

İÇİNDEKİLER

	Sayfa
1. ENVIRONMENTAL ASPECTS OF OFFSHORE ACTIVITIES IN ARCTIC (Review).....	3-17
2. A FUZZY BAYESIAN NETWORK APPROACH FOR RISK ANALYSIS OF HAZARDOUS CARGO SHIPS (Research Article).....	18-37
3. A REVIEW OF SEA ICE TRENDS ON POLAR REGIONS (Review).....	38-54
4. SERBEST SU YÜZEYİNE YAKIN DERİNLİKTEKİ DENİZALTININ MANEVRA SORUNLARININ İNCELENMESİ (İnceleme Makalesi)	55-65
5. Geri Çekildi: 2D BACKWARD FACING STEP FLOW SIMULATION BY FINITE DIFFERENCE METHOD (Research Article).....	66-79

ENVIRONMENTAL ASPECTS OF OFFSHORE ACTIVITIES IN ARCTIC

Kubilay DOKUMCU

Istanbul Technical University | dokumcu21@itu.edu.tr | ORCID 0000-0002-6006-9742

ÖZET

Dünya çapında artmakta olan enerji talebi, dünyanın ilgisini nispeten daha az keşfedilmiş ve zengin hidrokarbon kaynaklarına sahip Arktik bölgesine çekmiştir. Bu çalışmada, Arktik bölgesinde yürütülen açık deniz faaliyetlerinin, güncel durumu, karşılaşılan zorluklar ve olası çevresel etkileri değerlendirilmiştir. Arktik iklim ve çalışma şartları açısından zorlu bir coğrafya olup bu bölgede açık deniz faaliyetleri icra edilirken buzlanma, yüksek maliyetli operasyonel gereksinimler ve entegre esnasında zorluklar ile karşılaşabilmektedir. Bunun yanında faaliyetler esnasında petrol sızıntısı, su altı patlaması, atmosfere yüksek sera gazı salınımı, atık su deşarjları gibi önemli yan etkiler ortaya çıkmaktadır. Alınabilecek tedbirler kapsamında yeni ve çevre dostu teknolojilerin kullanımı, yerinde yakma, sıfır deşarj politikası, faaliyet öncesinde tüm olasılıkların değerlendirilebileceği hazırlık ve planlama faaliyetleri gerçekleştirilebilir. Arktik'in gelecek dönemlerde açık deniz faaliyetlerine daha fazla ev sahipliği yapacağı, bu maksatla çevresel etkilerin ve alınabilecek önlemlerin daha detaylı incelenmesi gerekli olduğu değerlendirilmektedir.

Anahtar Kelimeler: Açık deniz faaliyetleri, Arktik, Çevresel etki, Hidrokarbon kaynaklar.

Makale geçmişi: Gönderim 25 Aralık 2022; Kabul 16 Mart 2023

ABSTRACT

Increasing worldwide energy demand has drawn the world's attention to the Arctic region, which is relatively less explored and has rich hydrocarbon resources. In this study, the current status, difficulties and possible environmental impacts of offshore activities carried out in the Arctic region were evaluated. The Arctic is a challenging geography in terms of climate and operating conditions, icing, high-cost operational requirements, great energy demand for extraction and difficulties encountered during integration while performing offshore activities. In addition, important effects such as oil spills, underwater blasts, high greenhouse gas emissions into the atmosphere and produced water discharges may occur during activities. Within the scope of the measures that can be taken, the use of new and environmentally friendly technologies, in situ burning, zero discharge policy, preparation and well-planning before the activity can be carried out. It is considered that the Arctic will host more offshore activities in the future, and for this purpose, it is necessary to examine the environmental effects and the measures that can be taken in more detail.

Keywords: Offshore activities, Arctic, Environmental impact, Hydrocarbon resources.

Article history: Received 25 December 2022; Accepted 16 March 2023

1. Introduction

The Arctic Ocean is the smallest and shallowest of the five ocean basins of Earth, mainly covered by sea ice in winter but with more than half of the area ice-free during the permanently summer season [1]. Arctic Circle is the most widely used indicator to define the Arctic area but also the less accurate as it does not take into consideration any climatological or other geographical variations. According to this indicator, Arctic is an ocean placed in the north of the Arctic Circle (above the latitude of 66° 33' 44") [2]. If climatology is taken into consideration, the definition commonly accepted in engineering practices, "Arctic" refers to those places where the average temperature for the warmest month of the year is less than 10 °C [3].

The expanding demand for the oil and gas drives the explorations of the petroleum to the Arctic region [5, 6]. In 2008, the United States Geological Survey has assessed the area north of the Arctic Circle by using a probabilistic geology-based methodology and concluded that 22% of world hydrocarbon reserves (30% of the world's undiscovered gas and 13% (412 billion barrels) of the world's undiscovered oil) within these areas, mostly offshore under less than 500 meters of water and approximately 84% of such sources is expected to be found in offshore areas [7, 8, 9, 10, 11, 12, 13]. Undiscovered natural gas is three times more abundant than oil in the Arctic and is largely concentrated in Russia. Oil resources, although important to the interests of Arctic countries, are probably not sufficient to substantially shift the current geographic pattern of world oil production [14].

In this study, it is aimed to explain the current status of offshore activities in Arctic and the challenges encountered, and to review the environmental impacts and the measures to be taken by compiling different studies.

2. Offshore Activities in Arctic

2.1. Current Status

The Arctic environment is responding very sensitively to global warming, and the Arctic Ocean sea-ice is decreasing at a pace exceeding scientific predictions. Currently, the increasing meltdown of summer polar ice in the Arctic Ocean encourages the Arctic nations to perform offshore hydrocarbon exploration activities [2, 15].

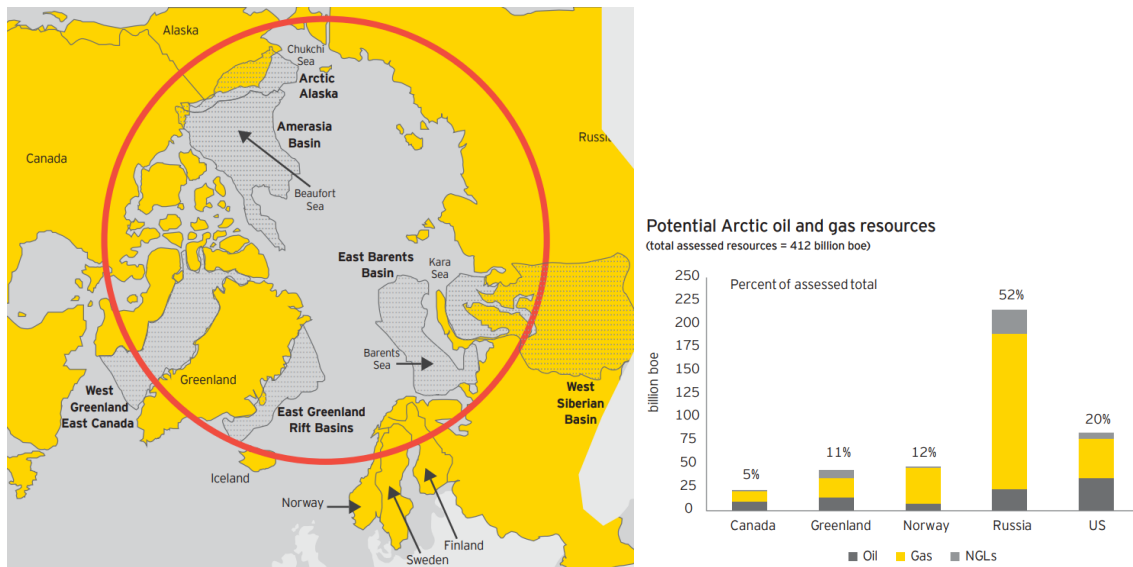


Figure 1. Probability of the presence of undiscovered oil/gas fields [9].

Figure 1 [9] shows the circumpolar Arctic region, the countries it includes, the most significant oil reserves, and the location of the Arctic Circle (see also in Section 1). Allocating the estimated resources/provinces to the nearest country (with “shared” provinces allocated equally), Russia is estimated to hold more than half of the total Arctic resources. Russia also holds the largest amount of natural gas resources, while the largest oil resources are in the US portion of the Arctic (Alaska). While Norway's offshore oil and gas reserves are beneath the North Norwegian and Barents seas, in Atlantic Canada, oil and gas activity occurs offshore the provinces of Newfoundland and Labrador, and Nova Scotia [17]. The largest oil and gas reserves in the Arctic are found in Russia. In Alaska there are six, in Canada eleven, and finally in Norway there is one large, discovered field [10, 18].

According to Novitsky et al. [19], offshore platforms can be divided into four groups based on operating depth: shallow (≤ 30 m), average depth (30-150 m), deep water (150-350 m), and ultra-deep water (≥ 350 m). Figure 2 shows various types of offshore structures and their operating depths. From a structural point of view, an offshore platform can be either fixed at the seabed or buoyant. Fixed platforms (fixed platform, compliant tower etc.), which are typically made of steel or concrete and are permanently anchored to the seabed. These platforms are more stable and less vulnerable to ice damage, but they are only suitable for use in relatively shallow waters. Buoyant platforms (tension leg platform, mini-tension leg platform, SPAR platform, floating production system, floating production, storage, offloading system) operate in deeper areas. These platforms are designed to move with the ice, allowing them to operate in shallow and frozen waters. The biggest challenge with buoyant platforms is the potential for ice damage, which can require significant maintenance and repair.

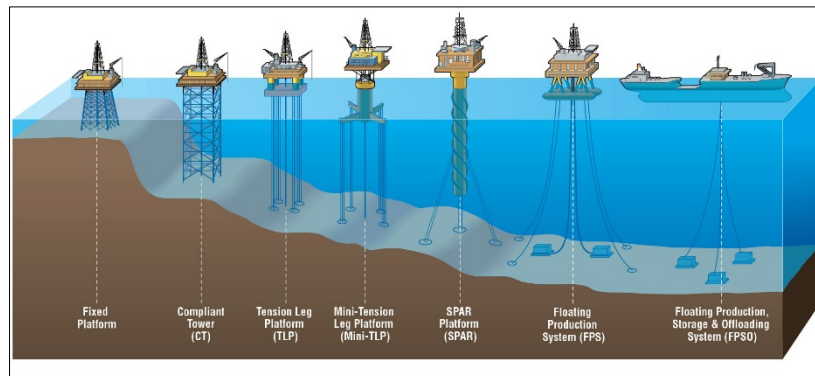


Figure 2. Types of offshore structures [60].

2.2. Challenges Encountered

Offshore activities in Arctic also bring a series of critical challenges to address:

Climate/Weather factors: The Arctic is characterized by a harsh climate with extreme variation in light and temperature, short summers, extensive snow and ice cover in winter, and large areas of permafrost [4]. The weather may deteriorate facility components at a higher rate, and delay operations, emergency and evacuation procedures. The remote and harsh environment is characterized by extreme waves, winds, storms, currents, icebergs, sea ice, and fog that hinder drilling operations and cause structural failures of critical offshore infrastructures. Moreover, these regions host unique ecosystems, and their preservation is a worldwide priority. For this reason, a comprehensive and systematic approach for risk analysis is necessary to prevent major accidents and comply with Arctic pollution control. Climate has considerable influence on the choice of design, operations, and maintenance [20, 21, 22]. From the past experiences, it is generally seen that bad weather causes loss of station keeping due to high winds and rough seas for floating structures and falling loads due to storms for fixed structures. Besides, high vulnerability to natural events of offshore infrastructure during transfer operations has resulted in numerous incidents [23]. Uncertainty on the influence of Arctic low temperature on offshore platform mechanical properties, which represents a topic for further investigation [6].

Icing: In his article, Barabadi et al. [24], emphasized that icing is a challenge for offshore structures and evaluated it by dividing it into two categories in general: atmospheric icing and sea spray icing. Atmospheric icing is defined as the processes where falling or drifting raindrops, refrozen wet snow, or drizzle form accretions on an object that is exposed to the atmosphere. Atmospheric ices are explained generally as hitting the deck of offshore structures; such as glaze (precipitating cold-water droplets), snow accumulation, rime (resulting from droplets in fog, sea smoke, or cloud drops), frost (direct transformation of water vapor to ice), sleet/ice pellets (accumulating loosely on horizontal surfaces such as decks, stairs, hatches, and helicopter landing pads). In the case of sea spray icing, the sea spray droplets are carried by the wind and hit objects in their way. Waves, volume of spray flux, and salinity of seawater are important factors that affect rate of sea spray. Sea spray accumulation occurrence is very rapid when there are high winds, low air temperature, and low sea temperature. Platform legs, bracing, blowout-preventer guidelines, mooring chains, marine risers, and flexible kill and choke lines in the splash zone 5–7 m above the sea are some potential areas for sea spray icing accumulation. Sea spray ice can

reduce rig stability, damage rig structure due to changes in stress on structural components, cause slipping hazards, render deck cargo unavailable, disable winches, cranes, and antennas, cover windows, rescue equipment, hatches, firefighting equipment, valves, and radomes [15, 24].



Figure 3. Icing effects on offshore structures [15].

Great energy demand for extraction: The extraction of oil and gas resources requires greater amounts of energy for lifting fluid to the surface. The energy demand for lifting fluid to the surface in the Arctic is likely to be higher than in other offshore environments due to the cold temperatures and the need for additional heating and insulation. Besides, in Arctic, the cold temperatures can cause the viscosity of oil to increase, making it more difficult to transport and process. To reduce the viscosity, the method often used is extra heating. But, heating the oil can require a significant amount of energy, which can be expensive and potentially increase greenhouse gas emissions [25, 26].

High operational costs: Higher wages and salaries are required to induce highly qualified personnel to work in the isolated and inhospitable Arctic. Transportation of materials and equipment is extremely expensive (logistic challenges). The icepack can hinder shipment of personnel, materials, equipment, and oil for long time periods. Furthermore, long supply lines from the world's manufacturing centers require equipment redundancy and a larger inventory of spare parts to insure reliability [2]. Also in Arctic conditions, clean-up costs are likely to be significantly greater than in less remote areas with more developed infrastructure, and milder weather conditions [27].

Strict regulations: Following the Deep-Water Horizon oil spill in the Gulf of Mexico in 2010, regulations on offshore drilling have been tightened, thereby limiting access and increasing costs further [2]. However, although these regulations may seem harsh, it is an undeniable fact that they will be beneficial in reducing environmental impacts, as will be explained in the next sections.

Reliability and integrity challenges: Every offshore activity can have risks like; hull structural failures, riser system failures, mooring line failures, umbilical system failures and human failures by its nature [2].

3. Environmental Impacts of Offshore Activities in Arctic

3.1. Possible Hazards

Health effects of oil spills: New economic developments in the Arctic, such as shipping and oil exploitation, bring along unprecedented risks of marine oil spills [28]. Oil spill is the major threat for these kinds of activities. Over the past 100 years, 7 million tons of oil has been spilled into the global environment from over 140 major incidents in addition to an estimated 600,000 tons of oil released annually from natural seeps [29, 30, 31]. For Arctic, A 2013 BOEM analysis of oil spills in the North Slope area between 1971 and 2011 identified 10 spills larger than 660 tons, and 2 spills larger than 1,300 tons [61]. In the report that Eger et al. [32] prepared, the reasons of oil spills could be from process leak, blowout, riser/pipeline/subsea structure leak, object on collision course; damage to structure; leak during loading/offloading. Differences in temperature between Arctic and temperate systems may alter the physical behavior of oil [5], hence oil spills can have more severe effects to living creatures: They can have negative impacts on local food sources because of contaminants and toxic substances that accumulate in the food chain of animals consumed as traditional foods [33, 34]. They may cause a loss of coastal areas and/or subsidence of land, contamination of beaches and rocks negative impacts on wildlife, including the killing of mammals, fish stocks, seabirds and shorebirds and various marine resources. Loss of land may also be due to the handling of contaminated waste, or by setting up a quarry on land to store oil from beaches. Such quarries may cause risks to wildlife, especially birds that may mistakenly identify it as a water source [33]. It should not be forgotten that Arctic plants and animals need a longer time to recover from damage because oil breaks down more slowly under cold conditions than warmer environments [2, 35]. Also shallow water sediments may become contaminated due to oil spills, as well as coastal vegetation, which may accelerate rates of erosion, wetlands may be lost, in addition to damage to “deep-sea coral communities” and “seaweed habitats harboring deep-sea shrimp, crab, and lobsters” [33]. Besides animals, they have effects to human health indirectly: Unpleasant oil smells and/or smoke/air pollution from a fire are also likely consequences of oil spills [33]. The health risks from oil and gas extraction are not only through air pollution but also through contaminated drinking water sources with chemicals that lead to cancer, birth defects, and liver damage [4]. Arctic oil spill response is challenging because of extreme weather and environmental conditions; the lack of existing or sustained communications, logistical and information infrastructure; significant geographic distances; vulnerability of Arctic species, ecosystems, and cultures. Timely and effective response to oil spills requires containment, recovery and restoration [2]. Johannsdottir and Cook [33] highlighted that oil spill response viability varies greatly throughout the year, with the situation better during summer months (July to October), when most areas are ice-free. However, during winter months, responses may not be as favorable. Location is another key aspect affecting likely response times. Oil spill responses are more favorable in the Bering Sea, Barents Sea, Norwegian Sea, Baffin Bay, Hudson Bay, and North Atlantic, while the situation is less favorable in other areas within the Polar region [36]. As a result, oil spills in ice infested waters are harder to deal with than open water, and that Arctic waters “might never recover from an environmental catastrophe like the one in the Gulf of Mexico” [37].

Harm to marine life due to underwater blasts: An underwater blast is accompanied by large amounts of air bubbles rising to the surface for a few minutes [38]. Underwater blasting can cause a range of impacts from the motile biota escaping the area of operation to lethal injuries or

immediate death, the impacted animals ranging in size from fish larvae and small fishes to large marine mammals [38, 39, 40]. According to Kjesbu et al. [55], underwater blasts cause significant behavioral changes in cod and herring, leading to decreased feeding and increased stress levels. Additionally, underwater blasts can result in physical damage to marine organisms. In a study of beluga whales in the Beaufort Sea, researchers found that exposure to underwater blasts caused damage to the whales' auditory systems, leading to hearing loss and potential impairments in their ability to communicate and navigate [56]. Furthermore, the effects of underwater blasts on the Arctic ecosystem extend beyond direct physical harm to individual organisms. These blasts can also cause migration of marine species, leading to changes in population dynamics and potentially disrupting the delicate balance of the ecosystem. In a study of narwhals in the Canadian Arctic, researchers found that underwater blasts resulted in the animals shifting their migratory patterns and moving away from their usual habitats [57].

Underwater blasts and dredging's suspended sediments and effects to benthic communities:

Studies of dredging activities have shown that spreading of suspended sediment takes place, e.g., near the surface or near the bottom, depending on the type of dredge being used [38]. These sediments mainly have effects to benthic communities. Benthic data is regularly collected worldwide to assess the environmental quality of marine ecosystems, by comparing proportions of species tolerant or favored by pollution, to species representative of unpolluted conditions. Arctic benthic communities are more vulnerable to petroleum compounds than those of temperate regions [41]. The reason could be that because Arctic region is characterized by low temperatures and a lack of sunlight, which results in slower rates of biodegradation and a longer persistence of pollutants in the environment [59]. This means that petroleum components are more likely to remain in the environment for a longer period of time, increasing the risk of exposure for benthic communities. In areas where the sediments at the seabed are polluted, operations such as underwater blasting and dredging could lead to the mobilization and spreading of the pollutants. In comparison it would seem that underwater blasting creates much more vigor and brings far more sediment into suspension and that this sediment becomes suspended at all possible levels throughout the water column. Blasting leads to a wider spreading of sediment, but that dredging leads to a wider spreading of the organic part of the sediment [38]. Barite and related compounds discharged at sea have an environmental impact on the benthos. Barite is a weight material used in drilling fluids, and barium and other heavy metals are found at high concentrations in it [41, 42]. Dredging of sediments has been shown to cause removal or destruction of the biota in the dredged material, coverage of the benthos in the vicinity of the site of operation by settlement of suspended sediment, and increased turbidity, resulting in decreased primary production of both phytoplankton and phytobenthos [38]. Besides, Roca et al. [43] demonstrated that high sedimentation rate can be the cause for a catastrophic, long-term impact on a nearby seagrass meadow and ecosystem.

Greenhouse gas emissions into the atmosphere: Oil and gas industry is one of the largest emitters of carbon dioxide [44]. Large power demand of offshore installations in the Arctic area is, in most cases, covered by their own gas, and greenhouse gas emissions from power production are high. Ice-protection techniques with a high consumption of energy have negative impacts on the sensitive environment and wilderness in the Arctic. The use of hazardous chemical ice protection causes degradation of the environmental quality; it also increases the produced waste and serious environmental consequences [24, 45].

Produced water discharges: Production of oil and gas generates large volumes of produced water. Produced water is a complex mixture of formation water (water trapped for millions of

years in a geologic reservoir, condensation water and occasionally injection water) injected in the well to maintain production levels. It contains numerous dissolved and particulate organic and inorganic substances with a concentration largely depending on reservoir characteristics. These substances include inorganic salts, metals, radioisotopes and organic compounds, such as polycyclic aromatic hydrocarbons, alkylphenols [46, 47, 48]. Beyer et al. [49] examined the environmental effects of offshore produced water and it is summarized that the accumulated ecotoxicological knowledge of offshore produced water discharges. The discharges contain organic acids (64%), metals (25%), dispersed crude oil (4%), alkylphenols (1%), polycyclic aromatic hydrocarbons (0.3%), and many other constituents of environmental relevance. Monitoring surveys find detectable exposures in caged mussel and fish several km downstream from produced water outfalls. Besides, increased concentrations of DNA adducts are found repeatedly in benthic fish populations, especially in haddock. But is uncertain whether increased adducts could be a long-term effect of sediment contamination due to ongoing produced water discharges, or earlier discharges of oil-containing drilling waste. According to Camus et al. [5], Arctic marine species are not less sensitive than their temperate counterparts to artificial produced water. But according to Geraudie et al. [50], overall long-term effects of produced water discharges to the marine environment are likely to be small.

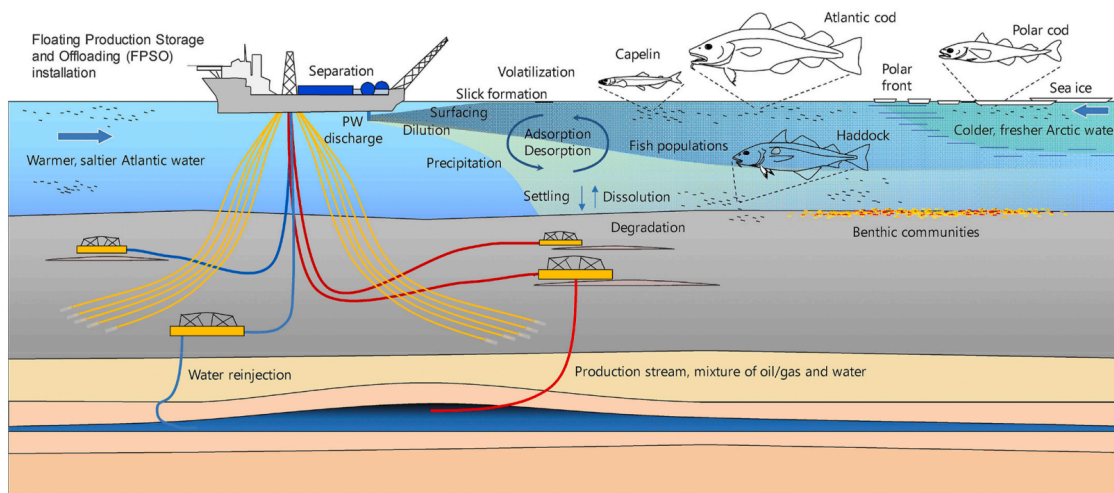


Figure 4. Produced water discharged from offshore oil and gas production and its effects [49].

Other effects: The accidents of Piper Alpha and the Gulf of Mexico, among other cases, show devastating outcomes, causing the semi-submersible platform's sinking, offloading, topside systems and helicopter accidents. It should not be forgotten that the similar disasters can happen in Arctic, too [22].

3.2. Precautions And Countermeasures To Be Taken

In-situ burning: The spilled oil not only harms the marine ecological environment, but it also can affect the shoreline ecological system and socioeconomic features, thereby endangering human health [51, 52, also see in section 3.1]. Once oil reaches or even strands on shorelines, cleanup and recovery are more difficult. The wind and atmosphere stability also play an important role in pollution dispersion. Lower wind and temperature inversion can seriously hinder the diffusion of pollutants. One of the widely used remediation strategies to prevent oil spreading is in-situ burning (also called controlled burning) when the oil is still floating on the ocean's surface

in offshore areas. Several studies, laboratory research and field experiments have proven that controlled burning in ice-affected waters is efficient in oil spill response, and it has been successfully applied in Arctic regions [53].

The usage of modern technology: There are various types of available offshore structures operated successfully in the Arctic region, but most of these structures are still limited by water depths and are incapable of year-round operations in extremely harsh ice environments. Hence, the need for new concepts or improvements to produce a feasible, reliable, and economical structure that permits continual year-round operation for the Arctic offshore drilling and production of oil and gas. The suitable concept of the structure should possess high resistance to extreme ice loadings, high resistance to freeze and thaw, easy site installations, and short site construction time [6]. It should be taken into consideration that the offshore platforms powered by renewable energy, including solar panels and wind turbines, and equipped with a wastewater treatment system and other environmentally friendly features should be used for better future. Today more and more companies are turning to environmentally friendly practices and technologies to reduce their impacts on the region's fragile ecosystem. Here are just a few examples of environment-friendly offshore activities in the Arctic. One example of environment-friendly offshore activities in the Arctic is the use of advanced drilling technology. This includes the use of subsea blowout preventers, which can help to prevent oil spills, as well as the deployment of remote operated vehicles (ROVs) for inspection and maintenance activities. By using these advanced technologies, companies can reduce the risks of accidents and spills, helping to protect the environment and wildlife in the Arctic. Another example of environment-friendly offshore activities in the Arctic is the use of environmental monitoring systems. These systems, which use sensors and other technology, can help to monitor water quality, air quality, and other environmental factors in real-time. This can help to identify potential environmental impacts of offshore operations, allowing companies to take timely and effective action to mitigate these impacts. Additionally, many companies operating in the Arctic are adopting best practices and standards for offshore activities. This includes the development of comprehensive emergency response plans, as well as the adoption of strict regulations and guidelines for offshore operations. By implementing these best practices and standards, companies can ensure that their operations are conducted in a responsible and sustainable manner, minimizing their impacts on the Arctic environment [58]. Besides, in Newfoundland and Alaska platforms have been designed to be able to withstand floating icebergs, and in Norway (e.g. Snøhvit) subsea installations have made gas transportation safer [10].

Zero-discharge policy: Andrade and Renaud [41] explored the polychaete/amphipod data ratio along the entire extent of the Norwegian continental shelf (North to Barents Seas) to evaluate its performance, specifically for impacts related to petroleum activities, as an environmental indicator for oil and gas impacts. The Barents Sea is managed under a zero-discharge policy, that is, no chemicals, oils and/or wastewater can be discharged to sea. The results give encouraging evidence that operation under the zero-discharge policy, combined with subsea installation and processing on land, does not seem to affect benthic communities, at least to the same extent as in other areas where discharges are permitted, and permanent surface installations exist [41, 54].

New environment-friendly policies: The Arctic Council initiated a project, 'Emergency Prevention, Preparedness and Response' (EPPR) for oil spill risks and published a subsequent technical report on circumpolar oil spill response [33, 36]. The report discusses weather conditions in the Arctic, i.e. "effects of wind, waves effects of wind, waves, air temperature, wind chill, sea ice, superstructure icing, horizontal visibility, and daylight/ darkness" on particular oil

spill response systems [36]. These systems are mechanical of vessels, ranging from 1 to 3 ships taking part in the recovery, dispersants from the vessel, aircraft or a helicopter, or in-situ burning techniques of vessels or helicopters. The Arctic Council's working groups and task forces, current and previous, are instrumental in initiating work that may reduce oil related risks in the region, as they are or have been focusing on issues such as telecommunication and connectivity, marine oil pollution prevention, preparedness and response, and search and rescue [35].

Preparedness and well-planning: The environmental impact of underwater blasting can probably be reduced considerably if the blast is timed favorably. If the desire is to reduce the far field environmental impacts such as spreading of organic material and fine-grained sediment, which might be carrying pollutants, then blasting should be carried out near slack tide, preferably in connection with neap tide, and when wind and waves are small. In addition, sediment is able to stay suspended at internal density gradients in the water column, periods should be preferred in which there is little input of buoyancy from freshwater or heating or when mixing of the water masses is strong. In arctic areas this is likely to happen during the fall where the freshwater runoff from land is ceasing and cooling from the atmosphere is increasing [38]. Another preparation is taking climate effects into consideration. For example, the extreme harsh environment where catastrophic hurricanes occur, requires a critical analysis of environmental loading on floating and fixed offshore structures at the operational phase [22].

Dispersants usage: Chemical usage (dispersants) during the clean-up phase of oil-spills may have positive effects, such as decreased amounts of toxic gases inhaled by clean-up participants [33].

4. Conclusions

In this study, environmental aspects of offshore activities in Arctic is examined. Increasing worldwide energy demand has drawn the world's attention to the Arctic region, which is relatively less explored and has rich hydrocarbon resources. Challenges during activities are classified as climate and weather factors, icing, great energy demand, strict regulations, reliability and integrity challenges. Environmental effects can be classified as health effects of oil spills, harms to marine life due to underwater blasts, underwater blasts and dredging's suspended sediments and effects to benthic communities, greenhouse gas emissions to Earth and produced water discharges. In order to prevent environmental impacts; in-situ burning and dispersant usage for oil spills, preparedness and well-planning to avoid accidents, the improvement of modern technology for harsh circumstances, and creating new environment-friendly policies can be used.

According to experts, we are “more than likely” to witness a substantial increase in oil and gas activities in the Arctic in the years to come, it should not be forgotten that the Arctic will become the center for oil and gas between 2030–2050 [10]. For this purpose, it is necessary to examine the environmental effects and the countermeasures that can be taken in more detail.

5. Acknowledgement

First, I would like to thank my lecturer, Dr. Sevil Deniz YAKAN DÜNDAR, who led me to this study and never spared her support and comments. In addition, I would like to thank the Istanbul Technical University Faculty of Naval Architecture and Ocean Engineering and ITU GiDB Journal for giving me this opportunity. This study was carried out within the scope of the

ADM505E Environmental Aspects of Offshore Activities graduate course. Therefore, no interest groups were worked with during the study and no funds were used.

References:

- [1] Ilicak, M., Drange, H., Wang, Q., Gerdes, R., Aksenov, Y., Bailey, ... Yeager, S.G. An assessment of the Arctic Ocean in a suite of interannual CORE-II simulations. Part III: Hydrography and fluxes. *Ocean Modelling*, 2016; 100: 141-161. <https://doi.org/10.1016/j.ocemod.2016.02.004>
- [2] European Commission, Joint Research Centre, Flitris, E., Rossotti, A., Tarantola, S., Safety aspects of offshore oil and gas operations in arctic and sub-arctic waters. Publications Office, 2019, <https://data.europa.eu/doi/10.2760/866261>
- [3] Freitag, D.R., McFadden, T.T. Introduction to Cold Regions Engineering. ASCE Publications, p. 2, 110. Gorynin, V., Malushevskiy, P., 2007. Creating and introducing of new materials. *Morskoy Vestnik*, 1997; 3 (6): 74-77.
- [4] Khare, N. and Khare, R. Environmental risk from exploitation of the Arctic. *The Arctic*, 2021.
- [5] Camus L., Brooks S., Geraudie P., Hjorth M., Nahrgang J., Olsen G.H., Smit M.G.D. Comparison of produced water toxicity to Arctic and temperate species. *Ecotoxicology and Environmental Safety*, 2015; 113: 248–258.
- [6] Yan J.B., Liu X.M., Liew J.Y.R., Qian X., Zhang M.H. Steel–concrete–steel sandwich system in Arctic offshore structure: Materials, experiments, and design. *Materials and Design*, 2016; 91: 111-121. <https://doi.org/10.1016/J.MATDES.2015.11.084>.
- [7] Gudmestad, O., Løset, S., Alhimenko, A., Shkhinek, K., Tørum, A., Jensen, A. Engineering aspects related to Arctic offshore developments. St. Petersburg, 2007.
- [8] Bird, K.J., Charpentier, R.R., Gautier, D.L., Houseknecht, D.W., Klett, T.R., Pitman, J.K., Moore, T.E., Schenk, C.J., Tennyson, M.E., Wandrey, C.J. Circum-Arctic Resource Appraisal: Estimates of Undiscovered Oil and Gas North of the Arctic Circle. USGS Fact Sheet 2008-3049. <https://doi.org/USGS Fact Sheet, 2008; 2008-3049>.
- [9] USGS. Circum-Arctic Resource Appraisal: Estimates of Undiscovered Oil and Gas North of the Arctic Circle. Fact Sheet 2008–3049, 2008.
- [10] Harsem Ø. and Knut Heen A.E. Factors influencing future oil and gas prospects in the Arctic, 2011; 39: 8037-8045.
- [11] Brownfield, M.E., et al., 2012. An Estimate of Undiscovered Conventional Oil and Gas Resources of the World, U.S. Geological Survey, USGS Fact Sheet 2012–3042.
- [12] Bucelli, M., Paltrinieri, N. Landucci, G. Cozzani, V. Safety barrier management and risk assessment: integration for safer operations in the Oil & Gas industry. Institution of Chemical Engineers Symposium Series, 2017-May (162).

- [13] Ilinova A. and Chanyшева A. Algorithm for assessing the prospects of offshore oil and gas projects in the Arctic. *Energy Reports*, 2020; 6: 504-509. <https://doi.org/10.1016/j.egy.2019.11.110>.
- [14] Gautier D.L., Bird K.J., Charpentier R.R., Arthur G., Houseknecht D.H., Klett T.R., Moore T.E., Pitman J.K., Schenk C.J., Schuenemeyer J.H., Kai S., Tennyson M.E., Valin Z.C., Wandrey C.J. Assessment of undiscovered oil and gas in the Arctic, *Science*, 2009; 324: 1175–1179.
- [15] Ryerson, C.C. Ice protection of offshore platforms. *Cold Reg. Sci. Technol.*, 2011; 65: 97–110.
- [16] Bai Y. and Jin W.L. *Marine Structural Design (Second Edition)*, Chapter 12 - Development of Arctic Offshore Technology, Butterworth-Heinemann, 2016; 229-243. <https://doi.org/10.1016/B978-0-08-099997-5.00012-5>.
- [17] Fidler C. and Noble B. Advancing strategic environmental assessment in the offshore oil and gas sector: Lessons from Norway, Canada, and the United Kingdom, 2012; 24: 12-21.
- [18] Budzik, P. Arctic Oil and Natural Gas Potential. US Energy Information Administration Office of Integrated Analysis and Forecasting Oil and Gas Division, 2009.
- [19] Novitsky, I.G., Portnoy, A.S., Razuvaev, V.N. Design of Offshore Platforms. Requirements of Standards (in Russian) SPBGMTY, 2009; pp. 8-10, 48-54, 72-75, 112-113.
- [20] Barabadi, A., Tobias Gudmestad, O., Barabady, J. RAMS data collection under Arctic conditions. *Reliab. Eng. Syst. Saf.*, 2015; 135: 92–99.
- [21] Bubbico R., Lee S., Moscati D., Paltrinieri N. Dynamic assessment of safety barriers preventing escalation in offshore Oil& Gas. *Safety Science*, 2020; 121: 319-330.
- [22] Adumene S. and Ikue-John H. Offshore system safety and operational challenges in harsh Arctic operations. *Journal of Safety Science and Resilience*, 2022; 3: 153-158.
- [23] Necci A., Tarantola S., Vamanu B., Krausmann E., Ponte L.. Lessons learned from offshore oil and gas incidents in the Arctic and other ice-prone seas. *Ocean Engineering*, 2019; 185: 12-26.
- [24] Barabadi A., Garmabaki A.H.S., Zaki R., Designing for performability: An icing risk index for Arctic offshore. *Cold Regions Science and Technology*, 2016; 124: 77-86.
- [25] Sujo-Nava D., Scodari L.A., Slater S.C., Dahm K., Savelski M.J. Retrofit of sour water networks in oil refineries: a case study, *Chem. Eng. Process. Process. Intensif*, 2009; 48 (April (4)): 892–901.
- [26] Khazaei A., Mohebbi V., Behbahani R.M., Ramazani S.A.A. Energy consumption in pervaporation, conventional and hybrid processes to separate toluene and i-octane, *Chem. Eng. Process. Process. Intensif*, 2018; 128 (June): 46–52.

- [27] Bonnieux, F., Rainelli, P. Learning from the Amoco Cadiz oil spill: damage valuation and court's ruling. *Ind. Environ. Crisis Q.*, 1993; 7 (3): 169–188.
- [28] Vergeynst L., Wegeberg S., Aamand J., Lassen P., Gosewinkel U., Fritt-Rasmussen J., Gustavson K., Mosbech A. Biodegradation of marine oil spills in the Arctic with a Greenland perspective. *Science of the Total Environment*, 2018; 626: 1243-1258.
- [29] NRC. *Oil in the Sea III: Inputs, Fates, and Effects*. National Academies Press (US), Washington, D.C, 2003.
- [30] Li, P., Cai, Q., Lin, W., Chen, B., Zhang, B. Offshore oil spill response practices and emerging challenges. *Mar. Pollut. Bull.*, 2016; 110: 6–27. <https://doi.org/10.1016/J.MARPOLBUL.2016.06.020>.
- [31] Bullock R., Perkins R., Aggarwal S. In-situ burning with chemical herders for Arctic oil spill response: Meta-analysis and review. *Science of the Total Environment*, 2019; 675: 705-716.
- [32] Eger K.M. *Effects of Oil Spills in Arctic Waters*, CHNL, 2010. <http://www.arctisearch.com/Effects+of+Oil+Spills+in+Arctic+Waters>
- [33] Johannsdottir L. and Cook D. Systemic risk of maritime-related oil spills viewed from an Arctic and insurance perspective. *Ocean and Coastal Management*, 2019; 179: 104853.
- [34] AMAP. *Arctic pollution issues 2014: trends in persistent organic pollutants, radioactivity, and human health in the Arctic - policymakers summary*, 2015. https://oaarchive.arctic-council.org/bitstream/handle/11374/1441/AMAP_POLLUTION_Doc1_Trends_in_POPs_Radioactivity_and_Human_Health_AC_SAO_CA04.pdf?sequence=1&isAllowed=y.
- [35] Arctic Council. *Arctic Oil and Gas*. Oslo, Norway, 2007.
- [36] EPPR. *Circumpolar Oil Spill Response Viability Analysis: Technical Report*. Tromsø, The Arctic Council, 2017.
- [37] Stotts, J. Arctic Council Deputy Ministers Meeting: Responding to Emerging Challenges in the Arctic, 2010. Available at: https://oaarchive.arctic-council.org/bitstream/handle/11374/768/EDOCS-%231977-v1-ACDMMDK01_COPENHAGEN_2010_ICC_statement.PDF?sequence=1&isAllowed=y.
- [38] Nielsen M.H., Bach S., Bollwerk, S.M. Spreading of sediment due to underwater blasting and dredging: Field observations from quay construction in Sisimiut, Greenland. *Ocean & Coastal Management*, 2015; 116: 512-522.
- [39] Buckstaff, K., Wells, R.S., Gannon, J.G., Novacek, D.P. Responses of bottlenose dolphins (*Tursiops truncatus*) to construction and demolition of coastal marine structures. *Aquat. Mamm.*, 2013; 39 (2): 174-186. <http://dx.doi.org/10.1578/AM.39.2.2013.174>.

- [40] Govoni, J.J., West, M.A., Settle, L.R., Lynch, R.T., Greene, M.D. Effects of underwater explosions on larval fish: implications for a coastal engineering project. *J. Coast. Res.*, 2008; 24 (2B): 228-233. <http://dx.doi.org/10.2112/05-0518.1>.
- [41] Andrade H. and Renaud P.E. Polychaete/amphipod ratio as an indicator of environmental impact related to offshore oil and gas production along the Norwegian continental shelf. *Marine Pollution Bulletin*, 2011; 62: 2836-2844.
- [42] Renaud, P.E., Jensen, T., Wassbotten, I., Mannvik, H.P. Botnen, H. Offshore sediment monitoring on the Norwegian shelf – a regional approach 1996-2006. Akvaplan-niva report no 3487-003, Akvaplan-niva, Tromsø, Norway, 2008.
- [43] Roca, G., Romero, J., Columbu, S., Farina, S., Pages, J.F., Gera, A., Inglis, G., Alcoverro, T. Detecting the impacts of harbour construction on a seagrass habitat and its subsequent recovery. *Ecol. Indic.*, 2014; 45: 9-17. <http://dx.doi.org/10.1016/j.ecolind.2014.03.020>.
- [44] Buslaev G., Morenov V., Konyaev Y., Kraslawski A. Reduction of carbon footprint of the production and field transport of high-viscosity oils in the Arctic region. *Chemical Engineering and Processing - Process Intensification*, 2021; 159: 108189.
- [45] Shi, X., Veneziano, D., Xie, N., Gong, J. Use of chloride-based ice control products for sustainable winter maintenance: a balanced perspective. *Cold Reg. Sci. Technol.*, 2013; 86: 104–112.
- [46] Durell, G., Utvik, T.R., Johnsen, S., Frost, T., Neff, J., 2006. Oil well produced water discharges to the North Sea. Part I: Comparison of deployed mussels (*Mytilus edulis*), semi-permeable membrane devices, and the DREAM model predictions to estimate the dispersion of polycyclic aromatic hydrocarbons. *Mar. Environ. Res.* 62, 194–223.
- [47] Johnsen, S., Utvik, T.I., Garland, E., de Vals, B., Campbell, J. Environmental fate and effects of contaminants in produced water. In: Paper Presented at the Seventh International Conference on Health, Safety and Environment in Oil and Gas Exploration and Production. Society of Petroleum Engineers, Richardson, Texas, , 2004; 9: SPE 86708.
- [48] Neff, J., Lee, K., DeBlois, E.M. Produced water: overview of composition, fates, and effects. In: Lee, K., Neff, J. (Eds.), *Produced Water*. Springer, NY, 2011.
- [49] Beyer J., Goksøyr A., Hjermmann D.Ø., Klungsoyr J. Environmental effects of offshore produced water discharges: A review focused on the Norwegian continental shelf. *Mar Environ Res.*, 2020; 162:105155. doi: 10.1016/j.marenvres.2020.105155. Epub 2020 Sep 21. PMID: 32992224.
- [50] Geraudie, P., Nahrgang, J., Forget-Leray, J., Minier, C., Camus, L. In vivo effects of environmental concentrations of produced water on the reproductive function of polar cod (*Boreogadus saida*). *J. Toxicol. Environ. Health Part A*, 2014; 77: 1–17.

- [51] Boufadel, M., Geng, X., An, C., Owens, E., Chen, Z., Lee, K., Taylor, E., Prince, R.C. A review on the factors affecting the deposition, retention, and biodegradation of oil Stranded on beaches and guidelines for designing laboratory experiments. *Curr. Pollut. Rep.*, 2019; 5: 407–423. <https://doi.org/10.1007/s40726-019-00129-0>.
- [52] Thibodeaux, L.J., Valsaraj, K.T., John, V.T., Papadopoulos, K.D., Pratt, L.R., Pesika, N.S. Marine oil fate: knowledge gaps, basic research, and development needs; a perspective based on the Deepwater Horizon spill. *Environ. Eng. Sci.*, 2011; 28: 87–93. <https://doi.org/10.1089/ees.2010.0276>.
- [53] Wang Z., Chunjiang An C., Lee K., Boufadel M., Feng Q. Dispersion modeling of particulate matter from the in-situ burning of spilled oil in the northwest Arctic area of Canada. *Journal of Environmental Management*, 2022; 301: 113913.
- [54] Olsen, G.H., Carroll, J., Dahle, S., Larsen, L.H., Camus, L. Challenges performing risk assessment in the arctic. In: Lee, K., Neff, J. (Eds.), *Produced Water*. Springer Science+Business Media, in press. doi:10.1007/978-1-4614-0046-2_28.
- [55] Kjesbu, O.S., Knutsen, T., Leknes, I., and Ovrevik, J. Effects of underwater blasts on cod and herring behavior. *Environmental Pollution*, 2018; 238: 902-910.
- [56] Houser, D.S., DeRuiter, S.L., Richardson, W.J., and Wartzok, D. Acoustic trauma in beluga whales (*Delphinapterus leucas*) exposed to underwater blasting. *Marine Pollution Bulletin*, 2016; 111(1): 345-353.
- [57] Heide-Jorgensen, M.P., Laidre, K.L., Dietz, R., Wiig, O., and Bech, C. Narwhal response to offshore oil and gas exploration in the Canadian Arctic. *Marine Pollution Bulletin*, 2017; 120(1-2): 402-409.
- [58] Kumar, P. and Patra, M. K. Environmental impacts of offshore oil and gas activities in the Arctic: A review. *Environmental Science and Technology*, 2018; 52(3): 1703-1712.
- [59] Gulliksen, B., Braithwaite, R., & Fossum, P. The Arctic: A vulnerable and fragile ecosystem. *Environmental Research Letters*, 2017; 12(3): 033001.
- [60] Stankiewicz S., https://www.coroflot.com/stevestankiewicz/digital-infographics?school_id=64332&msa=365&
- [61] Nuka Research and Planning Group. Oil Spill Occurrence Rates for Alaska North Slope Crude & Refined Oil Spills. Report to the Bureau of Ocean Energy Management. OCS Study BOEM, 2013: 205.

A FUZZY BAYESIAN NETWORK APPROACH FOR RISK ANALYSIS OF HAZARDOUS CARGO SHIPS

Gözde Nur Küçüksu¹, Ayhan MENTES², Hakan AKYILDIZ³

¹*Istanbul Technical University, Hidroteknik Nautical Design | kucuksu18@itu.edu.tr, gkucuksu@hidroteknik.net | ORCID 0000-0002-5003-3359*

²*Istanbul Technical University | mentes@itu.edu.tr | ORCID 0000-0003-1177-3212*

³*Istanbul Technical University | akyildiz@itu.edu.tr | ORCID 0000-0002-8554-2559*

ABSTRACT

The increasing global transportation raises some concerns over the handling of hazardous cargo vessels during berthing operations. This paper uses a Fuzzy Bayesian Network for the identification of various influencing factors, the inference, and analysis of these factors. The results show that dangerous cargo ships require more attention to resolve the risk probability. Human and environmental factors are the most prominent factors. On the other hand, training of ship personnel, wind force, water velocity, channel width, dock layout, and port location are other important factors to be taken into consideration. To conduct risk management for hazardous cargo vessels, port authorities need to focus on the invulnerable berthing of hazardous cargo vessels. The proposed model has prominent practical viability for governments, liner companies, and port authorities.

Keywords: Risk Analysis, Bayesian Network, Linguistic Variables, Fuzzy Set Theory, Berthing Operation.

Article history: Received 19 January 2023; Accepted 04 June 2023

1. Introduction

Shipping is becoming a bigger part of global trade, which depends on how well the maritime transport system and the seaport system work on the other hand, the increasing number of larger vessels brings more accidents and results in devastating consequences for human health and the environment (Murdoch et al., 2012). Most of the time, the presence of dangerous materials, which can leak out, explode, or catch fire, increases the chance of a terrible accident. Therefore, safety at sea is the most essential issue in the maritime industry. There are some international rules and applications by the ISPD (the International Ship and Port Facility Security Code), SOLAS (Safety of Life at Sea), IMO (International Maritime Organization), and the ISM Code (the International Safety Management Code).

The risk of accidents based on the existence of dangerous materials can result in devastating effects and consequences for human health and the environment when transported for commercial purposes (Inanloo and Tansel, 2015). These hazardous materials contain various petrochemical products that must be transported with enormous care (Akyuz and Celik, 2015).

The most recent incidents during the transport of hazardous materials include fire and explosion basically (Huang and Zhang, 2015). These accidents can be attributed to various factors that have diverted public attention to research on risk assessment and accident prevention (Zhao et al., 2012). Human error is considered an important factor in the maritime hazardous cargo risk assessment, which could be related to various characteristics of the carrying ships and the features of both the port facilities and the environment. This study develops insight into how the

sustainability and development of ports, in general, can be improved by analyzing the risk factors affecting the transport of hazardous materials using Fuzzy integrated Bayes Networks. Hence, the outcomes of this study can support the decision-making authorities in terms of adapted processes and sustained costs. To prevent any damage during the berthing operation, precise and gentle control is required. In any uncontrolled situation, several consequences such as a ship run aground, hitting the berth and colliding with other vessels can arise with alarming frequency, including loss of life, environmental pollution, and property damage (Murdoch et al., 2012) (John, et al., 2015). Evaluating the potential risks shows that a large number of accidents occur due to human error (Akyuz, 2016). Furthermore, most of the accidents have occurred because of fires or explosions in terms of hazardous cargo resulting in economic failure, loss of life, and injury.

This article uses the Fuzzy Bayes Networks to analyze the risks of dangerous cargo ships docking operations. In the berthing operations for a hazardous cargo vessel, the risk factors have been explained clearly using Bayesian Network and Fuzzy Set Theory with linguistic variables. The accident risk probabilities under various conditions were achieved through Expert Judgment and Binary Logistics regression. The contributing risk factors and sub-risk factors were determined, respectively, and their probabilities were calculated. It can be said that it is very important in terms of practical applications. Finally, the results and inferences have been given in detail.

2. Literature Review

In the literature, there are a number of ways to figure out how dangerous something is by using probability calculations and graphs, trees, flow charts, etc. to simulate them. It is important to understand the many effects of transporting hazardous materials and the role that the assessment and comparison of these risky play (Reniers et al., 2010). Overall, the risk of hazardous materials in maritime transportation has been measured in different ways and in different areas. With the help of event trees by Ronza et al. (2003), accident data from ports can be used to figure out what happened and in what order. A risk matrix (Cunningham, 2012) is a good way to show that accidents at the port terminal not only cause serious losses of life and property but also put the public's support for port operations at risk. According to Trbojevic and Carr (2000), putting up hazards control barriers and incorporating them into a safety management system can help manage or avoid the risks brought about by dangerous materials at the port. Kite-Powell et al. (1999) found that Bayesian networks can be used to find a link between the terminal environment and the reasons why a commercial ship ran aground. While approaching a terminal, LNG carriers are more susceptible to risks. Aside from the risks of transportation, it seems like a good target for terrorists and intentional damage can cause a release and a big fire that can spread up to 1500 meters (Bubbico et al., 2009). Also, recent studies on shipping suggest that the emission from the ship propulsion system and their environmental risk assessment are very necessary (Blasco et al., 2014). FST is also being used to evaluate the cargo ship risks along with the DEMATEL technique (Mentes et al., 2015).

Ren et al. (2007) have a study of the risk analysis of an offshore structure by the quantitative analysis of linguistic probabilities in a Bayesian Network. It has been evaluated the human factors affecting the collision risk between a Floating Production, Storage and Offloading (FPSO) unit, and an authorized vessel throughout the berthing process. Zhao et al. (2015) studied Bayesian Network to examine the safety of the LNG carrier system. It was calculated the likelihood of the accident and obtained the maximum chain by diagnostic reasoning in risk assessment. Akyuz (2016) studied a hybrid approach that integrated an Analytical Network Process (ANP) with a

Human Factors Analysis and Classification System (HFAC) to prevent loss of life or injury and enhance safety in maritime transportation. John et al. (2015) used both methods of the fuzzy logic-based approach and Bayesian network in the risk analysis to improve the resilience of a seaport system. Wen-hua et al. (2015) studied the major factors of oil spilling on ports and terminals during mooring and cargo handling. The Bayesian Network approach has been combining with the triangular fuzzy number approach to acquire the conditional probability of each variable. Chang et al. (2013) studied three major risk categories: information flow, physical flow, and payment flow by using both qualitative and quantitative methods.

John et al (2014) studied the safety assessment of seaport operations by using the integrated methods of Evidential Reasoning (ER) and Fuzzy Analytical Hierarchy (FAH). The risk factors were identified by an interview survey as a real case and then the relevant data were conducted by a questionnaire survey. In this study, the level of risks was identified by using a risk map, aiming to facilitate the treatment of uncertainties in seaport operations and optimize systematically the performance effectiveness. Hsu (2015) carried out a study of the risk assessment of ship berthing operation using the integration of a Safety Index (SI) and a Fuzzy Analytic Hierarchy Process (FAHP). This study was validated by investigation of berthing operation at Kaohsiung Port in Taiwan. Yeo et al. (2016) estimated the undesirable probability of an accident with Bayesian Network capability and conducted a dynamic safety analysis. The proposed method was performed on safety analysis for the offloading process of an LNG carrier. Pak et al (2015) conducted a study to evaluate and rank many factors that influence navigational safety in Korean ports. The weather-sea condition, channel condition, volume of traffic inside a port, ship types, and ship size were investigated as main factors by using the Fuzzy Hierarchical Process.

Ports systems consist of a vast variety of interconnected components, and the dynamic nature of these components makes the port operations systems complex. Exploring these systems from the perspectives of their interconnectivity that comprise of the infrastructure physiognomies, operational associations, environmental influences, technical competence, types of failure, and the situation in which the system operates provides a perception of the system intricacy. While reviewing the safety features of a seaport system, a rational tactic is to do itemization into the subsystems containing all the prominent functional components of the system to make decide at all the levels of the system's design, operations, and maintenance (Khan, R. U. et al., 2021). Therefore, port systems are considered an important entity to make this transport possible and hence play their role in the operations of cities and countries.

Generally, risk is the likelihood of an accident, determining the chances of an incident happening and the severity of aftereffects brought by it. Risk assessment for human, natural, and other associated stimuli is done through the combination of probability theory and statistical techniques as per their tolerability standards. Depending on the degree to which these factors and their analysis rely on numerical indicators, the methods used for their assessment could be classified as qualitative and quantitative methods, and as per situations, these methodologies are made hybrid as semi-quantitative. These hybrid semi-quantitative methods are found to be more accurate, broader, and successful as the qualitative method serves as the basis for all assessments. But quantitative methods are preferred as a result of their ability to cover both the probability and consequence of risks. Hence, quantitative methods are considered more useful as they can be consistently used to provide detailed statistical datasets, enhancing the ability to understand the magnitude and implication of risks.

Bayesian networks that incorporate the quantitative approach of risk assessment and provide viable results are a combination of graph theory and probability theory. The discrete properties of a BN include its ability to undertake the inference inversely, integrate new annotations to the network, handling incomplete and missing data, and provide a graphic illustration of the original cause and effect association (Ren et al., 2009). Bayesian methods have been used in various fields of transportation. In the marine transport and port systems, BNs is being used to evaluate the vessels evacuation in an accidental hazard situation by Eleye-Datubo et al. (2006), incorporation of human and organizational issues in the risk analysis by Trucco et al. (2008), and evaluation of the offshore safety by the integration of BN and the “Swiss Cheese” model by Ren et al. (2008). Apart from these BNs, they have been extensively used along with the uncertainty factors in various modeling approaches for the maritime traffic safety analysis (Hänninen et al., 2014) (Hänninen and Kujala, 2014) (Montewka et al., 2014). Increasing the size of vessels put the port infrastructure under pressure to facilitate the management of effective risk on the loading and unloading of these large vessels. The accident in the port operations system poses a threat not only to goods but also to the environment and human life. The port operational interruption factors may be attributed to vessel accidents and groundings, port machinery and equipment failures, spillage of hazardous materials, and petrochemicals (John et al., 2014). Human error and technical faults hold the major of the responsibility attributed to maritime accidents. Human capabilities in the analysis of maritime accidents have been evaluated previously (O’Neil, 2003) (Akyuz and Celik, 2015) (Hetherington et al., 2006) (Celik et al., 2009).

In addition to these works, there are also various forms of geological, atmospheric, and hydrological parameters of the natural environment for better understanding and handling of risks (Chauvin et al., 2013) (Kröger, 2008). These natural risks are held as the most loss-causing, recurring, and severe disruptions in seaport operations as they disturb the ship’s movements through increasing tides and velocity, visibility, increased wind speed, and floods (Lam and Su, 2015). Analyzing the offloading risks of LNG vessels through the dynamic failure modeling based on Bayesian networks indicates that collision can be the most commonly occurring accident at berths leading to calamitous consequences (Yeo et al., 2016). However, literature specifically related to risk assessment of berthing and departure of hazardous cargo ships under the effect of various contributing factors is scarce. Hence, it is of prodigious importance to carry out such studies and evaluate the most prominent and contributing factors to risks in dealing with hazardous cargo at ports.

2.1 Berthing Operation for Hazardous Cargo Ships

For a dangerous cargo ship to dock or berth, it must do a lot of maneuvering that requires a lot of people working together. Since oil and other hazardous materials are potentially inflammable and explosive by nature, an accident will result in fatalities and loss of property, and environmental pollution. After identifying the potential hazards due to the design of the vessel, process, equipment, manpower, materials, port environment, and facilities, it is of extreme vitality to improve the safety of hazardous cargo berthing operations (Hsu, 2015). The most important points of the berthing operation are slow speed, controlled approach, planning, teamwork, and checking equipment. Additionally, the professional skills of all ship personnel as well as knowledge about maneuvers and human mental situations have an essential effect on operations; a positive team approach increases efficiency and communication (Murdoch et al., 2012). In berthing operation, the pilot manages the ship handling and the maneuvering characteristics. Therefore, the pilot’s professional skills should be sufficient to manage the operation. On the other hand, poor

communication may result in misunderstanding and consequently result in safety problems in berthing operations because of different languages and different cultures.

All equipment must be checked to prevent any malfunction. Before approaching the berth, the main engine, thrusters, steering gears must be fully operational. Before arriving, the main engines should be tested, and remote controls should be checked. Also, all bridge equipment such as engine movement recorders, VDRs, radars, course recorders, echo sounders, and all remote read-outs should be controlled. Some tankers carrying oil and gas must be escorted by tugs in the harbor during berthing operation. Tugs escort the vessel when berthing alongside and departing by pulling and towing the vessel. Using tugs is needed when wind, tide, and current or the ship's handling characteristics cause difficult berthing conditions (Hsu, 2015), (Murdoch, Clarke, & Dand, 2012). While working with tugs, using bow thruster, when under-keel clearance is low, sailing in a narrow channel and when the ship close to another ship, the ship should avoid high forward speed for maneuvering. But at low speed, wind and current have a great effect on maneuvering. Also, the draft and trim information should be clear because they also affect maneuvering. Other important operations are dock operation, facilities and line handling operations. The port management policy has developed rules to manage the port operation of the growing ship density to ensure safety at the port during berthing operations. Complying with these rules may have a great effect on ensuring safety. The weather also creates risk for the berthing operation. Except for the visibility of navigation bridges, wind speeds, currents influence risk. In cold weather, the ship must be prepared for its equipment, such as mooring winches, cargo hose lifting gear, gangway hoists, water lines, and a firefighting system against freeze-up (Det Norske Veritas Inc., 2016).

Hazardous cargo has potential for spills, leaks, explosion, discharge, emission, and fire, and they have the risk to air, soil, sediment, groundwater, water, and habitats within the local port area and the wider environment. There are several reasons, including the presence of explosive, flammable, corrosive, noxious, poisonous, radioactive, and irritative substances, in commodities that emit poisonous vapor, pressurized gases, or bio-medical materials. The regulations for transportation of dangerous cargo have been determined by the International Maritime Organization (IMO). All organizations and port authorities should comply with the IMO regulations for storage, handling, loading, and discharge. IMO classifies the substance into nine groups: explosives, gases, flammable liquids, flammable solids, oxidizing substance and organic peroxides, toxic and infectious substance, radioactive material, corrosive substance, miscellaneous dangerous substance. IMO has a regulation for the shipping of hazardous cargo. As required by SOLAS (Safety of Life at Sea), all shipping of hazardous cargo must comply with the IMO's International Maritime Dangerous Goods (IMDG) code.

There are some studies about the safety problems of hazardous cargo. One of the main causes is the inconvenience of storage and segregation. The other causes are human factors. The lack of experienced staff will have very serious consequences. Not knowing any precaution for any dangerous cargo will result in fire, explosion, leakage, spilling, etc. The other human factor is misdeclaration or non-declaration of the cargo by shippers to save money, which is also improbable. In contrast to the shippers who try to save money, not taking any precaution or following the necessary rules will cause more money loss in any dangerous situation. Therefore, that makes risk assessment more important. In this study, the risk factor can be divided into five groups by considering both hazardous cargo vessel and berthing operations: "Human Factor", "Ship Factor", "Environmental Factor", "Operational Factor", and "Security".

3. Methodology

Risk is identified as the probability and consequence of uncertain events, and it brings an undesirable outcome such as loss, damage etc. Risk can be formulated as:

$$\text{Risk} = \text{Probabaility} \times \text{Consequences} \quad (1)$$

The scientific part of risk analysis is a risk assessment, which is about figuring out how likely something is to happen and what will happen if it does. One of the key points of risk assessment is a systematic and structured approach. The steps of methodology should be followed, which provide a good risk assessment (Gorris&Yoe, 2014).

Since maritime accident analysis became an important topic, studies have increased. There are several risk analysis methods such as Analytical Network Process by Akyuz (2016), Bayesian Network with Fuzzy Analytical Hierarchy Process by John et al. (2015), Zhao et al. (2015) and Wen-hua et al. (2015), questionnaire survey with mean value method, and stochastics dominance method by Chang et al. (2013), Evidential Reasoning and Fuzzy Analytical Hierarchy Process by John et al. (2014), Safety Index (SI) with a Fuzzy Analytic Hierarchy Process (FAHP) model by Hsu (2015), Formal Safety Assessment (FSA) by Wang&Foinikis (2001), Fuzzy Analytical Hierarchy Process by Pak et al. (2015) used in marine accidents.

Risk analysis can be defined as dealing with uncertainty, which can be classified as vagueness, randomness, and ignorance. Randomness is caused by unpredictable events, and probability theory can deal with randomness. Vagueness is caused by ill-defined situations, and Fuzzy can handle the vagueness. Finally, ignorance exists because of the weak correlation between factors and consequences identified by the experts. At this point, Bayesian Network provides enough correlation. Two ways have been asserted to control the risks in marine transportation: to reduce the accident probability and to control the accident extent (Zhao et al., 2015).

3.1 Bayesian Network & Fuzzy Numbers with Linguistic Judgments

Bayesian network is a kind of probabilistic reasoning and uncertainty analysis that has been in recent studies (Yeo et al., 2016) (Zhao & Soares, 2015). In risk analysis, Bayesian Network provides the causal relationships between risk factors and the related occurrence likelihood of each hazardous event (Ren et al., 2009). The Bayesians network model provides prior knowledge with prior probability and conditional probability to show knowledge uncertainty. The changes with new approaches, technologies, and hazardous cargoes create new risks and damages. Therefore, reducing the likelihood of occurrence becomes important.

Public health and safety require the prevention of accidents which makes risk assessment essential. After designating each set of events, a probability measure gives the quantification. But determining the value of the probability is generally impractical. That causes a nebulous probability for the event. Some judgments such as 'more or less likely', 'likely', 'possible', and 'impossible' may be used to specify the probability, instead of numerical value. Identifying the probability with linguistic terms as a result of fuzziness, that cannot be said that randomness (Karwowski & Mital, 1986). Evaluation of the risk factor expressed by human experts; these judgments can be transformed into crisp probabilities. Transformation of the linguistic judgments provides cost-saving and BN model modification and maintenance (Ren et al., 2007).

Stefanini et al. (2008) listed two features required to be satisfied to use of fuzzy numbers in applications, which are:

- An easy way to represent and model fuzzy information with enough or possible high flexibility of shapes, without being constrained to strong simplifications, e.g., allowing asymmetries or nonlinearities.
- The relative simplicity and computational efficiency required to perform exact fuzzy calculations or to obtain good or error-controlled approximations of the results.

In modeling the uncertainties, vagueness, uncertainties, fuzzy sets, and numbers are integrative to probability and statistics. The fuzzy sets are coming from the interval analysis which defines the rules error propagations. The mathematical model of a vaguely defined quantitative piece of information is the notion of a fuzzy quantity.

3.2 Theoretical Background

Bayesian Network

Bayes' rule is coming from conditional probability. As Devin Soni said (Soni, 2018), "*Bayes rule provides us with a way to update our beliefs based on the arrival of new, relevant pieces of evidence.*"

Bayes' theorem which used to calculate the conditional probability can be represented as follows (Ünal, 2018):

$$P(A|B) = (P(A)P(B|A))/P(B) \tag{2}$$

Where $P(A | B)$ is the probability of the happening of the A when the B has happened (posterior):

$P(A)$ is the probability of the happening of the A (likelihood):

$P(B | A)$ is the probability of the happening of the B when the A has happened (likelihood):

$P(B)$ is the probability of the happening of the B (marginal).

Let's apply the Bayesian Inference on a random variable X, which is any one of the sets of values. Assume that $V = \{X_1, X_2, \dots, X_n\}$ is a set of variables with X_i having a countable infinite space. The definition of joint probability distribution required that if the function of $P(X_1=x_1, X_2=x_2, \dots, X_n=x_n)$ satisfied the following conditions;

For every combination of values of the x_i 's

$$P \leq (X_1 = x_1, X_2 = x_2, \dots, X_n = x_n) \leq 1 \tag{3}$$

$$\sum_{x_1, x_2, \dots, x_n} P(X_1 = x_1, X_2 = x_2, \dots, X_n = x_n) = 1 \quad (4)$$

Directed acyclic graphs (DAG) are the basis of the probabilistic models, which are also known as Bayesian networks within cognitive science and artificial intelligence (Condary & Jouffe, 2013). The illustration of the Bayesian network can be specified with directional edges (Figure 1). A Bayesian network can be defined mathematically as a set of edges (Stephen, 2000):

Two important points of DAG can be shown in Figure 1:

- There is not any cyclic
- The edges are directed.

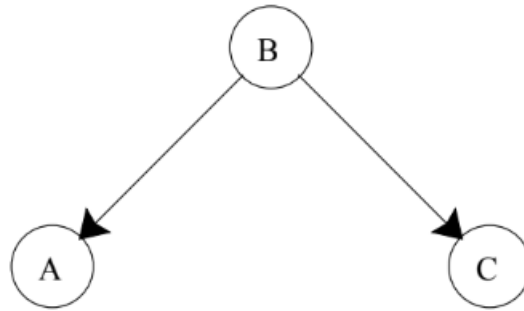


Figure 1. An example of the Bayesian network

The acyclic property provides to not cycle back means when you leave the initial node and go with the edge direction, you cannot back to the initial node again. The conditionally independent nodes in Figure 1 are A and C. The probabilities can be represented as followed (Stephen, 2000):

$$P(A|B, C) = P(A|B) \quad (5)$$

$$P(C|B, A) = P(C|B) \quad (6)$$

$$P(A, B, C) = P(A|B).P(B).P(C|B) \quad (7)$$

The joint distribution probability can be represented in general form as (Stephen, 2000);

$$P(X) = \prod_{i=1}^n [P(X_i | \text{parents}(X_i))] \quad (8)$$

and, then

$$\begin{aligned} P(A, B, C) &= P(A|B).P(B).P(C|B) = \frac{P(B|A)P(A)}{P(B)}.P(B).P(C|B) \\ &= P(B|A).P(A).P(C|B) \end{aligned} \quad (9)$$

A Bayesian network should satisfy the following two conditions:

- The structure of the directed network (DAG)
- Probability distribution

The goal of the Bayesian network is to show in a graph a number of conditionally independent relationships. A Bayesian network with several nodes and edges can be represented. Every node in the network is a forest if each node has either one or no parent. If one node has no parent, it is called a tree (Stephen, 2000). The final form of the Bayesian network has become as followed:

$$P(B | A) = (P(A; B; C))/P(A) = (P(A | B).P(B).P(C | B))/P(A) \tag{9}$$

Linguistic Variables and Fuzzy Sets

Assigning the numerical values of the risk factors gives a quantitative value of the risk. The risk score (S_{jk}) is calculated based on likelihood, exposure, and consequences. In general, the numeric values of the risk score are obtained from the judgments of the experts. But, in the given period, there is no unique risk that the hazard will happen. Therefore, risk analysis deals with imprecise and uncertain values based on personal experiences. This means that the experts’ judgments are generally verbal expressions. The risk scores were derived based on human judgments and their corresponding quantitative expressions were obtained by the analysts in the system safety area (Karwowski & Mital, 1986). As the likelihood is described vaguely and imprecisely, the probability of events P will also be described with linguistic variables. The linguistic values as very likely, likely, more-or-less likely, and others can notate as P_i and the numerical values are in the interval of $0 \leq P_i \leq 1$ (Karwowski&Mital, 1986). As described by Stefanini et al. (2008), the elements are defined by their membership function $\mu: X \rightarrow T \subseteq [0,1]$. The membership grade of the, $x \in X$ is notated with the value $\mu_u(x) \in [0,1]$. The u is assumed fuzzy set over X . The crisp value is defined as the subset of points of X called as support.

$$supp(u) = \{x | x \in X, \mu_u(x) > 0\} \tag{11}$$

For $\alpha \in [0,1]$, the α -cut of u is:

$$[u_\alpha] = \{x | x \in X, \mu_u(x) \geq \alpha\} \tag{12}$$

If $x \in supp(u)$ means that $\mu_u(x) > 0$, then:

$$\mu_u(x) = sup\{\alpha | \alpha \in [0,1] \text{ for which } x \in [u_\alpha]\} \tag{13}$$

When the $supp(u)$ has considered as a convex set, then the membership function is quasi-concave if α -cut of u are convex sets for all $\alpha \in [0,1]$. Detyniecki and Yager (2001) introduced the representative value, $Val(u)$ of a fuzzy number u as followed:

$$Val(u) = \frac{\int Average(u_\alpha).f(\alpha).d\alpha}{\int f(\alpha).d\alpha} \tag{14}$$

Where f is mapping from $[0, 1]$ to $[0, 1]$. There are two complementary parametrized functions: an increasing family of function and decreasing family of function.

The increasing family:

$$F: \alpha \rightarrow f(\alpha) = \alpha^q \text{ with } q \geq 0 \quad (15)$$

The decreasing family:

$$F: \alpha \rightarrow f(\alpha)(1 - \alpha)^q \text{ with } q \geq 0 \quad (16)$$

If the $q=0$, f becomes constant, which means it equals 1.

If the $q=\infty$, f becomes a direct function.

$q=0$:

$$Val(u(a, b, c, d)) = \frac{\left(\frac{b+c}{2}\right) + \left(\frac{a+d}{2}\right)}{2} \quad (17)$$

$q=\infty$:

$$Val(u(a, b, c, d)) = \left(\frac{b+c}{2}\right) \quad (17)$$

To make the judgments of experts more rational, they can adjust subjective parameter values by using different 'q' values in the f-weighted valuation function (Ren et al., 2007). In this study, two 'q' values have been used, and analyses have been completed for both.

4. Risk Analysis of Hazardous Cargo Ships

Following the structure of the risk analysis below is an important point for obtaining a realistic analysis. Therefore, the steps explained in the Methodology sections will be applied as a guideline for analysis. The test case is a risk analysis of the hazardous cargo vessel during the berthing operations. Fuzzy and linguistic judgment will be conducted with Bayesian Network for risk analysis. The proposed risk analysis in this study consists of the transformation of linguistic judgments into crisp values, creating a Fuzzy Set and Bayesian Inference. After determining and defining the problem, the risk analysis process can be divided into six steps as follows: Figure 2 shows the steps of the proposed method.

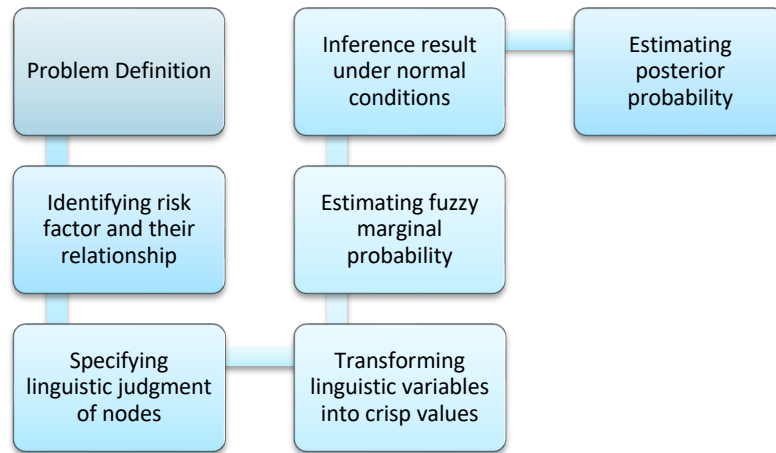


Figure 2. Flow diagram of the test case

- Step.1: Identifying risk factors and their relationship.
- Step.2: Specifying linguistic judgment of nodes.
- Step.3: Transforming linguistic variables into crisp values.
- Step.4: Estimating Fuzzy marginal probability.
- Step.5: Inference result under normal conditions.
- Step.6: Estimating Posterior Probability.

Step 1: Identifying risk factors and their relationship.

The first rule for berthing operation is slow and controlled speed and the second is bridge teamwork and preparation. Therefore, operational and human factors are handled in the test case. The operational factor is divided into three factors which are tugboat operation, dock operation, and port management policy. The human factor has two sub-factors: the pilot factor and the crew factor. All language and communication skills, operation knowledge, vessel knowledge are assessed under business skill for both pilot and crew factor. Also, mental skill is evaluated for both crew and pilot factor. Fuzzy and linguistic judgment was conducted with Bayesian Network for risk analysis. The risk factors that have been evaluated in the test case (see, Table 1).

Table 1. The evaluated risk factors in the test case.

Main Factor	Sub Factor	
Human Factor	Pilot Factor	Business skill
		Mental state
	Crew Factor	Business skill
		Mental state
Operational Factor	Tugboat Operation	
	Dock Operation	
	Port Management Policy	

The purpose of the test case is to evaluate the posterior probability of business skill of pilot factor (X1) when the hazardous cargo vessel risk (U1) is 100% (Figure 3)

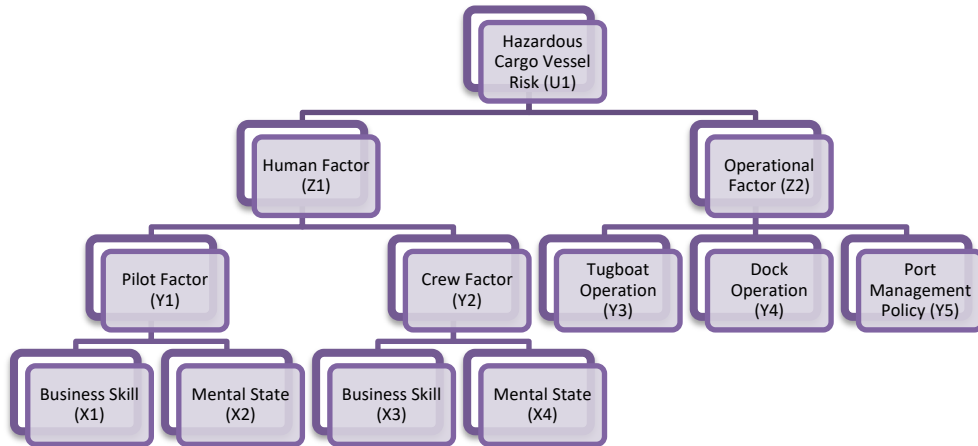


Figure 1. The structure of risk factors.

Step 2: Specifying linguistic judgment of nodes.

The linguistic judgment depends on the experts' experience. The risk level is determined verbally by the experts. The labels start with the event is occurred, which has been labeled as "Certain". The situation of an event that does not occur is labeled as "Impossible". Between "Impossible" and "Certain", there are 7 different linguistic labels. The Fuzzy membership functions vary between 0-1. The "Impossible" is accepted as 0 and the certain is accepted as 1.0. The interval linguistic labels and their membership functions are used (see, Table 2).

Table 2. Linguistic labels and their meanings.

Linguistic Label	Meaning	Fuzzy Membership Function
Impossible	Never occur	(0, 0, 0)
Nearly Impossible	The likelihood probability of occurrence is nearly impossible	(0.001, 0.002, 0.005) (0.040, 0.050, 0.080)
Very Unlikely	The likelihood probability of occurrence is very unlikely	(0.190, 0.200, 0.230) (0.220, 0.250, 0.260) (0.240, 0.250, 0.280)
Unlikely	The likelihood probability of occurrence is unlikely	(0.340, 0.350, 0.380) (0.390, 0.400, 0.430)
Even Chance	The likelihood probability of occurrence is even chance	(0.490, 0.500, 0.510)
Likely	The likelihood probability of occurrence is likely	(0.570, 0.600, 0.610) (0.620, 0.650, 0.660)
Very Likely	The likelihood probability of occurrence is very likely	(0.720, 0.750, 0.760) (0.740, 0.750, 0.780) (0.770, 0.800, 0.810)
Nearly Certain	The likelihood probability of occurrence is nearly certain	(0.920, 0.950, 0.960) (0.995, 0.998, 0.999)
Certain	Definitely occur	(1, 1, 1)

All prior probability calculations are completed according to the linguistic label of factor and corresponding Fuzzy Membership function. The linguistic label for the likelihood probability of Business Skill of Pilot (X1) is “Very Unlikely”, Mental Skill of Pilot (X2) is “Even Chance”, Business Skill of Crew (X3) is “Unlikely”, Mental Skill of Crew (X4) is “Very Unlikely”, Tugboat Operation (Y3) is “Even Chance”, Dock Operation (Y4) is “Unlikely”, and Port Management Policy (Y5) is “Likely”. The corresponding fuzzy membership functions are given (see, Table 3, Table 4, Table 5, Table 6, Table 7, Table 8, and Table 9).

Table 3. The Fuzzy occurrence probability of business skill of a pilot.

Business Skill of Pilot (X1)	
P(X1=1)	P(X1=0)
0.24	0.72
0.25	0.75
0.28	0.76

Table 4. The Fuzzy occurrence probability of mental state of a pilot.

Mental State of Pilot (X2)	
P(X2=1)	P(X2=0)
0.49	0.49
0.50	0.50
0.51	0.51

Table 5. The Fuzzy occurrence probability of business skill of crew

Business Skill of Crew (X3)	
P(X3=1)	P(X3=0)
0.34	0.62
0.35	0.65
0.38	0.66

Table 6. The Fuzzy occurrence probability of mental state of crew.

Mental State of Crew (X4)	
P(X4=1)	P(X4=0)
0.24	0.72
0.25	0.75
0.28	0.76

Table 7. The Fuzzy occurrence probability of tugboat operations.

Tugboat Operations (Y3)	
P(Y3=1)	P(Y3=0)
0.49	0.49
0.50	0.50
0.51	0.51

Table 8. The Fuzzy occurrence probability of dock operations.

Dock Operations (Y4)	
P(Y4=1)	P(Y4=0)
0.34	0.62
0.35	0.65

0.38	0.66
------	------

Table 9. The Fuzzy occurrence probability of Port Management Policy.

Port Management Policy (Y5)	
P(Y5=1)	P(Y5=0)
0.62	0.34
0.65	0.35
0.66	0.38

Step 3: Transforming linguistic variables into crisp values.

The crisp values have been evaluated by the value function. In this study, both values of q in the f -weighted valuation function are used ($q=0$ and $q=\infty$) (Table 10).

Table 10. The crisp values for the test case.

	The crisp values	
	$q=0$	$q=\infty$
P(X1=1)	0.255	0.250
P(X1=0)	0.745	0.750
P(X2=1)	0.500	0.500
P(X2=0)	0.500	0.500
P(X3=1)	0.355	0.350
P(X3=0)	0.645	0.650
P(X4=1)	0.255	0.250
P(X4=0)	0.745	0.750
P(Y3=1)	0.500	0.500
P(Y3=0)	0.500	0.500
P(Y4=1)	0.355	0.350
P(Y4=0)	0.645	0.650
P(Y5=1)	0.645	0.650
P(Y5=0)	0.355	0.350

The next steps can be named Bayesian Inference, which starts with the calculation of marginal probabilities and posterior probability calculation.

Step 4: Estimating Fuzzy marginal probability.

The marginal probabilities of Pilot Factor (Y1), Crew Factor (Y2), Human Factor (Z1), Operational Factor (Z2), and Hazardous Cargo Vessel Risk (U1) were calculated and given (see, Table 11).

Table 11. The marginal properties.

	P(Y1=1)	P(Y1=0)	P(Y2=1)	P(Y2=0)	P(Z1=1)	P(Z1=0)	P(Z2=1)	P(U1=1)	P(U1=0)
$q=0$	0.2065	0.7935	0.1737	0.8263	0.1228	0.8772	0.5000	0.1668	0.8332
$q=\infty$	0.2000	0.8000	0.1663	0.8338	0.1170	0.8830	0.5000	0.1616	0.8384

Step 5: Inference result under normal conditions

By using the results of marginal probabilities calculated in Step 4, the inference under normal conditions for both $q=0$ and $q=\infty$ are given in Table 12 and Table 13.

Table 12. The inferences under normal conditions for $q=0$.

X1-Business Skill	Y1-Pilot Factor	Z1-Human Factor	U1-Hazardous Cargo Vessel Risk
0.2550			
	0.2065		
X2-Mental Skill			
0.5000			
X3-Business Skill	Y2-Crew Factor	0.1228	
0.3550			
	0.1737		
X4-Mental Skill			
0.2550			
			0.1668
	Y3-Tugboat operation	Z2-Operational Factor	
	0.5000		
	Y4-Dock operation		
	0.3550	0.5000	
	Y5-Port Management Policy		
	0.6450		

Table 13. The inferences under normal conditions for $q = \infty$.

X1-Business Skill	Y1-Pilot Factor	Z1-Human Factor	U1-Hazardous Cargo Vessel Risk
0.2500			
	0.2000		
X2-Mental Skill			
0.5000			
X3-Business Skill	Y2-Crew Factor	0.1149	
0.3500			
	0.1663		
X4-Mental Skill			
0.2500			
			0.1595
	Y3-Tugboat operation	Z2-Operational Factor	
	0.5000		
	Y4-Dock operation		
	0.3500	0.5000	
	Y5-Port Management Policy		
	0.6500		

Step 6: Estimating Posterior Probability.

The final step of the methodology is the calculation of the posterior probability. The probability of business skill of pilot has been assessed when the hazardous cargo vessel risk is 100% ($U1=1$).

5. Results & Conclusion

This study presents an application of the Fuzzy Bayesian Network Approach of hazardous cargo vessels during berthing operations. The risk factors have been evaluated by the judgments of experts. The linguistic judgments in the methodology are expressed quantitatively with fuzzy membership functions. For the Bayesian inference evaluations, they have been transformed to crisp value with an f-weighted value function. The value of q has been applied with the value function ($q=0$ and $q=\infty$). Risk analysis can be considered as an assessment of uncertainty. In this case, three terms become important, namely vagueness, randomness, and ignorance. The Fuzzy handles the vagueness with occurs due to the ill-defined situations. Ignorance becomes a problem when experts are unable to make a strong connection between a factor and its consequences. The Bayesian network with a good correlation between factors and consequences eliminates ignorance.

Finally, probability theory can address the randomness resulting from unpredictable events. The human and operational factors have also been assessed. In this study, the mental state and business skills of the pilot and crew are the sub-factors for the human factor. The operational factors have been divided into tugboat operation, dock operation, and port management policy. The result for

both q values are very close: for the crisp value, $q=0$ the posterior probability $P(X1=1 \mid U1=1) = 0.260$, when the likelihood probability $P(X1=1) = 0.255$; for the $q=\infty$ the posterior probability $P(X1=1 \mid U1=1)=0.290$, when the likelihood probability $P(X1=1)=0.250$. When the posterior probability for both $q=0$ and $q=\infty$ are compared, the difference is very small. It can be indicated that the f -weighted value function is reasonable in both cases $q=0$ and $q=\infty$ and the occurrence of business skill for a pilot has increased. The correlation between hazardous cargo vessel risks and the business skill of a pilot is strong.

References

Akyuz, E., 2016. A marine accident analysing model to evaluate potential operational causes in cargo ships. *Safety Science*, 17-25.

Akyuz, E. & Celik, M., 2015. A methodological extension to human reliability analysis for cargo tank cleaning operation on board chemical tanker ships. *Safety Science*, 75, 146-155.

Akyuz, E. & Celik, M., 2016. A hybrid human error probability determination approach: The case of cargo loading operation in oil/chemical tanker ship. *Journal of Loss Prevention in the Process Industries*, 43, 424-431.

Blasco, J., Durán-Grados, V., Hampel, M. & Moreno-Gutiérrez, J., 2014. Towards an integrated environmental risk assessment of emissions from ships' propulsion systems.

Bubbico, R., Di Cave, S. & Mazzarotta, B., 2009. Preliminary risk analysis for LNG tankers approaching a maritime terminal. *Journal of Loss Prevention in the Process Industries*, 22, 634-638.

Celik, M., Er, I. D. & Topcu, Y. I., 2009. Computer-based systematic execution model on human resources management in maritime transportation industry: The case of master selection for embarking on board merchant ships. *Expert Systems with Applications*, 36, 1048-1060.

Chang, C.-H., Xu, J., & Song, D.-P., 2013. An analysis of safety and security risks in container shipping operations: A case study of Taiwan. *Safety Science*, 168-178.

Chauvin, C., Lardjane, S., Morel, G., Clostermann, J.-P. & Langard, B., 2013. Human and organizational factors in maritime accidents: Analysis of collisions at sea using the HFACS. *Accident Analysis & Prevention*, 59, 26-37.

Condary, S., & Jouffe, D. (2013). *Introduction to Bayesian Networks & BayesiaLab*.

Cunningham, L. K., 2012. *Risk Assessment Methodology for Marine Terminals*. Ports '01. ASCE Library.

Det Norske Veritas Inc., 2016. Canaport energy east marine terminal risk studies. Final Termopol Study Report: Element 3.15 Risk Assessment, Texas.

Detyniecki, M., & Yager, R. R. (2001). Ranking Fuzzy Numbers Using α -weighted Valuations. *International Journal of Uncertainty, Fuzziness and Knowledge-Based Systems*, 573-591.

Eleye-Datubo, A. G., Wall, A., Saajedi, A. & Wang, J., 2006. Enabling a powerful marine and offshore decision-support solution through Bayesian Network technique. *Risk Analysis*, 26, 695-721.

Gorris, L., & Yoe, C. (2014). *Risk Assessment: Principles, Methods, and Applications*. Elsevier Inc.

Hänninen, M. & Kujala, P., 2014. Bayesian Network modeling of port state control inspection findings and ship accident involvement. *Expert Systems with Applications*, 41, 1632-1646.

Hänninen, M., Valdez Banda, O. A. & Kujala, P., 2014. Bayesian Network model of maritime safety management. *Expert Systems with Applications*, 41, 7837-7846.

Hetherington, C., Flin, R. & Mearns, K., 2006. Safety in shipping: The human element. *Journal of Safety Research*, 37, 401-411.

Hsu, W. K., 2015. assessing the safety factors of ship berthing operations. *The Journal Of Navigation*, 576-588.

Huang, P. & Zhang, J., 2015. Facts Related to August 12, 2015 explosion accident in Tianjin, China. *Process Safety Progress*, 34, 313-314.

Inanloo, B. & Tansel, B., 2015. Explosion impacts during transport of hazardous cargo: GIS-based characterization of overpressure impacts and delineation of flammable zones for ammonia. *Journal of Environmental Management*, 156, 1-9.

International Maritime Organization (IMO), 2006. *International Maritime Dangerous Goods Code*. London: Polestar Wheatons Ltd, Exeter.

John, A., Yang, Z., Riahi, R., & Wang, J., 2015. A risk assessment approach to improve the resilience of a seaport system using Bayesian networks. *Ocean Engineering*, 136-147.

John, A., Paraskevadakis, D., Bury, A., Yang, Z., Riahi, R. & Wang, J., 2014. An integrated fuzzy risk assessment for seaport operations. *Safety Science*, 68, 180-194.

Karwowski, W., & Mital, A. (1986). Potential Application of Fuzzy Sets in Industrial Safety Engineering. *Fuzzy Sets and Systems* 19, 105-120.

Khan, R. U., Yin, J., Mustafa, F. S., & Anning, N. (2021). Risk assessment for berthing of hazardous cargo vessels using Bayesian networks. *Ocean & Coastal Management*, 210, 105673

Kite-Powell, H. L., Jin, D., Jebsen, J., Papakonstantinou, V. & Patrikalakis, N., 1999. Investigation of potential risk factors for groundings of commercial vessels in U.S. Ports. *International Journal of Offshore and Polar Engineering*, 9, 6.

Kröger, W., 2008. Critical infrastructures at risk: A need for a new conceptual approach and extended analytical tools. *Reliability Engineering & System Safety*, 93, 1781-1787.

Lam, J. S. L. & Su, S., 2015. Disruption risks and mitigation strategies: an analysis of Asian ports. *Maritime Policy & Management*, 42, 415-435.

Mentes, A., Akyildiz, H., Yetkin, M. & Turkoglu, N., 2015. A FSA based fuzzy DEMATEL approach for risk assessment of cargo ships at coasts and open seas of Turkey. *Safety Science*, 79, 1-10.

Montewka, J., Ehlers, S., Goerlandt, F., Hinz, T., Tabri, K. & Kujala, P., 2014. A framework for risk assessment for maritime transportation systems—A case study for open sea collisions involving RoPax vessels. *Reliability Engineering & System Safety*, 124, 142-157.

Murdoch, E., Clarke, C., & Dand, I. W., 2012. *The Standard and P&I Club: A Master's Guide to Berthing*. London.

O'NEIL, W. A. 2003. The human element in shipping. *WMU Journal of Maritime Affairs*, 2, 95-97.

Pak, J.-Y., Yeo, G.-T., Oh, S.-W., & Yang, Z., 2015. Port safety evaluation from a captain's perspective: The Korean experience. *Safety Science*, 172-181.

Reniers, G. & Dullaert, W. 2012. Tepitri: A screening method for assessing terrorist-related pipeline transport risks. *Security Journal*, 25, 173-186.

Reniers, G. L. L., Jongh, K. D., Gorrens, B., Lauwers, D., Leest, M. V. & Witlox, F. 2010. Transportation Risk Analysis tool for hazardous Substances (TRANS) – A user-friendly, semi-quantitative multi-mode hazmat transport route safety risk estimation methodology for Flanders. *Transportation Research Part D: Transport and Environment*, 15, 489-496.

Ren, J., Jenkinson, I., Wang, J., Xu, D. L. & Yang, J. B., 2009. An offshore risk analysis method using Fuzzy Bayesian Network. *Journal of Offshore Mechanics and Arctic Engineering*, 131, 1-12.

Ren, J., Wang, J., Jenkinson, I., Xu, D. L., Yang, J. B., & Yang, J. B., 2007. A Bayesian network approach for offshore risk analysis through linguistic variables. *China Ocean Engineering*, 371-388.

Ronza, A., Félez, S., Darbra, R. M., Carol, S., Vilchez, J. A. & Casal, J. 2003. Predicting the frequency of accidents in port areas by developing event trees from historical analysis. *Journal of Loss Prevention in the Process Industries*, 16, 551-560.

Trbojevic, V. M. & Carr, B. J., 2000. Risk-based methodology for safety improvements in ports. *Journal of Hazardous Materials*, 71, 467-480.

Trucco, P., Cagno, E., Ruggeri, F., Grande, O., 2008. A Bayesian Belief Network modeling of organizational factors in risk analysis: A case study in maritime transportation. *Reliability Engineering & System Safety* 93(6):845–856.

Soni, D., 2018. What is Bayes Rule? Retrieved from Towards Data Science: <https://towardsdatascience.com/what-is-bayes-rule-bb6598d8a2fd>.

Stephen, T. A., 2000. *An Introduction to Bayesian Network Theory and Usage*. Valais: IDIAP.

Stefanini, L., & Sorini, L., Guerra, M.L., 2008. Fuzzy Numbers and Fuzzy Arithmetic, *Handbook of Granular Computing*, 249 – 283.

Skowron, & V. Kreinovich, *Handbook of Granular Computing* (pp. 249-283). A John Wiley & Sons, Ltd, Publication.

Trucco, P., Cagno, E., Ruggeri, F. & Grande, O. 2008. A Bayesian Belief Network modeling of organizational factors in risk analysis: A case study in maritime transportation. *Reliability Engineering & System Safety*, 93, 845-856.

Wen-hua, W., Hou-ming, F., Wen-gang, C., & Yang, G., 2015. oil spill risk evaluation of ship mooring and cargo handling on ports using bayesian networks. *International Conference on Management Science & Engineering*, 394-402, Dubai.

Wang, J., & Foinikis, P. (2001). Formal safety assessment of containerships. *Marine Policy*, 143-157.

Yeo, C., Bhandari, J., Abbassia, R., Garaniyaa, V., Chaia, S., & Shomalib, B., 2016. dynamic risk analysis of offloading process in Floating Liquefied Natural Gas (FLNG) platform using bayesian network. *Journal of Loss Prevention in the Process Industries*.

Zhao, L., Wang, X. & Qian, Y. 2012. Analysis of factors that influence hazardous material transportation accidents based on Bayesian Networks: A case study in China. *Safety Science*, 50, 1049-1055.

Zhao, S., Zhu, H., & Soares, C. G., 2015. A Bayesian network modeling and risk analysis on LNG carrier anchoring system. *The 3rd International Conference on Transportation Information and Safety*, (pp. 432-436). Wuhan.

A REVIEW OF SEA ICE TRENDS ON POLAR REGIONS

Kubilay DOKUMCU

Istanbul Technical University | dokumcu21@itu.edu.tr | ORCID 0000-0002-6006-9742

ABSTRACT

This paper aims to establish a comprehensive trend database for sea ice extent (SIE), sea ice volume (SIV), and sea ice thickness (SIT) in polar regions, with the influence of global climate change. The analysis predominantly spans between 1979-2018, coinciding with the onset of satellite-based sea ice measurements. Arctic exhibits coherent negative trends in SIE, SIV, and SIT; conversely, in Antarctic, the trends in SIE and SIV are generally positive. Though, a comparison of the SIE trends and data for July 2023 in both polar regions reveals concerning results. The Arctic's SIE significantly deviates from the reference period average, surpassing the worst-case climate change projections, while Antarctic displays extreme levels of decline, deviating from previously observed positive trends. The underlying reasons for these deviations necessitate urgent investigation and further research, as they hold significant implications for Earth's polar regions and require heightened scientific attention.

Keywords: Arctic, Antarctic, Sea ice extent, Sea ice volume, Sea Ice thickness, Climate change

Article history: Received 18 March 2023; Accepted 29 May 2023

1. Introduction

The Arctic Ocean is the smallest and shallowest of the five ocean basins of Earth, mainly covered by sea ice in winter but with more than half of the area ice-free during the permanently summer season (Ilicak et al. 2016). Its sea ice cover receives net heat input in summer, as shortwave radiation and sensible heat fluxes directly heat the sea ice, including its snow layer (Itoh et al. 2011). Being an expansive region, the Antarctic, covers the area below the starting latitude of Antarctic Circle (66°S) and includes the Southern Ocean together with the continent of Antarctica (Watt, 2023). With around 90% of the world's total surface fresh water and 60% of the world's total fresh water, Antarctic holds a significant portion of the planet's water resources. Antarctic is divided into five sectors: the Weddell Sea (WS), the Indian Ocean (IO), the western Pacific Ocean (WPO), the Ross Sea (RS), and the Bellingshausen and Amundsen Seas (BAS) as seen in Figure 1 (NASA, 2016).

The excessive increase of greenhouse gases in the atmosphere causes global warming and climate change. According to US National Aeronautics and Space Administration the air temperature around the world increase between 1980 and 2020 was approximately 1.0°C (NASA, 2020). In the third Special Report to be produced in the Intergovernmental Panel on Climate Change's Sixth Assessment Report (AR6), projected change in global mean surface air temperature in our world would be increasing up to 4.8 °C until 2100 (IPCC, 2019). Global climate change exhibits a significant interconnection with the polar regions, stemming from the persistent poleward transfer of atmospheric thermal energy and moisture, the climate of the polar regions is highly influenced by the climate at lower latitudes (Ilicak et al. 2016). At seasonal to interannual time scales, sea ice may influence the climate of mid-high-latitude regions (Francis et al. 2009). The response to

an increase in atmospheric greenhouse gases concentration simulated by general circulation models is generally stronger at high latitudes than at lower latitudes (e.g. Manabe et al. 1991; Houghton et al. 1996). Especially the warming in the Arctic has been much faster than in the rest of the world, a phenomenon known as Arctic amplification. According to Rantanen et al. (2021) that region has warmed four times faster than the globe since 1980. Climate change impacts the sea ice by reducing its coverage, which means that more solar radiation is absorbed by the ocean instead of being reflected back into space by the ice (Parkinson, 2014). This change in the physical properties of sea ice creates annual trend. Measurements of sea ice levels have increased since 1979 when the continuously satellites monitoring of the sea ice began. In this study, it is aimed to show the effects of the climate change to the sea ice by creating sea ice trends lists via using different studies and different measurement devices. The variation trends of sea ice extent (SIE), sea ice volume (SIV) and sea ice thickness (SIT) in the polar regions are analyzed in detail.

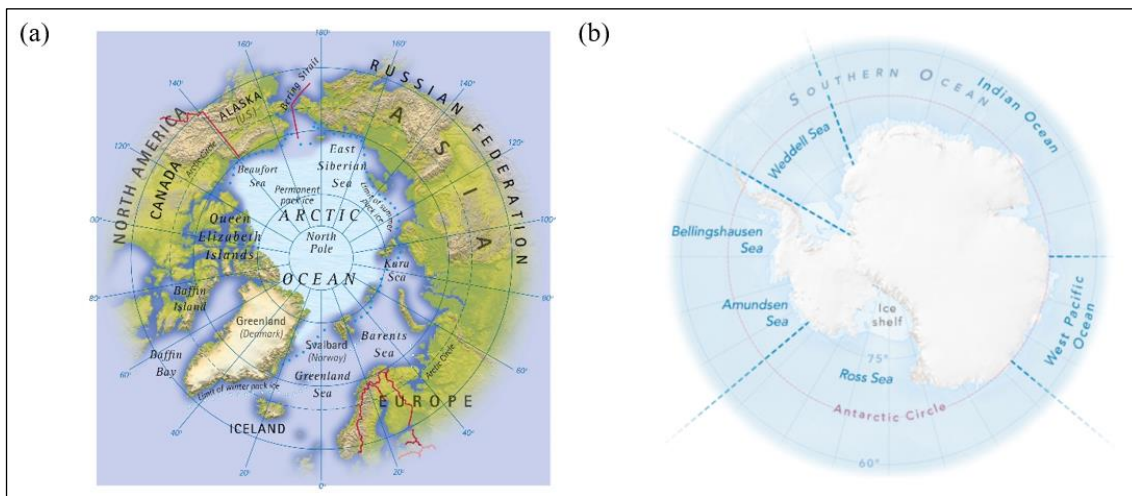


Figure 1. (a) Arctic (National Geographic, 2021) and (b) Antarctic (NASA, 2016) general view.

2. Sea Ice Data Systems

Various measurement techniques were employed in the generation of trend values described in the studies. These measurement systems possess distinct characteristics, which are briefly outlined: Submarine measurements were conducted using upward looking sonar instruments installed on Navy submarines, employing digital or analog recording methods. Satellite measurements are made by different satellites. Satellite measurements involved different satellites, such as the Ice, Cloud, and Land Elevation Satellite (ICESat), which serves as the reference Earth Observing System mission for measuring ice sheet mass balance ("ICESat", 2017). The CryoSat (CS) satellite measures sea ice by gauging 'freeboard,' the difference in height between sea ice and adjacent water, as well as ice sheet altitude, enabling the monitoring of changes in ice thickness ("CryoSat", 2021). Coupled models are computer-based models of the earth's climate, in which different parts (such as atmosphere, oceans, land, ice) are "coupled" together, and interact in simulations (Gerald et al., 1997). The Pan-Arctic Ice-Ocean and Assimilating System (PIOMAS) is a sea ice-ocean model with sea ice concentration and sea surface temperature assimilation using optimal interpolation by National Centers for Environmental Prediction/National Center for Atmospheric Research (NCEP/NCAR) reanalysis data which is globally gridded atmospheric data set (Lindsay and Zhang, 2006; Schweiger and others, 2011). The Coupled Model Intercomparison Project Phase (CMIP5 and CMIP6) is a

collaborative framework designed to improve knowledge of climate change. The Nucleus for European Modelling of the Ocean (NEMO) is a framework of ocean related engines for ocean dynamics and thermodynamics ("NEMO", 2021). The MIT General Circulation Model (MIT GCM) uses the finite volume method to accurately represent the bottom boundary position (Adcroft et al., 1998). The National Snow and Ice Data Center (NSIDC) combines remote sensing, satellites and model data for determining SIE loss. Microwave radiometers (MR) are instruments that measure the power of the thermal noise emitted at a physical temperature larger than 0 Kelvin-absolute zero and can provide observations with all-time and all-weather coverage and has high sensitivity to sea ice permittivity (Emery and Camps, 2017; Wang et al., 2020).

3. Methods

The studies reviewed in this article used the linear trend method to determine the trends of values, despite the use of various sea ice data systems mentioned earlier.

$$y = a + bx$$

Linear trend refers to a pattern or tendency where the dependent variable (usually denoted as "y") changes in a linear manner over time (represented by the independent variable, denoted as "x"). In other words, the relationship between the two variables can be described by a straight line. To determine the linear trend, data is collected from past periods and analyzed using the equation as seen above. In this equation, "a" represents the constant coefficient or the intercept of the line, and "b" represents the slope or the trend of the line. The value of "x" represents time, which is used to estimate the value of "y" at different points in time. (Dokumcu, 2021). In this study, different time intervals of trend values are standardized annually. The fact that data has been obtained since 1979 considered in trend calculations meets the concept of a 30-year data set, which World Meteorological Organization (2017) claims is more accurate in normal and trend analysis. Trend list is listed on the basis of the date when the trend period started (if there is more than one trend in the same study, on the basis of reference). If a trend value is seasonal or for specific month it is specified after the period (i.e. 1979-2012 September, 2003-2013 Autumn).

4. Results and Discussion

Sea ice is the layer of ice formed on top of the sea when it freezes which is a sensitive indicator of climate change for the polar regions and beyond, so monitoring sea ice is important ("How we measure sea ice", 2021). The state of the sea ice is determined by its extent, thickness and volume ("SIE", 2020).

4.1 SIE Trends

SIE is a measurement of the area of the ocean where the integral sum of the areas of all grid cells with minimum ice concentration. Usually threshold of minimum concentration is defined to mark the ice edge; and "15 percent cutoff" provides the most consistent agreement between satellite and ground observations (Candanosa 2021; "Quick facts", 2021).

Table 1. Arctic SIE Trends.

Period	Method	SIE Trend ($10^3 \text{ km}^2 \text{ y}^{-1}$)	Reference
1979-2014 September	Satellites	-82 ± 18	Shu et al., 2020
	CMIP6	-70 ± 6	
2002-2017 July-October	CryoSat	-19	Wang et al., 2020
2002-2017 April-May		-2	
1972 – 2002	MR	-30 ± 3	Cavalieri et al., 2003
1979–2018 September	Satellites	-82.3 ± 7.3	Kumar et al. 2020
1979–2018 March	MR	-42.1 ± 3.53	
1979-2015	Satellites	-43.5 ± 4.1	Shu et al. 2015
	CMIP5	-37.1 ± 1.9	
1979-2012	Satellites	-51	Huang et al., 2017
1979-2012 March		-23	
1979-2012 June		-40	
1979-2012 September		-95	
1979-2012 December		-35	
2013-2100 RCP 4.5	CMIP5	-36	
2013-2100 March-RCP 4.5		-21	
2013-2100 June-RCP 4.5		-28	
2013-2100 September-RCP 4.5		-37	
2013-2100 December-RCP 4.5		-38	
2013-2100 RCP 8.5		-81	
2013-2060 March-RCP 8.5		-36	
2013-2060 June-RCP 8.5		-49	
2013-2060 September-RCP 8.5		-82	
2013-2060 December-RCP 8.5		-71	
1978-2013	NSIDC	-54.58 ± 3.70	Simmonds, 2015
1979-2007	MR	-65	Deser, 2013
1979-2010	MR	-14.6 ± 2.3	Cavalieri and Parkinson, 2012

Upon examination of the trend values for Arctic SIE in Table 1, a consistent and persistent negative trend is observed, notwithstanding variations in measurement techniques and time intervals. This decline in Arctic SIE can be attributed to various physical factors, including increased solar energy absorption by open water, strong southerly winds transporting warm temperatures, an intensified wind-driven transpolar drift leading to substantial ice outflow through

Fram Strait or ice accumulation at the edge of the Canadian Arctic Archipelago basin, and downward energy fluxes from the atmosphere and northward ocean heat transport (Kumar et al., 2020). Notably, the most significant decreasing trends in Arctic SIE occur during the autumn period. Furthermore, projections for future trend values are provided, considering two distinct scenarios: RCP 4.5 and RCP 8.5. Under RCP 4.5, a medium-mitigation emission scenario where radiative forcing levels stabilize at 4.5 W/m² before 2100, Arctic SIE is anticipated to continue declining across all seasons from 2013 to 2100. Conversely, under RCP 8.5, a high-emission scenario where radiative forcing levels stabilize at 8.5 W/m² before 2100, Arctic SIE is expected to decrease more rapidly in each month from 2013 to 2060, particularly in September and December. This projection suggests that the Arctic may experience ice-free conditions, where SIE decreases to less than 1×10^6 km², as early as September 2053 (Huang et al., 2017).

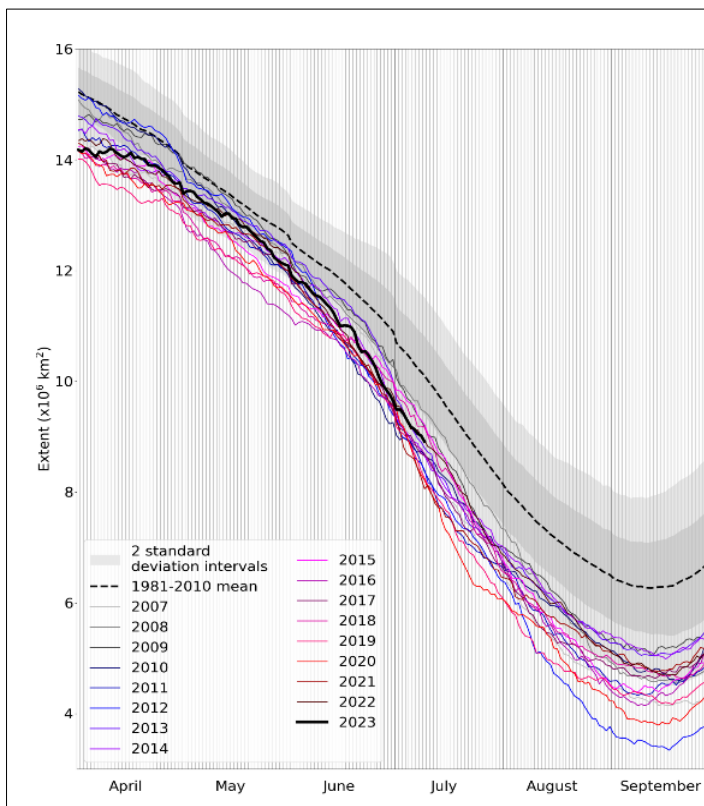


Figure 2. Arctic sea ice extent (Met Office, 2023).

Comparing the trends (Table 1) with July 2023 data (Figure 2) reveals worse results. In July 2023, SIE in the Arctic was recorded as 8.91×10^6 km² (Met Office, 2023), while the average extent for the reference period of 1981 to 2010 was 10.1×10^6 km². This significant difference of 1.19×10^6 km² (equivalent to an annual decline of 92×10^3 km²y⁻¹) surpasses the projected annual decline of 81×10^3 km²y⁻¹ for the RCP 8.5 scenario until 2100, as documented in Table 1 (Huang, 2017). These observations imply that the current decrease in SIE exceeds the predictions for even the worst climate change scenario, raising substantial concerns for the future state of the Arctic region and its ecological implications.

Table 2. Antarctic SIE Trends.

Period	Method	SIE Trend ($10^3 \text{ km}^2 \text{ y}^{-1}$)	Reference
1972 – 2002	MR	-15 ± 8	Cavalieri and Parkinson, 2003
1979-2005	GIOMAS	$+12.9 \pm 5.7$	Shu et al., 2015
	CMIP5	-3.36 ± 1.5	
1979-2013	NSIDC	+18.6	Turner et al., 2015
1978-2013	NSIDC	$+15.29 \pm 3.85$	Simmonds, 2015
1979-2018	Satellites	$+4.0 \pm 3.5$ (WS)	Parkinson, 2019
		$+2.6 \pm 1.8$ (IO)	
		$+2.6 \pm 1.3$ (WPO)	
		$+5.8 \pm 2.9$ (RS)	
		-3.7 ± 1.8 (BAS)	
		$+11.3 \pm 5.3$	
1979-2014	CMIP6	-70 ± 6	Shu et al., 2020
1979–2015	SB2	$+20.2 \pm 4.0$	Comiso et al., 2017
1979-2013	NSIDC	+4.8 (WS)	Turner et al., 2016
		+5.6 (IO)	
		+2.3 (WPO)	
		+11.9 (RS)	
		-5.1 (BAS)	
		+19.5	
1992-2008	SICCI	$+17.75 \pm 11.50$	He et al., 2016
1979-2012	NSIDC	+18	Turner et al., 2013a
1979-2005	CMIP5	+12.7	Turner et al., 2013b
1979-2005 September		-40	
1981-2000	NSIDC	$+14.7 \pm 8.6$ (RS)	Laine, 2008
		-13 ± 6.4 (BAS)	

When analyzing the comprehensive records from 1979 presented in Table 2, a general positive trend in yearly average Antarctic SIE is observed. However, notable exceptions to this trend are found in the Bellingshausen/Amundsen Seas and CMIP5 measurements. The Bellingshausen/Amundsen Seas region displays a significant 40-year negative trend, characterized by decreasing yearly average ice extents during the initial three decades, reaching a minimum in 2007, followed by an overall upward trend since then. This behavior represents a reversal in the opposite direction compared to the other four sectors and the Antarctic sea ice cover as a whole (Parkinson, 2019). Additionally, it is evident that the CMIP5 models exhibit a remarkable deficiency in reproducing the observed increase in Antarctic sea ice extent. Despite attempts to implement the effects of ozone in these models, they still fail to capture the actual trend, highlighting the need for further refinement and improvement in modeling approaches (Maiming et al., 2017). These findings underscore the complex and region-specific dynamics governing Antarctic sea ice trends and emphasize the importance of advancing modeling capabilities to better comprehend and predict sea ice variations in the region.

Despite numerous proposed mechanisms, the underlying cause of the increasing trend in Antarctic sea ice extent (SIE) remains ambiguous, with ongoing debates about its anthropogenic or natural origins (Naiming et al., 2017). Polvani et al. (2013) argue that attributing the observed SIE trends to anthropogenic forcing is challenging. In contrast, Mahlstein et al. (2013) propose that the positive SIE trend observed via satellite data may be the result of natural variation combined with external forcing. Turner et al. (2014) identify a dominant positive trend in the RS sector, where SIE shows a significant correlation with the depth of the Amundsen Sea Low (ASL), which has intensified since 1979.

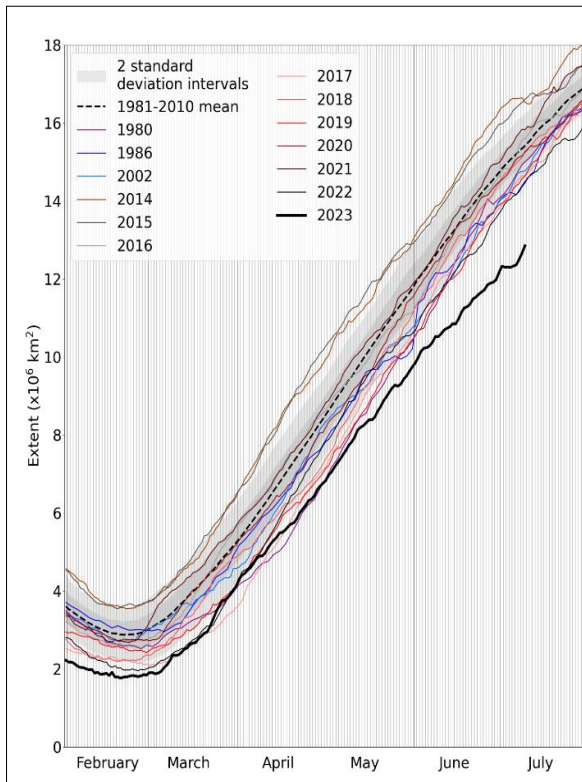


Figure 3. Antarctic sea ice extent (Met Office, 2023).

Analysis of July 2023 data in Antarctic (Figure 3) displays extreme levels of decline and creates opposition to positive trend bias. Although 1981 and 2010 average SIE was $15.41 \times 10^6 \text{ km}^2$, it decreased to $14.46 \times 10^6 \text{ km}^2$ in 2022, and further plummeted to $12.85 \times 10^6 \text{ km}^2$ in 2023. $2.56 \times 10^6 \text{ km}^2$ difference between 2023 and 1981-2010 period ($197 \times 10^3 \text{ km}^2\text{y}^{-1}$) is far from correlating with the previously observed positive trend values (Table 2). This discrepancy raises concerns as it deviates from the expected positive trend values and the specific reasons behind this deviation have not been clearly identified in the available information, warranting further investigation and research in this area (The Guardian, 2023). The urgency to investigate these

unprecedented changes in SIE is evident, as it holds significant implications for the Earth's polar regions and beyond.

Table 3. Arctic and Antarctic Ensemble SIE Trends.

Period	Method	SIE Trend ($10^3 \text{ km}^2\text{y}^{-1}$)	Reference
1979–2013	Satellite	-35 ± 2.9	Parkinson, 2014
1979-1996		-21.5 ± 10.6	
1996-2013		-50.5 ± 20	
1979–2013 September		-68.2 ± 10.5	
1979–2013 May		-6.1 ± 10.6	
1978-2013	NSIDC	-35.29 ± 5.75	Simmonds, 2015

Parkinson (2014) and Simmonds et al. (2015) also calculated total loss of SIE of both Arctic and Antarctic regions ensemble. The values can be seen in Table 3. The trend values of Parkinson (2014) between 1979-2013 are remarkable. The reduction values after 1996 are more than twice the values up to 1996.

4.2 SIV Trends

SIV is a crucial parameter influencing the Earth's energy and water budget, but its direct observations are severely limited. Nevertheless, it can be estimated by integrating data from sea ice cover and SIT measurements spanning the entire Arctic region (Bunzel et al., 2018). Unlike SIE, SIV exhibits a more direct connection with climate forcing, making it an essential climate indicator in climate research (Shu et al., 2015).

Table 4. Arctic SIV Trends.

Period	Method	SIV Trend (km^3/year)	Reference
1979-2010	PIOMAS	-280	Schweiger et al., 2011
1979-2011 September	CMIP5	-226	Song, 2016
	Satellites	-321	
1979-2012 March	PIOMAS	no trend (Fram Strait)	Zhang et al., 2017
1979-2015	PIOMAS	-214 ± 14	Shu et al. 2015
	CMIP5	-145 ± 5	
1979-2016	PIOMAS	-310	Labe, 2017
1979-2018 September	Satellites	-300 ± 20	Kumar et al., 2020
1984-2008	Submarines (1984-2000) ICESat (2003-2008)	-411	Liu et al., 2020
1992-2014	Submarines Satellites	no trend (Fram Strait)	Spren et al., 2020

2002-2010	Envisat	-177 (min)	Li et al., 2021
	PIOMAS	-360 (max)	
2003-2008 Autumn	ICESat	-1450 ± 530	Zygmuntowska et al., 2014
2003-2008 Spring		-880 ± 260	
2003-2013 Autumn	ICESat (2003-2008)	-210.8	Bi et al., 2018
2003-2013 Winter	CSt-2 (2011-2013)	-320.6	
2003-2014 Winter	ICESat-2, CS-2	-417	Kwok and Cunningham, 2015
2003-2014 Autumn		-776	
2003-2014 Winter	ICESat	-862	
2003-2014 Autumn		-1237	
2003-2015 Autumn	ICESat (2003-2008)	-390	Bi et al., 2018
2003-2015 Spring	CS-2 (2011-2015)	-121.6	
2003-2018 Winter	Submarines	-287	Kwok, 2018
2003-2018 Fall	ICESat CS-2	-513	
2004-2014 Winter	ICESat (2004-2008)	-402	Labe, 2017
2004-2014 Summer	CS-2 (2011-2014)	-760	
2010-2018	CS-2	no clear trend	Li et al., 2021
	PIOMAS		

Upon scrutinizing the trend list for SIV in Table 4, a consistent and pervasive negative trend in the Arctic region becomes evident. Intriguingly, no discernible trend values were identified in the Fram Strait, a critical linkage zone between Greenland and Svalbard, connecting the Atlantic Ocean to the polar seas. The absence of a discernible trend there merits further investigation and may offer critical insights into the intricate dynamics governing sea ice volume transport and distribution in this significant region. Notably, the autumn season displays the most pronounced negative trend values, mirroring the pattern observed in SIE.

Table 5. Antarctic SIV Trends.

Period	Method	SIV Trend (km ³ /year)	Reference
1979-2004	NCEP-NCAR	+20	Zhang, 2007
1980-2008	NEMO-LIM2	+35.5 ± 33.8	Massonet et al., 2013
		+15 ± 12.4 (RS)	
		+20.9 ± 36.2 (WS)	
		-4.5±5.4 (BAS)	
1990-2010	MITgcm	+30	Holland et al., 2014
2003-2008 Spring	ICESat	-266	Kurtz and Markus, 2012

2003-2008		-160	
Summer			

When analyzing the trend list for Antarctic SIV in Table 5, a general increasing pattern in SIV values, SIE values, is observed. However, it is important to note that the article by Kurtz and Markus (2012) reports a contrasting negative trend, particularly more pronounced during spring than in summer. Remarkably, positive values in the trend list correspond to modeling results, while negative values are derived from satellite data. This pattern mirrors the findings observed in the SIE trend list, wherein satellite-derived data exhibit negative trends, while model-based data present positive trends.

4.3 SIT Trends

Table 6. Arctic SIT Trends.

Period	Method	SIT Trend (cm/year)	Reference
1980-2007	ICESat	-6.1	Kwok and Untersteiner, 2011
2000–2013	Satellites, Submarines	-5.8 ± 0.7	Lindsay and Schweiger, 2014
2002-2017 Autumn	Envisat, CS	-1.5	Wang et al., 2020
2002-2017 Winter		-1.8	
2002-2017		-5.1 (Hudson Bay)	
2003-2011	PIOMAS	-6 ± 0.4	Lindsay and Schweiger, 2014
2003-2011 Spring	ICESat	-7.5	Laxon et al., 2013
2011-2017 May-October	CS-2	-3, -4.5	Gao et al., 2021

SIT data is necessary for assessing sea ice mass balance, the surface energy budget, seasonal and annual sea ice prediction, and changes in the polar climate system (Labe, 2017). Observations of SIT are very sparse, compared to other observations which have a continuous satellite record from 1979 to the present. SIT is not measured directly by satellite due to the remote location of polar regions, and the difficulty of satellites signals to penetrate through the sea. Rather, it is freeboard that measured, or the height of the sea ice above the ocean surface, from which SIT may be calculated, given the depth of snow on top of the sea ice and hydrostatic equilibrium. One satellite mission (ICESat) evaluating SIT does not provide continuous measurements; rather, they only offer readings over two periods of the annual cycle, close to the minimum SIT in fall and close to the maximum SIT in spring. While the other satellite mission (CS-2) provides weekly and monthly data, its SIT estimates are only available during the cold season due to melt pond formation in the summertime. Only observations from submarines offer direct measurements of SIT, but those measurements are limited by small areal extent and sporadic temporal coverage (Massonet et al., 2013; Labe and Magnusdottir, 2018). Reconstructions using numerous observational sources show a 65% decline in annual mean SIT in the central Arctic since the 1970s (Lindsay and Schweiger, 2015). Looking at the trend list in Table 6, there are only satellite or submarine measurements and there is a consistent decrease in the Arctic region, as in SIE and

SIV; however in the Antarctic region, it can be seen that the value obtained with the satellite is negative, and the model and MR calculations are not negative as in Table 7.

Table 7. Antarctic SIT Trends.

Period	Method	SIT Trend (cm/year)	Reference
1990-2010	MITgcm	+0.15	Holland et al., 2014
1992-2011	MR	no negative trend	Aulicino et al., 2013
2003-2008 Spring, Summer	ICESat	-3	Kurtz and Markus 2012

5. Conclusions

The primary objective of this paper is to establish a fundamental trend database for SIE, SIV and SIT data of polar regions. The underlying driving force behind these trends is attributed to global climate change. Notably, trend analyses predominantly commence from the year 1979, coinciding with the initiation of satellite-based sea ice measurements. This time frame is deemed optimal for trend analysis, encompassing a 30-year period, which is considered more robust for assessing long-term variations. The research commonly employs satellite measurements, microwave radiometer remote sensing techniques, and numerical model calculations. Notably, the number of SIE and SIV data is greater compared to SIT. This discrepancy arises due to the challenges associated with accurately calculating SIT. SIE, SIV and SIT trend values are coherently negative in the Arctic region. For the seasonal and monthly trend, autumn, especially September, has the higher trend values than other seasons in negative direction. It is remarkable that in SIE; the negative trend values after 1996 are more than twice the values up to 1996. For future projections, it is predicted that the SIE value will decrease by more than $3 \times 10^6 \text{ km}^2$ by 2100 in the Arctic under the RCP 4.5 scenario. If RCP 8.5 scenario happens, the Arctic will be almost free of ice in September before 2060, at approximately 2053. The similar thing is valid for SIV data. Under the RCP4.5 scenario after 2060, SIV in the Arctic becomes persistent around $1.2 \times 10^3 \text{ km}^3$. If RCP 8.5 scenario happens, SIV value will be below $1 \times 10^3 \text{ km}^3$ before 2060, just as in the SIE. In the Antarctic, as different from Arctic, SIE and SIV trends are generally positive. Some studies found the negative trend values, contrarily. The comparison of the trends and July 2023 SIE data in both the Arctic and Antarctic presents intriguing and concerning findings. In the Arctic, July 2023 SIE significantly deviates from the reference period average, surpassing even the worst climate change scenario projections. This unprecedented decrease raises substantial concerns for the future state of the Arctic region. Similarly, in Antarctic, the data for July 2023 reveals extreme levels of SIE decline, diverging from previously observed positive trend values. The reasons behind this deviation remain unclear, demanding urgent investigation and further research. Unprecedented changes in sea ice hold significant implications for the Earth's polar regions and beyond, necessitating heightened attention and scientific inquiry into this critical area of concern.

References

- Aderoft, A.J., Hill, C.N. and Marshall, J. Representation of topography by shaved cells in a height coordinate ocean model. *Mon Wea Rev*, 1998; 125: 2293-2315.
- Aulicino, G., Fusco, G., Kern, S., and Budillon, G. 1992-2011 sea ice thickness estimation in the ross and Weddell seas from SSM/I brightness temperatures. Paper presented at the European Space Agency, (Special Publication) ESA SP, 2013; 712.
- Bi, H., Zhang, J., Wang, Y., Zhang, Z., Zhang, Y., Fu, M., . . . Xu, X. Arctic sea ice volume changes in terms of age as revealed from satellite observations. *IEEE Journal of Selected Topics in Applied Earth Observations and Remote Sensing*, 2018; 11(7): 2223-2237. doi:10.1109/JSTARS.2018.2823735
- Bo e, J., Hall, A. & Qu, X. September sea-ice cover in the Arctic Ocean projected to vanish by 2100. *Nature Geoscience*, 2019; 2:341–343. <https://doi.org/10.1038/ngeo467>
- Bunzel, F., Notz, D. and Pedersen, L. T. Retrievals of Arctic sea-ice volume and its trend significantly affected by interannual snow variability. *Geophysical Research Letters*, 2018; 45: 11,751– 11,759. <https://doi.org/10.1029/2018GL078867>
- Bushuk, M., Msadek, R., Winton, M., Vecchi, G. A., Gudgel, R., Rosati, A., and Yang, X. Summer enhancement of Arctic sea ice volume anomalies in the September-ice zone. *Journal of Climate*, 2017; 30(7): 2341-2362.
- Candanosa, R.M. NASA Finds 2021 Arctic Summer Sea Ice 12th Lowest on Record. NASA's Climate Change News. Retrieved from <https://climate.nasa.gov/news/3114/nasa-finds-2021-arctic-summer-sea-ice-12th-lowest-on-record/> Accessed at: 2021, September 22.
- Cavalieri, D. J. and Parkinson, C. L. Arctic sea ice variability and trends, 1979-2010. *Cryosphere*, 2012; 6(4), 881-889. doi:10.5194/tc-6-881-2012
- Cavalieri, D. J., Parkinson, C. L., & Vinnikov, K. Y. 30-year satellite record reveals contrasting arctic and Antarctic decadal sea ice variability. *Geophysical Research Letters*, 2003; 30(18): CRY 4-1-4-4. doi:10.1029/2003GL018031
- CryoSat. 2021. Retrieved from <https://earth.esa.int/eogateway/missions/cryosat>
- Deser, C. and Teng, H. Recent trends in arctic sea ice and the evolving role of atmospheric circulation forcing, 1979-2007. *Arctic sea ice decline: Observations, projections, mechanisms, and implications*, 2013; pp. 7-26. doi:10.1029/180GM03
- Dokumcu, K. Investigation Of The Effects Of The Climate Change On The Oceanographic Conditions Of The East Marmara Sea (Master's thesis). Institute of Marine Sciences and Management, İstanbul, 2021.
- Emery W. and Camps A. *Introduction to Satellite Remote Sensing*, 2017; 131-290, <https://doi.org/10.1016/B978-0-12-809254-5.00004-X>

Francis, J. A., Chan W., Leathers D. J., Miller J. R., and Veron D. E. Winter Northern Hemisphere weather patterns remember summer Arctic sea-ice extent. *Geophys. Res. Lett.*, 2009; 36: L07503, doi:10.1029/2009GL037274.

Gao, X., Pang, X., and Ji, Q. Spatiotemporal variation of sea ice freeboard in the Antarctic weddell sea based on CryoSat-2 altimeter data. *Wuhan Daxue Xuebao (Xinxi Kexue Ban)/Geomatics and Information Science of Wuhan University*, 2021; 46(1): 125-132. doi:10.13203/j.whugis20180504

Gerald M.A., Boer G.J., Covey C., Latif M. and Stouffer R.J. Intercomparison makes for a better climate model. *EOS Science News*, 1997; 78(41): 445-451. <https://doi.org/10.1029/97EO00276>

Holland, P. R., Bruneau, N., Enright, C., Losch, M., Kurtz, N. T., and Kwok, R. Modeled trends in antarctic sea ice thickness. *Journal of Climate*, 2014; 27(10): 3784-3801. doi:10.1175/JCLI-D-13-00301.1

Houghton J., Meira Filho L.G., Callander B.A., Harris N., Kattenberg A. and Maskell K. (Eds) *Climate change 1995. The science of climate change*. Intergovernmental Panel on Climate Change. Cambridge University Press, 1996; pp 572.

How we measure sea ice, 2021. Retrieved from <https://www.metoffice.gov.uk/research/climate/cryosphere-oceans/sea-ice/measure>

Huang, F., Zhou, X., and Wang, H. Arctic sea ice in CMIP5 climate model projections and their seasonal variability. *Acta Oceanologica Sinica*, 2017; 36(8). doi:10.1007/s13131-017-1029-8 ICESat. Retrieved from <https://icesat.gsfc.nasa.gov/>

Ilicak, M., Drange, H., Wang, Q., Gerdes, R., Aksenov, Y., Bailey, ... Yeager, S.G. An assessment of the Arctic Ocean in a suite of interannual CORE-II simulations. Part III: Hydrography and fluxes. *Ocean Modelling*, 2016; 100: 141-161. <https://doi.org/10.1016/j.ocemod.2016.02.004>

IPCC, 2019. Technical Summary [H.-O. Pörtner, D.C. Roberts, V. Masson-Delmotte, P. Zhai, E. Poloczanska, K. Mintenbeck, M. Tignor, A. Alegría, M. Nicolai, A. Okem, J. Petzold, B. Rama, N.M. Weyer (eds.)]. In: *IPCC Special Report on the Ocean and Cryosphere in a Changing Climate* [H.- O. Pörtner, D.C. Roberts, V. Masson-Delmotte, P. Zhai, M. Tignor, E. Poloczanska, K. Mintenbeck, A. Alegría, M. Nicolai, A. Okem, J. Petzold, B. Rama, N.M. Weyer (eds.)]. Cambridge University Press, Cambridge, UK and New York, NY, USA, pp. 39–69. <https://doi.org/10.1017/9781009157964.002>

Itoh, M., Inoue J., Shimada K., Zimmermann S., Kikuchi T., Hutchings J., McLaughlin F.A., and Carmack E. Acceleration of sea ice melting due to transmitted heat through pounded ice area in the Arctic Ocean: Results of in situ observation from icebreakers in 2006 and 2007. *Ann. Glaciol.*, 2011; 52: 249–260. doi:10.3189/172756411795931471

Kumar, A., Yadav, J., Mohan, R. Global warming leading to alarming recession of the Arctic sea-ice cover: Insights from remote sensing observations and model reanalysis. *Heliyon*, 2020; 6(7). doi: 10.1016/j.heliyon.2020.e04355

Kurtz, N. T., and Markus, T. (2012). Satellite observations of Antarctic sea ice thickness and volume. *Journal of Geophysical Research: Oceans*, 117(8) doi:10.1029/2012JC008141

Kwok, R. Arctic sea ice thickness, volume, and multiyear ice coverage: Losses and coupled variability (1958-2018). *Environmental Research Letters*, 2018; 13(10). doi:10.1088/1748-9326/aae3ec

Kwok, R. and Untersteiner N. The Thinning of Arctic Sea Ice. *Physics Today*, 2011; 64 (4): 36–41.

Labe, Z., National Center for Atmospheric Research Staff (Eds). *The Climate Data Guide: Sea Ice Thickness Data Sets: Overview & Comparison Table*. 2017. Retrieved from <https://climatedataguide.ucar.edu/climate-data/sea-ice-thickness-data-sets-overview-comparison-table>.

Labe, Z.M., Magnusdottir, G., and Stern, H.S. Variability of Arctic Sea Ice Thickness Using PIOMAS and the CESM Large Ensemble. *Journal of Climate*, 2018; 31, 3233-3247.

Labe, Z. Arctic Sea Ice Volume/Thickness, 2021. Retrieved from <https://sites.uci.edu/zlabe/arctic-sea-ice-volumethickness/>

Laxon, S. W. and Coauthors. Cryosat-2 estimates of Arctic sea ice thickness and volume. *Geophys. Res. Lett.*, 2013; 40: 732–737. doi:10.1002/grl.50193.

Li, M., Ke, C., Shen, X., Cheng, B. and Li, H. Investigation of the Arctic Sea ice volume from 2002 to 2018 using multi-source data. *International Journal of Climatology*, 2021; 41: 2509-2527. doi:10.1002/joc.6972.

Li, M., Ke, C., Shen, X., Cheng, B., Li and H. Investigation of the Arctic Sea ice volume from 2002 to 2018 using multisource data. *International Journal of Climatology*, 2021; 41: 2509-2527. doi:10.1002/joc.6972.

Lindsay, R. and Zhang J. Arctic Ocean ice thickness: Modes of variability and the best locations from which to monitor them. *J. Phys. Oceanogr.*, 2006; 36: 496–506, <https://doi.org/10.1175/JPO2861.1>.

Lindsay, R. and Schweiger, A. Arctic Sea Ice Thickness Loss Determined using Subsurface, Aircraft, and Satellite Observations. *The Cryosphere Discussions*, 2014; 8. 10.5194/tcd-8-4545-2014.

Liu, Y., Key, J. R., Wang, X., & Tschudi, M. Multidecadal arctic sea ice thickness and volume derived from ice age. *Cryosphere*, 2020; 14(4), 1325-1345. doi:10.5194/tc-14-1325-2020

M. Zyguntowska M., Rampal P., Ivanova N. and Smedsrud L. H. Uncertainties in Arctic sea ice thickness and volume: new estimates and implications for trends. *Cryosphere*, 2014; 8: 705-720. doi:10.5194/tc-8-705-2014

Manabe S., Stouffer R.J., Spelman M.J. and Bryan K. Transient responses of a coupled atmosphere–ocean model to gradual changes of atmospheric CO₂. I. Annual mean response. *J Clim*, 1991; 4: 785–818.

Massonnet F., Mathiot P., Fichet T., Goosse H., Beatty C., Vancoppenolle M. and Lavergne T. A model reconstruction of the Antarctic sea ice thickness and volume changes over 1980–2008 using data assimilation. *Ocean Modelling*, 2013; 64: 67-75. <https://doi.org/10.1016/j.ocemod.2013.01.003>.

Met Office. Briefing on Arctic and Antarctic Sea Ice - July 2023. Accessed at: 2023, July 29. <https://www.metoffice.gov.uk/research/approach/monitoring/sea-ice/2023/briefing-on-arctic-and-antarctic-sea-ice---july-2023>.

NASA, GISS. Global temperature, climate change, 2020. Retrieved from <https://climate.nasa.gov/vital-signs/global-temperature/>

National Geographic. Arctic Ocean map, 2021. Retrieved from Arctic-map.jpg (4179×4200) (nationalgeographic.org)

NEMO, 2021. Retrieved from <https://www.nemo-ocean.eu/doc/node4.html>

Parkinson, C. L. Global Sea Ice Coverage from Satellite Data: Annual Cycle and 35-Yr Trends, *Journal of Climate*, 2014; 27(24): 9377-9382. <https://journals.ametsoc.org/view/journals/clim/27/24/jcli-d-14-00605.1.xml>

Quick facts, 2021. Retrieved from <https://nsidc.org/cryosphere/quickfacts/seaice.html#:~:text=Arctic%20sea%20ice%20keeps%20the%20polar%20regions%20cool,the%20ocean%20absorbs%2090%20percent%20of%20the%20sunlight>.

Rantanen M., Karpechko A., Lipponen A., Nordling K., Hyvärinen O., Ruosteenoja K., Vihma T. and Laaksonen A. The Arctic has warmed four times faster than the globe since 1980, 2018. <https://doi.org/10.21203/rs.3.rs-654081/v1>

Schweiger, A., Lindsay R., Zhang J., Steele M., Stern H., and Kwok. R. Uncertainty in modeled Arctic sea ice volume. *J. Geophys. Res.*, 2011; 116: C00D06, <https://doi.org/10.1029/2011JC007084>.

NASA, 2016. Antarctic Sea Ice. Retrieved from <https://www.earthobservatory.nasa.gov/features/SeaIce/page4.php>

Shu, Q., Song, Z. and Qiao, F. Assessment of sea ice simulations in the CMIP5 models. *Cryosphere*, 2015; 9(1): 399-409. doi:10.5194/tc-9-399-2015

Shu, Q., Wang, Q., Song, Z., Qiao, F., Zhao, J., Chu, M., and Li, X. Assessment of sea ice extent in CMIP6 with comparison to observations and CMIP5. *Geophysical Research Letters*, 2020; 47(9). doi:10.1029/2020GL087965

- SIE, 2020. Retrieved from <http://polarportal.dk/en/sea-ice-and-icebergs/sea-ice-extent0/>
- Simmonds, I. Comparing and contrasting the behavior of arctic and Antarctic sea ice over the 35-year period 1979-2013. *Annals of Glaciology*, 2015; 56(69): 18-28. doi:10.3189/2015AoG69A909
- Song M.R. Change of Arctic sea-ice volume and its relationship with sea-ice extent in CMIP5 simulations, *Atmospheric and Oceanic Science Letters*, 2016; 9:1: 22-30, doi:10.1080/16742834.2015.1126153
- Spreen, G., de Steur, L., Divine, D., Gerland, S., Hansen, E., and Kwok, R. Arctic sea ice volume export through Fram Strait from 1992 to 2014. *Journal of Geophysical Research: Oceans*, 2020; 125(6). doi:10.1029/2019JC016039
- The Guardian, 2023. Something weird is going on: search for answers as Antarctic sea ice stays at historic lows. Retrieved from https://www.theguardian.com/world/2023/jul/29/something-weird-is-going-on-search-for-answers-as-antarctic-sea-ice-stays-at-historic-lows?CMP=Share_AndroidApp_Other Accessed at: 2023, July 29.
- Turner, J., Hosking, J. S., Phillips, T., and Marshall, G. J. Temporal and spatial evolution of the antarctic sea ice prior to the september 2012 record maximum extent. *Geophysical Research Letters*, 2013a; 40(22): 5894-5898. doi:10.1002/2013GL058371
- Turner, J., Bracegirdle, T. J., Phillips, T., Marshall, G. J., and Scott Hosking, J. An initial assessment of Antarctic sea ice extent in the CMIP5 models. *Journal of Climate*, 2013b; 26(5): 1473-1484. doi:10.1175/JCLI-D-12-00068.1
- Turner, J., Hosking, J. S., Bracegirdle, T. J., Marshall, G. J., and Phillips, T. Recent changes in Antarctic sea ice. *Philosophical Transactions of the Royal Society A: Mathematical, Physical and Engineering Sciences*, 2015; 373(2045). doi:10.1098/rsta.2014.0163
- Turner, J., Hosking, J.S., Marshall, G. J., Phillips, T., and Bracegirdle, T. J. Antarctic sea ice increase consistent with intrinsic variability of the Amundsen sea low. *Climate Dynamics*, 2016; 46(7-8), 2391-2402. doi:10.1007/s00382-015-2708-9
- Wang, Z., Li, Z., Zeng, J., Liang, S., Zhang, P., Tang, F., . . . Ma, X. Spatial and temporal variations of arctic sea ice from 2002 to 2017. *Earth and Space Science*, 2020; 7(9). doi:10.1029/2020EA001278
- Watt, L.M., 2023. Antarctica. *Encyclopedia Britannica*, 30 Mar. 2023. <https://www.britannica.com/place/Antarctica>. Accessed 25 June 2023.
- World Meteorological Organization. WMO Guidelines on the Calculation of Climate Normals, 2017; 4: 9. Chairperson, Publications Board, Geneva 2, Switzerland.
- Zhang J. Increasing Antarctic sea ice under warming atmospheric and oceanic conditions. *Journal of Climate*, 2007; 20(11): 2515-2529. <https://doi.org/10.1175/JCLI4136.1>

Zhang, Z., Bi, H., Sun, K., Huang, H., Liu, Y. and Yan, L. Arctic sea ice volume export through the Fram strait from combined satellite and model data: 1979–2012. *Acta Oceanologica Sinica*, 2017; 36(1): 44-55. doi:10.1007/s13131-017-0992-4

SERBEST SU YÜZEYİNE YAKIN DERİNLİKTEKİ DENİZALTININ MANEVRA SORUNLARININ İNCELENMESİ

Kağan YÜCE¹, Devrim Bülent DANIŞMAN²

¹*İstanbul Teknik Üniversitesi | yuce20@itu.edu.tr | ORCID 0000-0003-1703-9481*

²*İstanbul Teknik Üniversitesi | bulent.danisman@itu.edu.tr | ORCID 0000-0001-6320-5351*

ÖZET

Gizlilik, denizaltıların en etkili özelliklerinden birisi olup; periskop derinliğinde bu özelliğini kaybetmeden görevlerini icra etmesi gerekmektedir. Ancak denizaltıların sahip olduğu form nedeniyle serbest su yüzeyine yakın derinlikte oluşan basınç dağılımı denizaltıyı başlı bir şekilde dalma yönünde harekete zorlamaktadır. Bu durumu nümerik olarak incelemek amacıyla DARPA SUBOFF AFF-8 geometrisi ile OpenFOAM açık kaynak kodlu yazılımın çok fazlı akış çözücüsü kullanılmıştır. Ağ yapısı olarak da oluşturulan model, akış hacminden bağımsız dinamik hareket edebilen ‘overset’ hacmine yerleştirilmiştir. Oluşturulan ağın Hesaplamalı Akışkanlar Dinamiği (HAD) analiz sonuçlara etkisinin olup olmadığını incelemek amacıyla da ‘Ağ Yakınsaklık İndeksi’ hesaplamalarıyla doğrulama çalışması yapılmıştır. Analiz sonuçlarında çapının 1,1 katı derinliğe yerleştirilen model, 0 (sıfır) derece açı değerinde bulunan dümenleri ve baştan 2,009 metre olarak belirlenen ağırlık merkezi ile başlı bir şekilde dalma hareketini yapmıştır. Bu manevra sorununu giderebilmek için ufki dümenlere aşağı yönde açı vermek ve baş taraftan balast atmak denizaltıcıların uyguladığı yöntemler olduğu öğrenilmiştir. Gelecek çalışmalarda bu çözümlerin etkisi parametrik olarak incelenecektir.

Anahtar kelimeler: Denizaltı, manevra, serbest su yüzeyi, OpenFOAM, DARPA.

Makale geçmişi: Gönderim 19 Mayıs 2023; Kabul 24 Mayıs 2023

1. Giriş

Denizaltılar ve sualtı araçları, sahip oldukları sınırlı hacim nedeniyle farklı yollarla üretilen enerjinin en verimli şekilde kullanılması gereken platformlardır. Genellikle askeri amaçla kullanılan bu platformlar hakkındaki bilgiler gizlilik nedeniyle ulaşılması güç olsa da günümüze kadar birçok jenerik denizaltı formu oluşturulmuştur. Araştırmacılar bu jenerik denizaltı geometrilerini kullanarak deneysel ve nümerik çalışmalar yapmışlardır. Son zamanlarda, denizaltıların sahip olduğu form nedeniyle ortaya çıkan manevra karakteristikleri ve sorunları araştırmacıların ilgisini çekmektedir. Bu sorunlardan bir tanesi de batarya imlası ve keşif faaliyetlerini yürütmesi için periskop derinliğinde ilerlemesi gereken denizaltıların serbest su yüzeyine yakın olması nedeniyle ortaya çıkan manevra sorunudur.

Sualtı araçlarının manevra karakteristiklerini incelemek için sayısal ve deneysel çalışmalar yürütülse de açık kaynak kodlu ve ticari yazılımlardaki gelişmeler sayesinde sayısal çalışmalar daha etkin biçimde kullanılmaktadır. Takahashi [1] sualtı araçlarının hidrodinamik performansını simüle etmekte kullanılmak üzere çalışmanın ana esaslarını belirleyen kılavuz niteliğinde bir

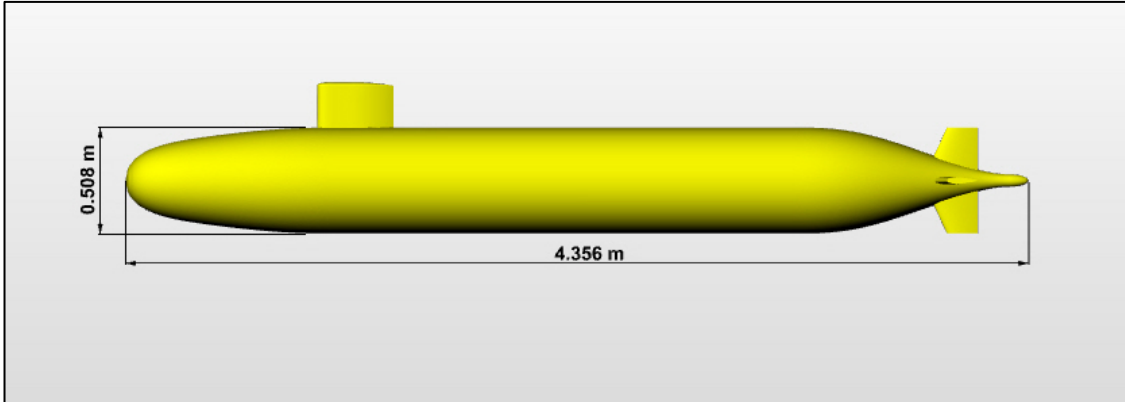
prosedür hazırlamıştır. Kim ve diğerleri [2] 6 serbestlik derecesi ile hareket eden sualtı araçlarının manevra karakteristiklerini hesaplamalı akışkanlar dinamiği (HAD) ile belirlemek üzere yapılan çalışmada katsayıları deneysel verilerle azami %7,26 sapma oranı ile hesaplamışlardır. The Defence Advanced Research Projects Agency (DARPA) tarafından geliştirilen 8 farklı denizaltı modeli de hidrodinamik alanında çalışma yürüten araştırmacılar tarafından kullanılmaktadır. Denizaltıların hidrodinamik karakteristiğini belirlemek için kullanılan HAD'ın potansiyeli, DARPA modelini kullanarak farklı hız ve dönme açılarında incelenmiştir [3]. Kale [4] AFF-1 ve AFF-8 modellerini kullanarak yaptığı çalışmada ANSYS FLUENT ve Open Field Operation and Manipulation (OpenFOAM) programları ile nümerik sonuçları deneysel verilerle kıyaslamıştır. Jenerik denizaltı geometrilerinden olan Joubert BB2 modeli de Carrica ve diğerleri [5] tarafından farklı hızlarda dikey zig-zag manevrasının incelenmesinde kullanılmıştır.

Denizaltı manevra karakteristiğini belirlemenin yanısıra kontrol yüzeylerinin optimizasyonu ve denizaltı formunun iyileştirilmesi konuları da araştırmacıların ilgisini çekmektedir. Hussain ve diğerleri [6] AFF-8 modelini kullanarak iki farklı kış dümen konfigürasyonunda HAD analizleri yapmışlardır. Çalışmaya göre haç biçimindeki dümen yapısı denizaltıyı daha stabil hale getirir iken çarpaz biçimindeki dümen yapısı denizaltıya daha yüksek manevra kabiliyeti sağlamaktadır. AFF-8 modelinin kış amudi dümenini üç farklı dönme açısında iki farklı sayısal metotla inceleyen Li ve diğerleri [7] ise 'Unsteady Reynolds-Averaged Navier Stokes (URANS)' metodunun 'Delayed Detached Eddy Simulation (DDES)' akış hatlarını belirlemede daha üstün olduğunu tespit etmiştir. Denizaltının kış formu optimizasyonu üzerine yapılan Özden ve diğerlerinin [8] yaptığı çalışmada INSEAN E1619 yedi kanatlı pervaneye sahip AFF-8 modeli farklı kış form açıları parametrik olarak incelenmiştir. Sezen ve diğerleri [9] de AFF-1 ve AFF-8 modellerini kullanarak farklı hızlarda direnç analizleri yaparak kapsamlı bir çalışma gerçekleştirmiştir.

Bu çalışmada, DARPA SUBOFF AFF-8 jenerik denizaltı modeli periskop derinliğinde iken ortaya çıkan manevra sorunları OpenFOAM açık kaynak HAD yazılımı ile incelenmiştir. Serbest su yüzeyine yakın seviyelerdeki denizaltılar hakkında Efremov ve Milanov [10], deneysel çalışmalar yürütmüş, AFF-8 modelinin amudi dümenlerinin verimliliği incelemişlerdir. Quintana ve Paredes [11], farklı derinlik ve froude sayılarında serbest su yüzeyinin direnç etkisi ile hız sensörlerinin yerleştirilebilecek bölgeleri araştırmışlardır. Amiri ve diğerleri [12], periskop derinliğindeki denizaltılara gelen baş ve kış dalgaların hidrodinamik etkilerini incelemişlerdir.

2. HAD Analizlerinde Kullanılan Geometri

Bu çalışma kapsamında yapılan HAD analizlerinde DARPA'nın SUBOFF programı ile geliştirilen denizaltı modellerinden AFF-8 modeli kullanılmıştır. Model, Groves ve diğerleri [13] tarafından hazırlanan dokümana göre Rhinoceros programı ile oluşturulmuştur. Model, fonksiyonel bir ifadeyle elde edilebilecek aksel simetrik bir gövdeye sahiptir. Yelken, kış ufki ve amudi dümenleri de modelin takıntılarını oluşturmaktadır. Üç boyutlu modelin yan görünüşü ve boyutsal özellikleri Şekil-1'de verilmiştir.



Şekil 1. AFF-8 Model Geometrisi.

1/24 ölçeğinde olan model denizaltının hacmi 0.708 m^3 olup; Roddy [14]'nin 1990 yılında yaptığı deneysel çalışmalarda olduğu gibi yapılan HAD analizlerinde boyuna ağırlık merkezi baştan 2,009 m olarak belirlenmiştir.

3. HAD Analizi Detayları

3.1 Hesaplama Yöntemi

Sayısal analizlerde OpenFOAM yazılımı ile ‘Sonlu Hacimler Yöntemi’ kullanan ‘interFoam’ çözücüsünün ‘overset’ ağ metodunun kullanıldığı ‘overInterDyMFOam’ çözücüsü kullanılmıştır. ‘overInterDyMFOam’, ‘Reynolds Averaged Navier Stokes (RANS)’ denklemleri ile izotermal ve birbirine karışmayan sıkıştırılmaz iki akışkan için nümerik olarak çözümü gerçekleştirmektedir.

Süreklilik denklemi Denklem (1)’de gösterilmektedir.

$$\frac{\partial u_j}{\partial x_j} = 0 \quad (1)$$

Momentum denklemi Denklem (2) olarak sunulmuştur.

$$\frac{\partial(\rho u_i)}{\partial t} + \frac{\partial}{\partial x_j}(\rho u_j u_i) = -\frac{\partial p}{\partial x_i} + \frac{\partial}{\partial x_j}(\tau_{ij} + \tau_{t_{ij}}) + \rho g_i + f_{\sigma i} \quad (2)$$

u	:	Hız
g_i	:	Yerçekimi ivmesi
p	:	Basınç
τ_{ij} ve $\tau_{t_{ij}}$:	Viskozite ve türbülans gerilimi
$f_{\sigma i}$:	Yüzey gerilimi

Momentum denkleminde yoğunluğu ifade eden ρ Denklem (3)’de görülmektedir.

$$\rho = \alpha \rho_1 + (1 - \alpha) \rho_2 \quad (3)$$

Denklemdaki ' α ' ifadesi birinci akışkan için 1, diğer akışkan için 0 olup; ara fazda bulunan akışkan için bu değer 0 ile 1 arasındadır.

Yüzey gerilimini ifade eden $f_{\sigma i}$ ve eğriliğin yaklaşık hesaplama denklemi Denklem (4) ve (5) olarak gösterilmiştir.

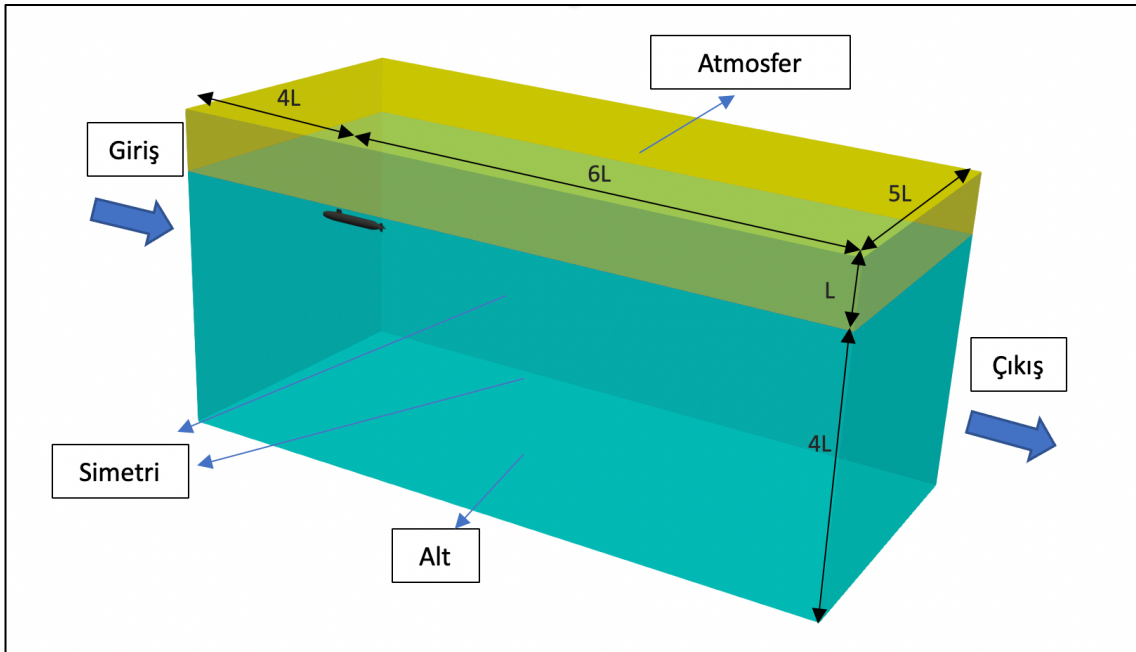
$$f_{\sigma i} = \sigma \kappa \frac{\partial \alpha}{\partial x_i} \quad (4)$$

σ : Yüzey gerilim sabiti
 κ : Eğrilik

$$\kappa = -\frac{\partial n_i}{\partial x_i} = -\frac{\partial}{\partial x_i} \left(\frac{\partial \alpha / \partial x_i}{|\partial \alpha / \partial x_i|} \right) \quad (5)$$

3.2 Sınır Koşulları ve Ağ Yapısı

'L' model boyu olmak üzere, dikdörtgen prizmadan oluşan akış hacmi 10L uzunluğunda, 5L genişliğinde ve su hattının altında kalan derinlik 4L olmak üzere toplam 5L yüksekliğindedir. Başlangıç konumu $H/D=1.1$ derinlikte olan model, 2L uzunlukta, L genişliğinde ve L yüksekliğinde 'overset' hacminin içerisine yerleştirilmiştir. Akış hacminin boyutların ve sınırların isimleri Şekil-2'de gösterilmektedir.



Şekil 2. Akış hacmi boyutları ve sınır isimlendirmesi.

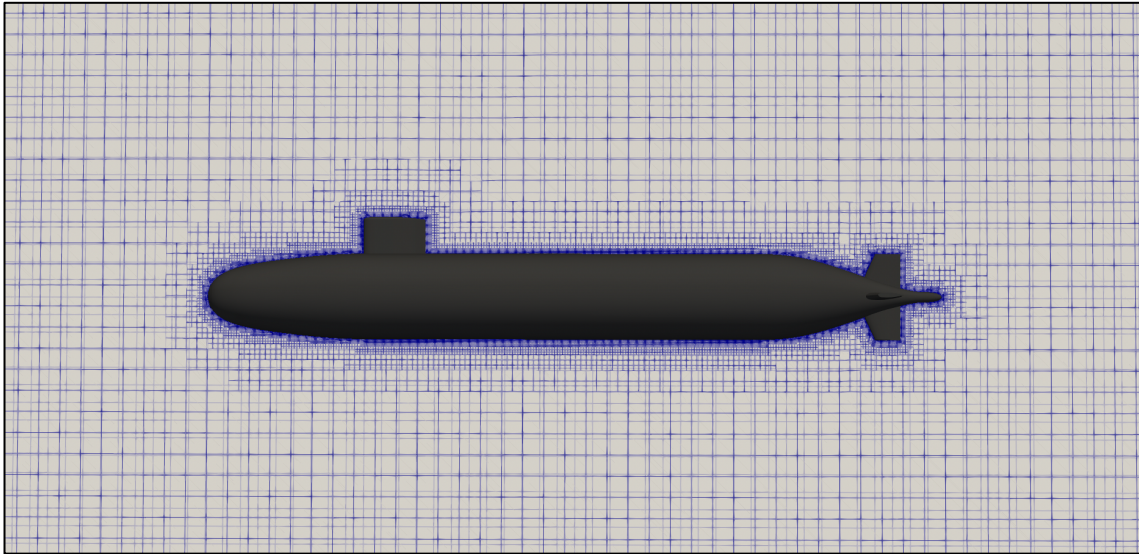
Hesaplamalarda kullanılan sınır koşulları Tablo 1’de özetlenmiştir.

Tablo 1. Sınır koşulları.

Sınır İsmi	U (Hız)	p_rgh
Giriş	fixedValue	fixedFluxPressure
Çıkış	outletPhaseMeanVelocity	zeroGradient
Atmosfer	pressureInletOutletVelocity	totalPressure
Alt	symmetryPlane	symmetryPlane
Simetri	symmetryPlane	symmetryPlane
AFF-8	movingWallVelocity	fixedFlucPressure

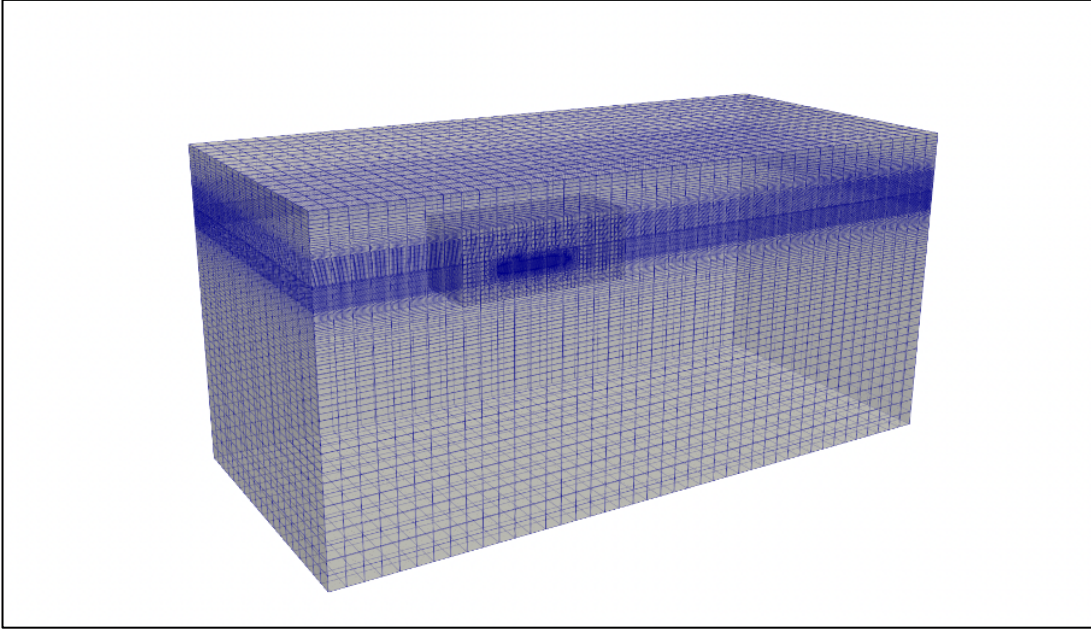
Çalışmada kullanılan akış hacmi içerisinde ‘overset’ olarak isimlendirilen ve geometriyi içine alan bir hacim kullanılmıştır. Bu hacim, akış hacminden bağımsız dinamik bir ağ oluşturmak için kullanılmakta olup; sınır koşulları ‘overset’ olarak belirlenmiştir. Bu yöntemde deforme olan ağ türünün dezavantajları olmadan çok fazlı akıştaki kompleks geometrilerin hareketleri interpolasyon ile çözülebilmektedir. Bu yöntem kullanılabilmesi için, OpenFOAM dosya düzeninde bulunan ‘constant’ klasöründe yer alan ‘dynamicMeshDict’ dizininde ‘dynamicOversetFvMesh’ ağ tipi seçilmiştir.

Rhinoceros programı ile oluşturulan AFF-8 yüzeyi ‘Standard Triangle Language (STL)’ formatında OpenFOAM dosya dizinine eklenmiş olup; ‘snappyHexMesh’ ağ üreticisi ile ağ oluşturulmuştur. ‘snappyHexMesh’ ile oluşturulan ağ yapısı Şekil-3’de görülmektedir.



Şekil 3. ‘snappyHexMesh’ ile oluşturulan ağ yapısı.

Serbest su yüzeyi bölgesindeki akışı daha iyi çözümlmek maksadıyla su hattı bölgesinde ağ yoğunluğu artırılmış olup; ‘blockMesh’ komutu ile oluşturulan arka plan ağ yapısı Şekil-4’de gösterilmektedir.



Şekil 4. 'blockMesh' ile oluşturulan arka plan ağ yapısı.

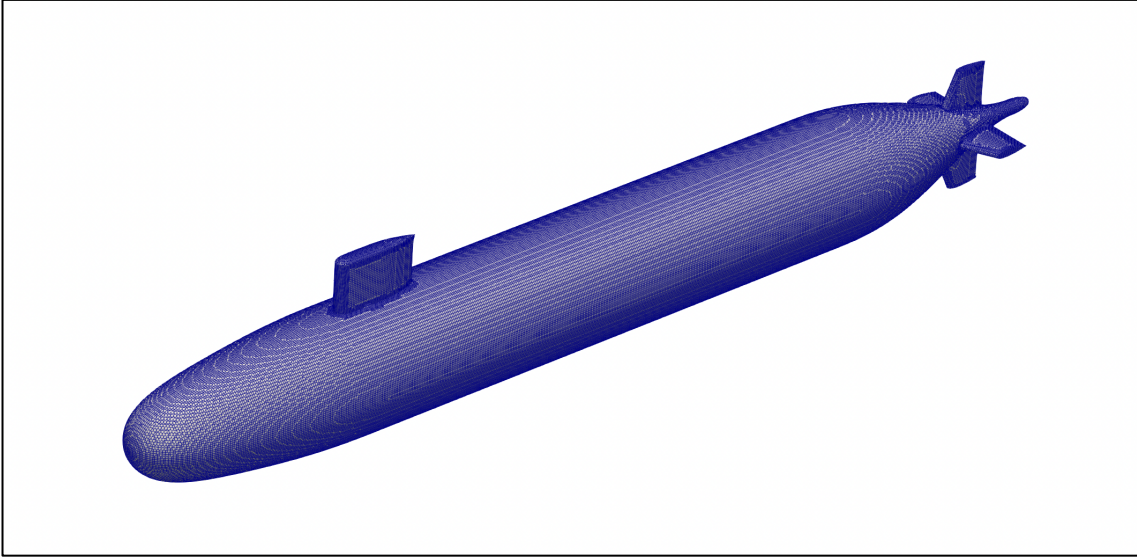
4. Doğrulama Çalışması

HAD analiz sonuçlarının kullanılan ağdan bağımsız olup olmadığını belirlemek amacıyla Çelik ve diğerleri [15] tarafından oluşturulan 'Ağ Yakınsaklık İndeksi (Grid Convergence Index – GCI)' hesaplamalarıyla doğrulama çalışması yapılmıştır. Hesaplama, toplam hücre sayısı artış oranı en az 1,3 olacak şekilde üç farklı çözünürlükteki ağ kullanılmıştır. Yapılan 'Ağ Yakınsaklık İndeksi' hesaplaması sonuçları Tablo-2'de olduğu gibidir.

Tablo 2. Doğrulama çalışması sonuçları.

Ağ Adı	Hücre Sayısı	Ortalama y^+	Sürüklenme Değeri (N)	Ağ Yakınsaklık İndeksi (%)
A	4024391	34	281	1,45
B	2006418	42	278	2,82
C	1183792	51	274	-

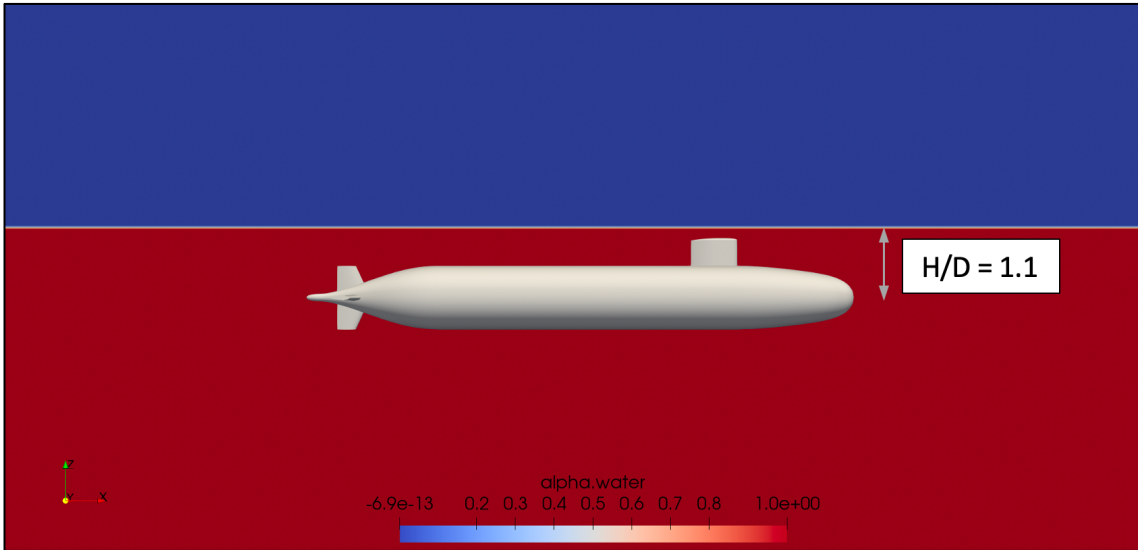
Hesaplama sonuçlarına göre, sık ağ yapısının (A) toplam sürüklenme değeri hesabında ağdan bağımsızlık indeksinin % 1,45 olduğu tespit edilmiş olup; yapılacak HAD çalışmalarında bu ağ yapısı kullanılmıştır. Analizlerde kullanılan ağ yapısının genel görünümü Şekil-5'de gösterilmiştir.



Şekil 5. Doğrulama çalışması sonrasında seçilen ağ yapısı.

5. Sonuç

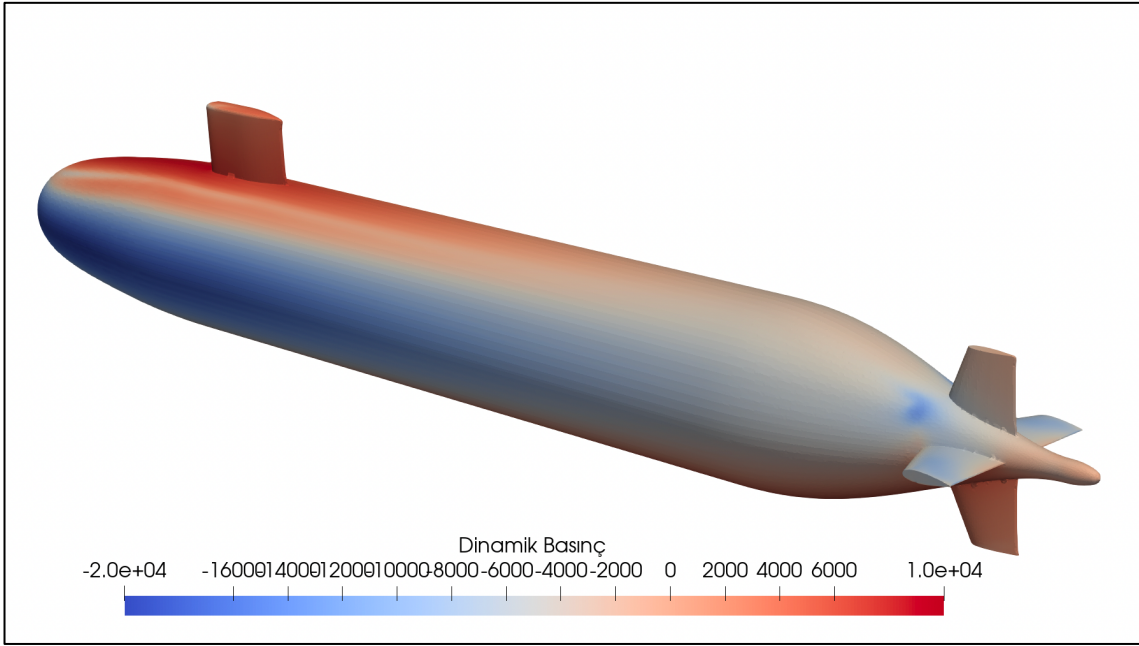
Bu çalışmada periskop derinliğinde bulunan denizaltıların manevra sorunlarını ortaya çıkarmak amacıyla model, $H/D=1.1$ derinliğe konumlandırılmıştır. Modelin su hattına göre konumu Şekil-6'da şematik olarak gösterilmiştir.



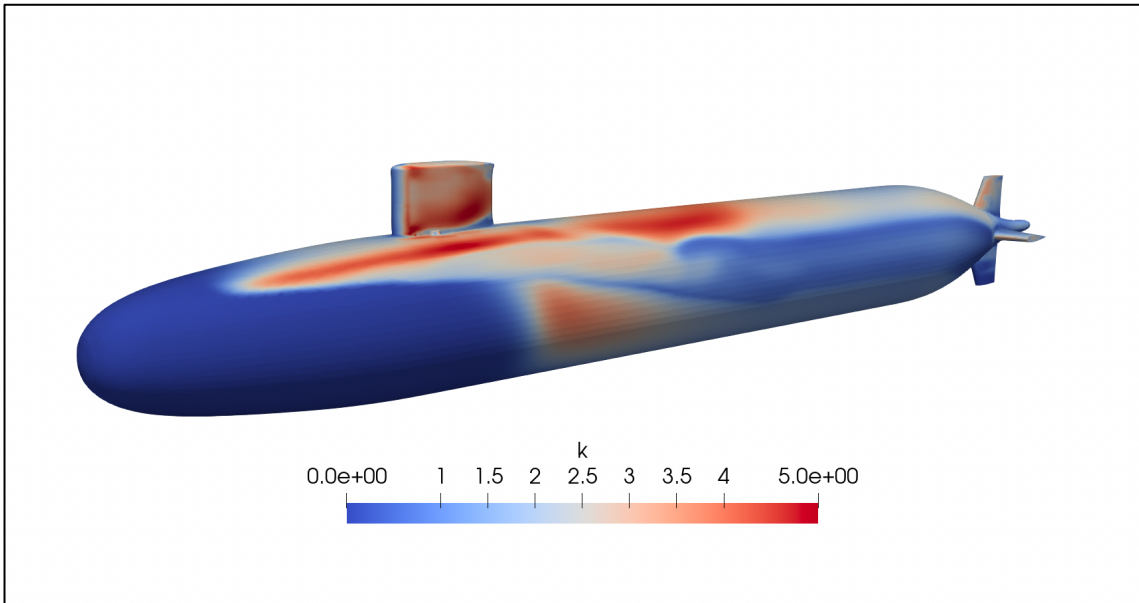
Şekil 6. Model konumu $H/D=1.1$.

6 serbestlik derecesine sahip denizaltının sualtı hareketleri 'sixDoFRigidBodyMotion' çözücüsü ile incelenmiştir. Denizaltının periskop derinliğindeki hareketlerini incelediğimiz için, 'dynamicMeshDict' dizininde model hareketi sadece boyuna (-x eksen) ve düşey (-z eksen) yönde doğrusal; baş kış dönme hareketi (-y eksen) yapacak biçimde rotasyonel olarak sınırlandırılmıştır. Bu sayede hesaplama maliyeti düşürülmüştür. Hesaplamalarda 'kOmegaSST' türbülans modeli kullanılmış olup; akış hızı 5,144 m/s olarak belirlenmiştir.

Denizaltılar, ufki kontrol yüzeylerini kullanarak ve uygun balast operasyonları ile dalıp çıkma hareketini yapmaktadır. Ancak periskop derinliğinde gizliliğini koruyarak göreve devam edebilmesi için denizaltının, su hattının hemen altında belirli bir derinlikte seyretmesi gerekmektedir. Denizaltının sahip olduğu form nedeniyle oluşan basınç dağılımı (Şekil-7) denizaltının başlı bir şekilde dalmaya zorlamaktadır. Bunu engellemek maksadıyla ufki dümenlere açı vermek, balast operasyonu yapmak gibi önlemler alınmaktadır. Ayrıca model etrafında oluşan türbülans kinetik enerjisi dağılımı da Şekil-8'de sunulmuştur.

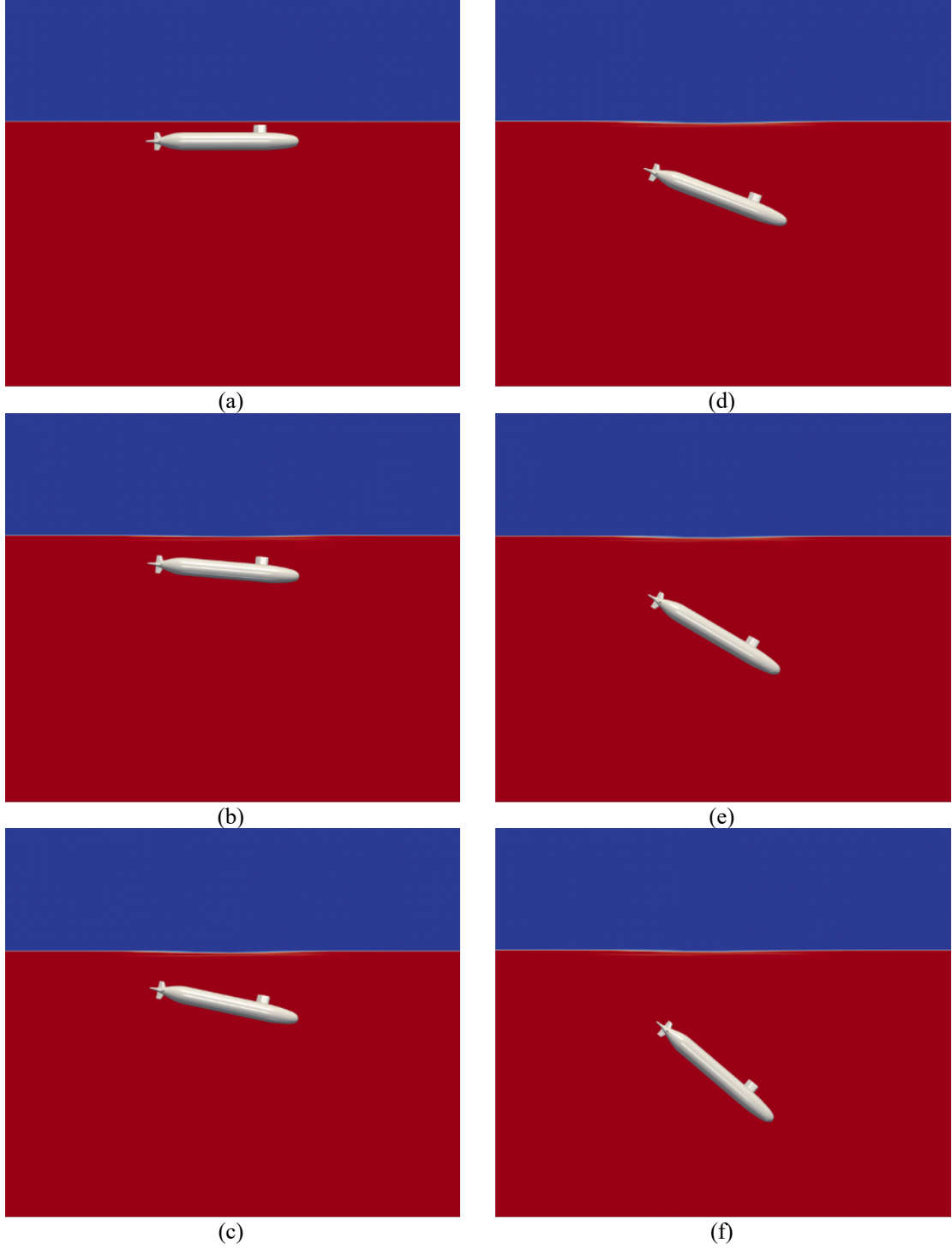


Şekil 7. Model etrafında oluşan dinamik basınç dağılımı.



Şekil 8. Model etrafında oluşan türbülans kinetik enerjisi.

'oversetInterDyMFoam' çözücüsü ile yapılan HAD analizlerinde önceki bölümlerde anlatılan geometri, sınır koşulları ve ağ örgüsüyle denizaltının başlı bir şekilde dalma hareketini yaptığı Şekil-9'da görülebilmektedir.



Şekil 9. HAD analiz sonuçları.

Yapılan HAD analizinde görüldüğü gibi model üzerinde bulunan kontrol yüzeylerine müdahale edilmezse denizaltı dalma hareketine devam etmektedir. Bu durumu engellemek amacıyla periskop derinliğinde kış kontrol yüzeylerine kumanda edilmektedir. Bu sayede model üzerinde oluşan basınç kaynaklı oluşan kuvvetlere karşı kuvvet üretilmektedir. Sonuç olarak denizaltı periskop derinliğindeki görevlerini icra edebilmekte ve gizliliğini koruyabilmektedir.

Kaynaklar

- [1] Takahashi, Kenshiro. Numerical simulations of comprehensive Hydrodynamic performance of DARPA SUBOFF submarine. Diss. 2019.
- [2] Kim, Howan, et al. "Six-DOF simulations of an underwater vehicle undergoing straight line and steady turning manoeuvres." *Ocean Engineering*, 2018.
- [3] Takahashi, Kenshiro, and Prasanta K. Sahoo. "Fundamental CFD study on the Hydrodynamic Performance of the DARPA SUBOFF submarine." *International Conference on Offshore Mechanics and Arctic Engineering*. Vol. 58776. American Society of Mechanical Engineers, 2019.
- [4] Kale, Fatih Mehmet. Numerical investigation of flow around a submarine by openfoam and ansys fluent. Diss. Master's Thesis]. Istanbul Technical University Institute of Science, Istanbul, Turkey, 2020.
- [5] Carrica, P. M., Y. Kim, and J. E. Martin. "Vertical zigzag maneuver of a generic submarine." *Ocean Engineering* 219, 2021.
- [6] Hussain, Arif, et al. "To study the effectiveness of stern appendages (Cruciform & X Shaped configurations) for maneuverability of autonomous underwater vessel using computational fluid dynamics." *Ocean Engineering* 272, 2023.
- [7] Guo, Haipeng, Guangnian Li, and Lin Du. "Investigation on the flow around a submarine under the rudder deflection condition by using URANS and DDES methods." *Applied Ocean Research* 131, 2023.
- [8] Özden, Yasemin Arıkan, M. Cansın Özden, and Fahri Çelik. "Numerical investigation of submarine tail form on the hull efficiency." *Proceedings of the fifth international symposium on marine propulsors*. 2017.
- [9] Sezen, Savas, et al. "Investigation of self-propulsion of DARPA Suboff by RANS method." *Ocean Engineering* 150, 2018.
- [10] Efremov, D. V., and E. M. Milanov. "Hydrodynamics of DARPA SUBOFF submarine at shallowly immersion conditions." *TransNav: International Journal on Marine Navigation and Safety of Sea Transportation* 13.2, 2019.
- [11] Quintuña, María T., and Rubén J. Paredes. "Free Surface Effect Assessment of the Flow Around the DARPA SUBOFF-5470 Submarine Using OpenFOAM." *International Conference*

on Offshore Mechanics and Arctic Engineering. Vol. 85185. American Society of Mechanical Engineers, 2021.

[12] Amiri, Mojtaba Maali, et al. "How does the free surface affect the hydrodynamics of a shallowly submerged submarine?." Applied ocean research 76, 2018.

[13] Groves, Nancy C., Thomas T. Huang, and Ming S. Chang. Geometric characteristics of DARPA (Defense Advanced Research Projects Agency) SUBOFF models (DTRC model numbers 5470 and 5471). David Taylor Research Center Bethesda MD Ship Hydromechanics Dept, 1989.

[14] Roddy, Robert F. Investigation of the stability and control characteristics of several configurations of the DARPA SUBOFF model (DTRC Model 5470) from captive-model experiments. David Taylor Research Center Bethesda MD Ship Hydromechanics Dept, 1990.

[15] Celik, Ishmail B., et al. "Procedure for estimation and reporting of uncertainty due to discretization in CFD applications." Journal of fluids Engineering-Transactions of the ASME 130.7, 2008.

2D BACKWARD FACING LAMINAR STEP FLOW SIMULATION BY FINITE DIFFERENCE METHOD

Cihad ÇELİK¹, Devrim Bülent DANIŞMAN², Barış BARLAS³,

¹*Istanbul Technical University, Faculty of Naval Architecture and Marine Engineering | celikciha@itu.edu.tr*

²*Istanbul Technical University, Faculty of Naval Architecture and Marine Engineering |
bulent.danisman@itu.edu.tr*

³*Istanbul Technical University, Faculty of Naval Architecture and Marine Engineering | barlas@itu.edu.tr*

ABSTRACT

In the current study, a backward-facing step flow (BFS) by finite difference discretization is solved in 2D Cartesian coordinate system. The governing equations of the problem are the incompressible Navier-Stokes equations and the continuity equation. The no-slip boundary conditions are applied using ghost cells within the solid domain. The Dirichlet and Neumann boundary conditions are implemented at the inlet and outlet of the channel, respectively. MAC (Marker and Cell) method is utilized as a numerical scheme to solve the flow. The problem is considered as a Stokes flow ($Re = 0$). Results show good agreement with the data that is calculated by the commercial software. The code written in Matlab is provided in the Appendix.

Key Words: Backward-Facing Step Flow, Finite Difference Method, Stokes Flow, MAC Method.

1. Introduction

Stokes flow which was named after George Gabriel Stokes, is a type of fluid flow where advective inertial forces are small compared with viscous forces. The Reynolds number is very low ($Re \ll 1$). This is a typical situation in flows where the fluid velocities are very slow, the viscosities are very large. In practice this type of flow occurs in the swimming of microorganisms, sperm motility, the flow of lava, painting brush problem, lubrication between plates, microelectromechanical and nanoelectromechanical systems particularly those with moving parts, and in the flow of viscous polymers. Backward-Facing Step is widely known for its application in internal flow studies. The flow separation is caused due to the sudden changes in the geometry. This creates a zone of recirculation and a point of flow reattachment. Strong adverse pressure gradients arise through this process.

Experimental [1-2] and numerical [3-7] studies of backward-facing step flow have been carried out with different flow conditions, laminar [3], transitional and turbulent in detail.

A technique [7] is first presented by Harlow & Welch namely, the marker and cell method, implemented to numerically solve the time-dependent flow of an incompressible fluid by finite difference discretization. The pressure and the velocity components as the primary variables are defined at cell centers and cell boundaries, respectively, shown in Figure 1 (a). Further investigations have been performed to understand the effect of the expansion ratios, the ratio of the channel height (H) to the inlet channel height (h), at low and moderate Reynolds numbers. It is highlighted that the total pressure loss rises with the increasing step height ($H - h$) and decrease with increasing Re number ($0 < Re < 200$) [3]. Direct numerical simulation of BFS flow has been performed at $Re = 395$ and expansion ratio 2 in order to understand the strong adverse pressure gradients attached to the step's downstream

which leads to flow instabilities and defines the pressure increasing [5]. The BFS flow problem has also been investigated numerically and experimentally in the transitional flow regime, from laminar to the turbulent regime, in a water channel [2]. In the experimental part, electro-diffusion technique is implemented to measure the wall shear rate. Numerical simulations performed in FLUENT software using finite volume discretization in 2D. Numerical simulations show good agreement with the experimental ones, which depicted that the backward-facing flow structure becomes more complex while the expansion ratio increases.

In this study, a backward-facing step flow by finite difference discretization is solved in 2D Cartesian coordinate system at $Re = 0$ and the code written in Matlab is provided to the readers, can be found in the Appendix. The authors believe that the readers would benefit from the code and it is ensured that it could be further developed.

2. Mathematical and Numerical Formulation

The incompressible Navier-Stokes equations that govern the incompressible viscous fluid flow in the Cartesian coordinate system can be written in dimensionless form as follows;

The momentum equations along the x-axis and y- axis, respectively,

$$Re \frac{\partial u}{\partial t} + Re \frac{\partial(uu)}{\partial x} + Re \frac{\partial(uv)}{\partial y} + \frac{\partial p}{\partial x} = \frac{\partial^2 u}{\partial x^2} + \frac{\partial^2 u}{\partial y^2} \quad (1)$$

$$Re \frac{\partial v}{\partial t} + Re \frac{\partial(uv)}{\partial x} + Re \frac{\partial(vv)}{\partial y} + \frac{\partial p}{\partial y} = \frac{\partial^2 v}{\partial x^2} + \frac{\partial^2 v}{\partial y^2} \quad (2)$$

The continuity equation;

$$-\frac{\partial u}{\partial x} - \frac{\partial v}{\partial y} = 0 \quad (3)$$

In these equations (u, v) represents the velocity vector components, p is the pressure and Re is the dimensionless Reynolds number.

$$Re = Re_D = \frac{\rho u D}{\mu} \quad (4)$$

Where, ρ is the density, D is the hydraulic diameter of the inlet channel, that is equivalent to twice its height, μ is the dynamic viscosity. The primitive variables can be arranged as shown in Figure 1(a). The finite difference approximations to the momentum equations (1) and (2) can be written; [6-7]

The momentum equations along the x-axis;

$$Re \frac{u_{i,j}^{n+1} - u_{i,j}^n}{\Delta t} + Re \frac{(uu)_{i+1,j} - (uu)_{i-1,j}}{2\Delta x} + Re \frac{(uv)_{i,j+1} - (uv)_{i,j-1}}{2\Delta y} + \frac{p_{i,j} - p_{i-1,j}}{\Delta x} = \frac{u_{i+1,j} - 2u_{i,j} + u_{i-1,j}}{\Delta x^2} + \frac{u_{i,j+1} - 2u_{i,j} + u_{i,j-1}}{\Delta y^2} \quad (5)$$

The momentum equations along the y-axis;

$$Re \frac{v_{i,j}^{n+1} - v_{i,j}^n}{\Delta t} + Re \frac{(uv)_{i+1,j} - (uv)_{i-1,j}}{2\Delta x} + Re \frac{(vv)_{i,j+1} - (vv)_{i,j-1}}{2\Delta y} + \frac{p_{i,j} - p_{i,j-1}}{\Delta y} = \frac{v_{i+1,j} - 2v_{i,j} + v_{i-1,j}}{\Delta x^2} + \frac{v_{i,j+1} - 2v_{i,j} + v_{i,j-1}}{\Delta y^2} \quad (6)$$

The similar approximations to the continuity;

$$-\frac{u_{i+1,j} - u_{i,j}}{\Delta x} - \frac{v_{i,j+1} - v_{i,j-1}}{\Delta y} = 0 \quad (7)$$

The no-slip boundary conditions can be applied using ghost cells within the solid domain as shown in Figure 1(b). The application of $u_b = 0$ requires that $u_{i+1,j} = 0$. In a similar manner, the application of $v_b = 0$ requires that $v_{i+1,j} = -v_{i,j}$.

2.1 Stokes flow

Using the above described MAC (Marker and Cell) [7], [8] scheme to solve Stokes flow ($Re = 0$) within the backward step $[0,5] \times [0,1]$. The boundary conditions can be seen in Figure 2. The computation is proceeded using the local numbering similar to that of in Figure 3.

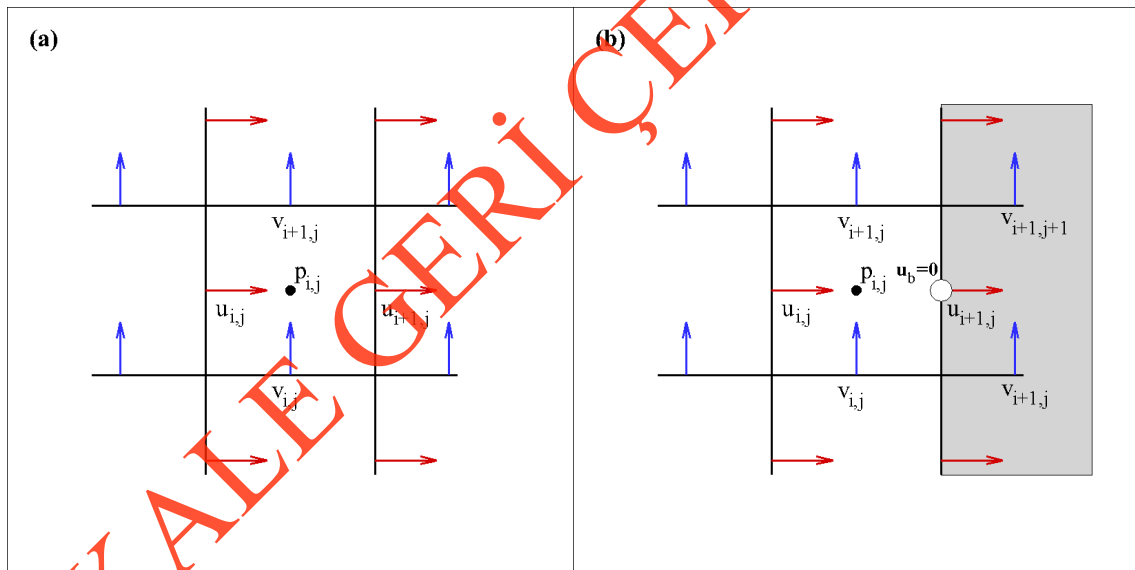


Figure 1: (a) The arrangement of primitive variables and (b) the application of no-slip boundary condition.

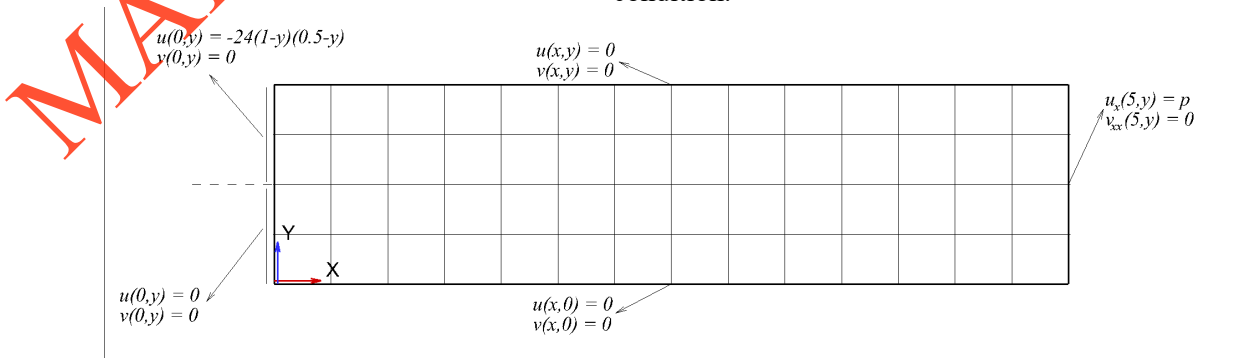
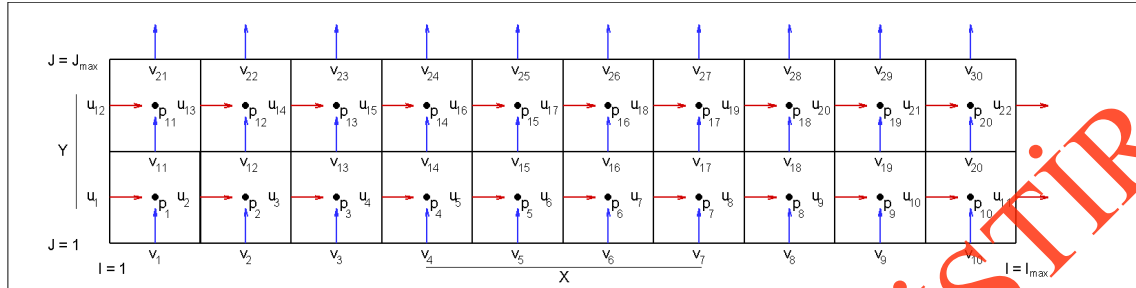


Figure 2: Computational domain and boundary conditions.**Figure 3:** The local numbering of primitive variables.

2.2 Boundary conditions

The boundary conditions were given below have been implemented to the inlet, outlet, top and bottom boundaries accordingly.

- **Inlet:** Dirichlet boundary condition was applied. The u velocity profile was given as parabolic function.

$$u(0, y) = -24(1 - y)(0.5 - y) \quad v(0, y) = 0 \quad y > 0.5$$

$$u(0, y) = \quad \quad \quad v(0, y) = 0 \quad y \leq 0.5$$

- **Bottom:** Dirichlet boundary condition was applied.

$$u(x, 0) = \quad \quad \quad v(x, 0) = 0$$

- **Top:** Dirichlet boundary condition was applied.

$$u(x, 1) = \quad \quad \quad v(x, 1) = 0$$

- **Outlet:** Neumann boundary condition was implemented.

$$\frac{\partial u}{\partial x} = p \quad \text{at } x = 5 \quad \frac{\partial^2 v}{\partial x^2} = 0 \quad \text{at } x = 5$$

3. Coding

The coefficients matrix A as depicted in Figure 4 includes the coefficients of u and v velocities and pressures in the X-Momentum, Y-Momentum and Continuity equations respectively. The matrix A is coded by considering the boundary conditions. Also, the right hand side matrix is defined according to the given boundary values. Finally, u and v velocities in the direction of X and Y with the pressure values defined in the cell centers is calculated by the matrix multiplication of inverse of A and the right hand side matrix. Pseudo code is found below.

A11: Coefficients of u velocities in the X-Momentum equation.

A12: 0

A13: Coefficients of pressures in the X-Momentum equation.

A21: 0

A22: Coefficients of v velocities in the Y-Momentum equation.

A13: Coefficients of pressures in the Y-Momentum equation.

A31: Coefficients of u velocities in the Continuity equation.

A32: Coefficients of v velocities in the Continuity equation.
A33: 0

$$\begin{bmatrix} A_{11} & A_{12} & A_{13} \\ A_{21} & A_{22} & A_{23} \\ A_{31} & A_{32} & A_{33} \end{bmatrix} \begin{bmatrix} u \\ v \\ p \end{bmatrix} = \begin{bmatrix} b \\ c \\ 0 \end{bmatrix}$$

→ X-Momentum
→ Y-Momentum
→ Continuity

Figure 4: The coefficients matrix structure

Table 1: Pseudo code for Stokes flow

```

1 - Define computational domain dimensions ([0,5] × [0,1])
2 - Define number of nodes along X and Y directions (Imax & Jmax)
3 - Create sparse matrix A which includes coefficients of X, Y – Momentums and Cont. equation
4 - Create X-Momentum coefficients in matrix A
for i = 1:Imax
    for j = 1:Jmax-1
        if i = 1 (Inlet boundary)
            if cc > 0.5
                Dirichlet boundary condition
            else
                No-slip boundary condition
            end if
        else if i = Imax (Outlet boundary)
            Out-flow boundary condition
        else
            Calculate pressure coefficients location in matrix A
            if j = 1 (Bottom boundary)
                No-slip boundary condition
            else if j = Jmax-1 (Top boundary)
                No-slip boundary condition
            else
                Inner cells
            end if
        end if
    end for
end for
5 - Create Y-Momentum coefficients in matrix A
for j = 1:Jmax
    for i = 1:Imax-1
        if j = 1 (Bottom boundary)
            No-slip boundary condition
        else if j = Jmax (Top boundary)
            No-slip boundary condition
        else
            Calculate pressure coefficients location in matrix A
            if i = 1 (Inlet boundary)
                No-slip boundary condition
            else if I = Imax-1 (Outlet boundary)

```

```

    Out-flow boundary condition
  else
    Inner cells
  end if
end if
end for
end for
6 - Create continuity equation coefficients in matrix A
for i = Imax-1
  for j = Jmax-1
    Inner cells
  end for
end for
7 - Calculate velocities in the direction of X-Y and pressures

```

4. Results

Backward-facing step flow has been solved with continuity and incompressible Navier-Stokes equations as governing equations. Finite difference method with the MAC scheme was implemented to compute the u, v velocities in the X-Y directions and pressure values in the cell centers. u velocity distribution can be seen in Figure 5. u velocity profile at $X=3$ was compared with the data calculated in FLUENT. It can be seen from Figure 6 that the numerical code shows good agreement with the verified data. v velocity and dynamic pressure distribution are depicted in Figure 7 and 8. The vertical velocity changes dominantly occur around the inlet boundary because of the geometrical discontinuity. The computations were proceeded with 101 and 21 finite difference nodes along the X and Y directions respectively. The comparison between the number of finite difference nodes on streamlines can be seen in Figure 9 and 10. Table 1 shows the comparison of error value for different number of finite difference nodes. The absolute error value has been decreased by increasing the nodes number.

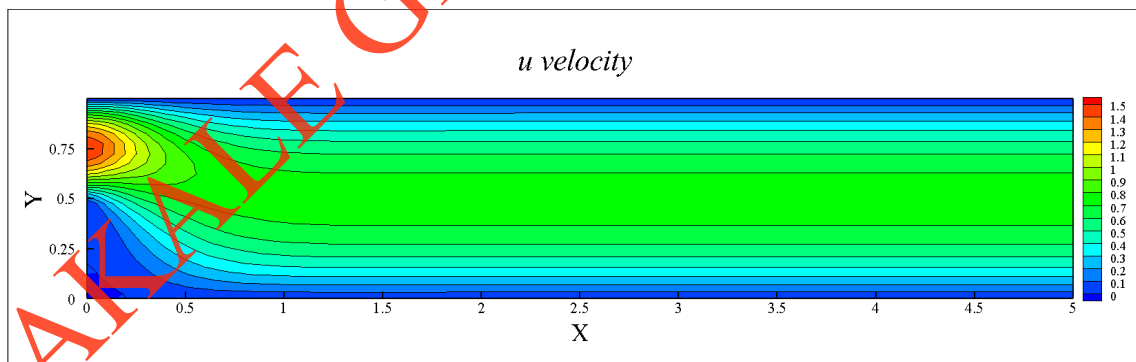


Figure 5: u velocity distribution with 101 and 21 finite difference nodes along the X and Y directions respectively.

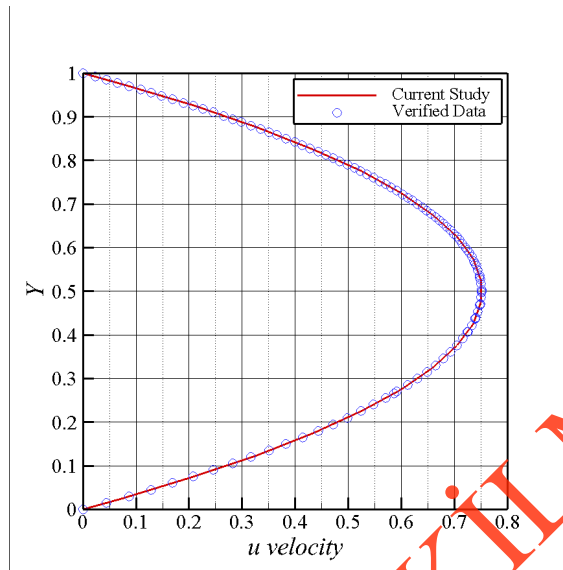


Figure 6: u velocity comparison between the current numerical study and data by Fluent at $X=3$.

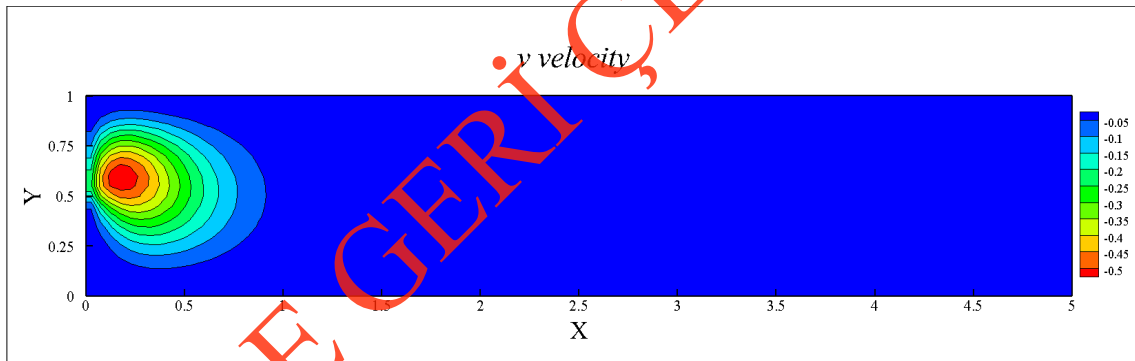


Figure 7: v velocity distribution with 101 and 21 finite difference nodes along the X and Y directions respectively.

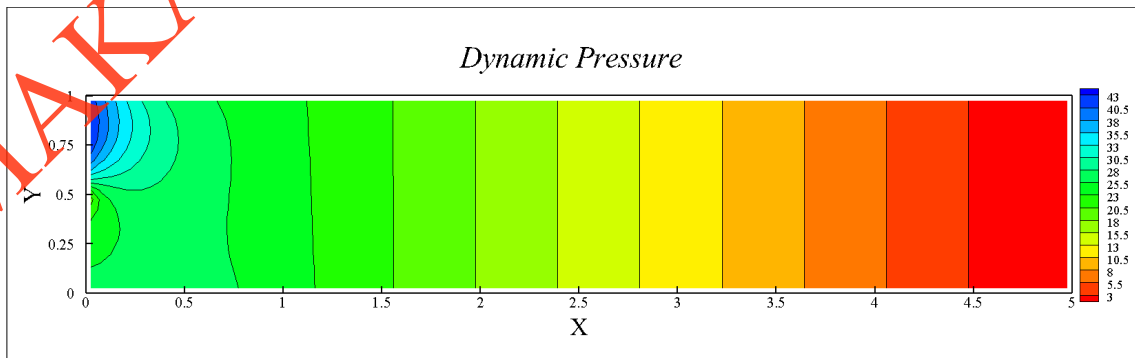
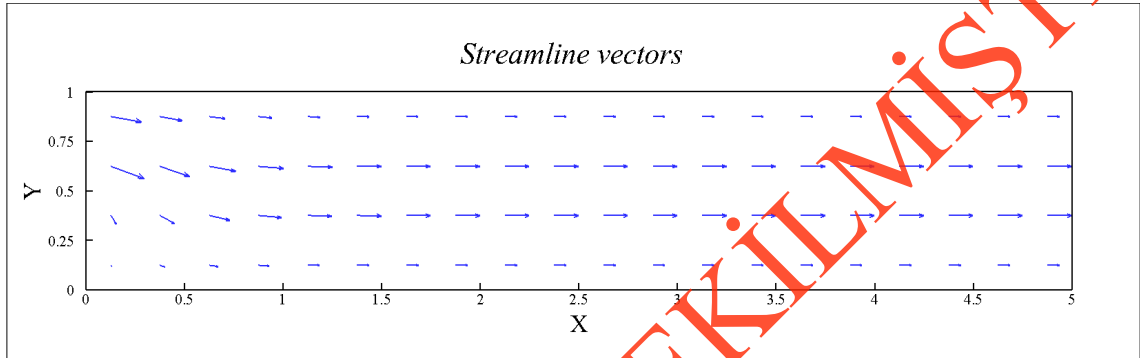
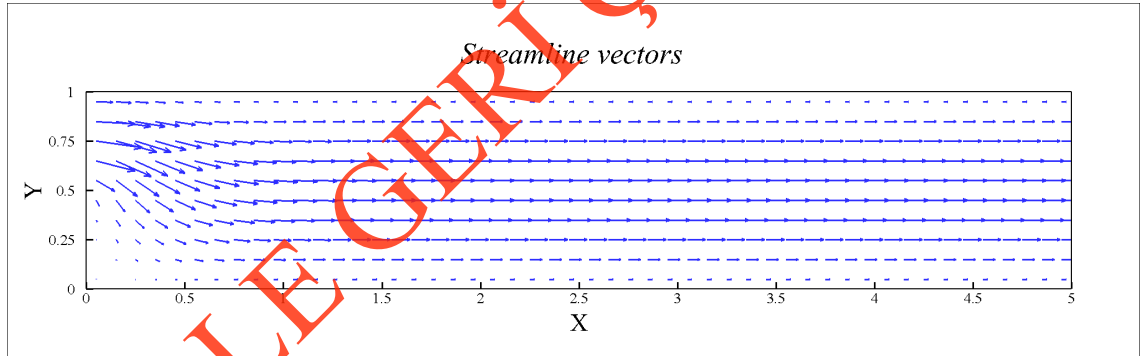


Figure 8: Dynamic pressure distribution with 101 and 21 finite difference nodes along the X and Y directions respectively.

Table 1. Comparison of error value for different number of finite difference nodes.

Exact	5x11	11x51	21x101
0.75000000000	0.75000002188	0.74999999943	0.74999999974
Error 10⁶(%)	2.92	0.08	0.03

**Figure 9:** Streamlines vectors with 21 and 5 finite difference nodes along the X and Y directions respectively.**Figure 10:** Streamlines vectors with 51 and 11 finite difference nodes along the X and Y directions respectively.

According to the provided parabolic function, the maximum u velocity is 1.5 in inlet section. In Figure 6, u velocity profile can be seen at section $X=3$ that is twice the inlet section. Here, the maximum velocity of u is 0.75, which shows that the problem provides the conservation of mass.

5. Conclusions

In this study, a backward-facing step flow by well-known finite difference discretization is solved in 2D Cartesian coordinate system using the incompressible Navier-Stokes momentum equations and the continuity equation. The convective terms in the momentum equations is discretized by using second order finite difference formulations, while pressure and time discretization is of first order. In the continuity equation the discretization in the main flow direction is of the first order and the cross flow is of the second order. The problem is considered as a Stokes flow. A Matlab code is written and

compared with the results of Fluent software. It can be seen from the results that the numerical code shows good agreement with the verified data. In the future, a 3D simulation of backward-facing step flow with and without the viscosity effect will be examined by finite difference and finite volume methods. Although the second order discretization could be problematic in 3D flow problems, higher order discretization along with averaging and smoothing methods will be planned to utilized.

References:

- [1] Armaly, B. F., Durst, F., Pereira, J. C. F., & Schönung, B. (1983). Experimental and theoretical investigation of backward-facing step flow. *Journal of fluid Mechanics*, 127, 473-496.
- [2] Tihon, J., Pěnkavová, V., Havlica, J., & Šimčík, M. (2012). The transitional backward-facing step flow in a water channel with variable expansion geometry. *Experimental Thermal and Fluid Science*, 40, 112-125.
- [3] Biswas, G., Breuer, M., & Durst, F. (2004). Backward-facing step flows for various expansion ratios at low and moderate Reynolds numbers. *J. Fluids Eng.*, 126(3), 362-374.
- [4] Chen, L., Asai, K., Nonomura, T., Xi, G., & Liu, T. (2015). A review of Backward-Facing Step (BFS) flow mechanisms, heat transfer and control. *Thermal Science and Engineering Progress*, 6, 194-216.
- [5] Pont-Vílchez, A., Trias, F. X., Gorobets, A., & Oliva, A. (2019). Direct numerical simulation of backward-facing step flow at $Re=395$ and expansion ratio 2. *Journal of Fluid Mechanics*, 863, 341-363.
- [6] Erturk, E. (2008). Numerical solutions of 2-D steady incompressible flow over a backward-facing step, Part I: High Reynolds number solutions. *Computers & Fluids*, 37(6), 633-655.
- [7] Harlow, F. H., & Welch, J. E. (1965). Numerical calculation of time-dependent viscous incompressible flow of fluid with free surface. *The physics of fluids*, 8(12), 2182-2189.
- [8] McKee, S., Tomé, M. F., Ferreira, V. G., Cuminato, J. A., Castelo, A., Sousa, F. S., & Mangiavacchi, N. (2008). The MAC method. *Computers & Fluids*, 37(8), 907-930.

Appendix

Matlab code for the backward step flow by finite difference method in 2D.

```
% Prepared by Cihad Çelik - 508192006
% Backward Step Flow by Finite Difference Method in 2D
% 29-01-2021

clear all
clc

% Computational domain dimensions
H = 1; % Height of the solution domain (Y direction)
W = 5; % Width of the solution domain (X direction)

Nodes = menu('# of nodes on Y and X axis', '5x21', '11x51', '21x101', 'Other');
if Nodes ==1; Jmax = 5;
elseif Nodes ==2; Jmax = 11;
elseif Nodes ==3; Jmax = 21;
elseif Nodes ==4; Jmax = input...
('Define # of nodes on Y axis (# of nodes on X axis calculated automatically): ');
end
dx = H/(Jmax-1);
dx2 = dx*dx;
Imax = W/dx+1;

t_u = (Jmax-1)*Imax; % number of u velocities
t_v = (Imax-1)*Jmax; % number of v velocities
t_p = (Jmax-1)*(Imax-1); % number of pressure point
t_uvp = (Jmax-1)*Imax+(Imax-1)*Jmax+(Jmax-1)*(Imax-1); % number of u+v+P

i=[]; j=[]; s=[];
b = t_uvp;
A = sparse(i, j, s, t_uvp, b);
RHS = sparse(i, j, s, t_uvp, 1);

x_axis = 0:dx:W;
x_axis_center = (dx/2):dx:(W-dx/2);
y_axis = 0:dx:H;
yac = (dx/2):dx:(H-dx/2); % y_axis_center

%% X - Momentum
s=0;
for i = 1:Imax
    for j = 1:Jmax-1
        m = (j-1)*Imax+1;
        if i == 1
            s=s+1;
            if yac(s) <= 0.5
                A(m,m) = 1;
                RHS(m) = 0;
            else
                % Dirichlet boundary condition
                A(m,m) = 1;
                RHS(m) = -24*(1-yac(s))*(0.5-yac(s));
            end
        elseif i == Imax
            n = ((j-1)*(Imax-1)+i-1)+(Jmax-1)*Imax+(Imax-1)*Jmax;
            % Out-flow boundary condition
            A(m,m) = -1/dx; A(m,m-1) = 1/dx;
            A(m,n) = 1;
            RHS(m) = 0;
        else
            n = ((j-1)*(Imax-1)+i)+(Jmax-1)*Imax+(Imax-1)*Jmax;
            if j == 1
                A(m,m) = 5/dx2; A(m,m+1) = -1/dx2; A(m,m-1) = -1/dx2; ...
                A(m,m+Imax) = -1/dx2;
            end
        end
    end
end
```

```

        A(m,n) = 1/dx; A(m,n-1) = -1/dx;
        RHS(m) = 0/dx2;
    elseif j == Jmax-1
        A(m,m) = 5/dx2; A(m,m+1) = -1/dx2; A(m,m-1) = -1/dx2; ...
        A(m,m-Imax) = -1/dx2;
        A(m,n) = 1/dx; A(m,n-1) = -1/dx;
        RHS(m) = 0/dx2;
    else
        A(m,m) = 4/dx2; A(m,m+1) = -1/dx2; A(m,m-1) = -1/dx2; ...
        A(m,m+Imax) = -1/dx2; A(m,m-Imax) = -1/dx2;
        A(m,n) = 1/dx; A(m,n-1) = -1/dx;
        RHS(m) = 0/dx2;
    end
end
end
end

%% Y - Momentum
for j = 1:Jmax
    for i = 1:Imax-1
        m = (j-1)*(Imax-1)+i+(Jmax-1)*Imax;
        if j == 1
            A(m,m) = 1;
            RHS(m) = 0;
        elseif j == Jmax
            A(m,m) = 1;
            RHS(m) = 0;
        else
            n = (j-1)*(Imax-1)+i+(Jmax-1)*Imax+(Imax-1)*Jmax;
            if i == 1
                A(m,m) = 5/dx2; A(m,m+1) = -1/dx2; A(m,m-(Imax-1)) = ...
                -1/dx2; A(m,m+(Imax-1)) = -1/dx2;
                A(m,n) = 1/dx; A(m,n-(Imax-1)) = -1/dx;
                RHS(m) = 0/dx2;
            elseif i == Imax-1
                % Out-flow boundary condition
                A(m,m) = 1/dx2; A(m,m-1) = -2/dx2; A(m,m-2) = 1/dx2;
                RHS(m) = 0/dx2;
            else
                A(m,m) = 4/dx2; A(m,m+1) = -1/dx2; A(m,m-1) = -1/dx2; ...
                A(m,m+(Imax-1)) = -1/dx2; A(m,m-(Imax-1)) = -1/dx2;
                A(m,n) = 1/dx; A(m,n-(Imax-1)) = -1/dx;
                RHS(m) = 0/dx2;
            end
        end
    end
end
end

%% Continuity
for i = 1:Imax-1
    for j = 1:Jmax-1
        m = (j-1)*(Imax-1)+i+(Jmax-1)*Imax+(Imax-1)*Jmax;
        m1 = (j-1)*(Imax-1)+i+(j-1);
        n1 = (j-1)*(Imax-1)+i+(Jmax-1)*Imax;
        A(m,m1) = -1/dx;
        A(m,m1+1) = 1/dx;
        A(m,n1) = -1/dx;
        A(m,n1+(Imax-1)) = 1/dx;
        RHS(m) = 0/dx;
    end
end
end

t_uv = t_u+t_v; % total number of u and v velocities

x = A\RHS;

%% Plot
u_vel = x(1:t_u);
u_vel = full(u_vel);

```

```

v_vel = x(t_uv+1:t_uv);
v_vel = full(v_vel);

P = x(t_uv+1:t_uvp);
P = full(P);

x_axis = 0:dx:W;
x_axis_center = (dx/2):dx:(W-dx/2);
y_axis = 0:dx:H;
y_axis_center = (dx/2):dx:(H-dx/2);

for i = 1:Imax
    for j = 1:Jmax-1
        m = (j-1)*Imax+i;
        u_vel_grid(j,i) = u_vel(m);
    end
end

for j = 1:Jmax
    for i = 1:Imax-1
        m = (j-1)*(Imax-1)+i;
        v_vel_grid(j,i) = v_vel(m);
    end
end

for i = 1:Imax-1
    for j = 1:Jmax-1
        m = (j-1)*(Imax-1)+i;
        P_grid(j,i) = P(m);
    end
end

figure('Name','u velocity','NumberTitle','off')
[X,Y] = meshgrid(x_axis,y_axis_center);
contourf(X,Y,u_vel_grid,10)
xlabel('x');
ylabel('y');
title('u velocity Stokes flow');
colorbar

figure('Name','v velocity Stokes flow','NumberTitle','off')
[X,Y] = meshgrid(x_axis_center,y_axis);
contourf(X,Y,v_vel_grid,10)
xlabel('x');
ylabel('y');
title('v velocity');
colorbar

figure('Name','Pressure Stokes flow','NumberTitle','off')
[X1,Y1] = meshgrid(x_axis_center,y_axis_center);
contourf(X1,Y1,P_grid,10)
xlabel('x');
ylabel('y');
title('Pressure');
colorbar

for i = 1:Imax-1
    for j = 1:Jmax-1
        u_cen(j,i) = (u_vel_grid(j,i+1)+u_vel_grid(j,i))/2;
    end
end

for j = 1:Jmax-1
    for i = 1:Imax-1
        v_cen(j,i) = (v_vel_grid(j+1,i)+v_vel_grid(j,i))/2;
    end
end

figure('Name','Stream Stokes flow','NumberTitle','off')

```

```
[mx,my]=meshgrid(x_axis_center,y_axis_center);  
XY = stream2(x_axis_center,y_axis_center,u_cen,v_cen,mx,my);  
streamline(XY);  
quiver(x_axis_center,y_axis_center,u_cen,v_cen);  
grid on
```

MAKALE GERİ ÇEKİLMİŞTİR

MAKALE GERİ ÇEKİLMİŞTİR